RL-TR-95-293
Final Technical Report
January 1996

HARDWARE COMPRESSIVE TRUE-TIME STEERING FOR CONTROL OF PHASED ARRAY ANTENNAS

Westinghouse Science and Technology Center

A.P. Goutzoulis, J.M. Zomp, D.K. Davies, I. Liberman,
A.H. Johnson, and P.D. Hrycak

APPROVED FOR PUBLIC RELEASE; DISTRIBUTION UNLIMITED.

Rome Laboratory
Air Force Materiel Command
Rome, New York

This report has been reviewed by the Rome Laboratory Public Affairs Office (PA) and is releasable to the National Technical Information Service (NTIS). At NTIS, it will be releasable to the general public, including foreign nations.

RL-TR-95- 293 has been reviewed and is approved for publication.

APPROVED: James R. Hunter

JAMES R. HUNTER
Project Engineer

FOR THE COMMANDER: Gary D. Barmore

GARY D. BARMORE, Major, USAF
Deputy Director of Surveillance & Photonics

If your address has changed or if you wish to be removed from the Rome Laboratory mailing list, or if the addressee is no longer employed by your organization, please notify Rome Laboratory/ (OCPC), Rome NY 13441. This will assist us in maintaining a current mailing list.

Do not return copies of this report unless contractual obligations or notices on a specific document require that it be returned.

REPORT DOCUMENTATION PAGE

Form Approved
OMB No. 0704-0188

1. AGENCY USE ONLY (Leave Blank)	2. REPORT DATE	3. REPORT TYPE AND DATES COVERED
	January 1996	Final Sep 91 - Nov 95

4. TITLE AND SUBTITLE

HARDWARE COMPRESSIVE TRUE-TIME STEERING FOR CONTROL OF PHASED ARRAY ANTENNAS

5. FUNDING NUMBERS

C - F30602-91-C-0111
PE - 63726F
PR - 2863
TA - 92
WU - 53

6. AUTHOR(S)

A.P. Goutzoulis, J.M. Zomp, D.K. Davies, I. Liberman, A.H. Johnson, P.D. Hrycak

7. PERFORMING ORGANIZATION NAME(S) AND ADDRESS(ES)

Westinghouse Science and Technology Center
1310 Beulah Road
Pittsburgh PA 15235

8. PERFORMING ORGANIZATION REPORT NUMBER

N/A

9. SPONSORING/MONITORING AGENCY NAME(S) AND ADDRESS(ES)

Rome Laboratory/OCPC
25 Electronic Pky
Rome NY 13441-4515

10. SPONSORING/MONITORING AGENCY REPORT NUMBER

RL-TR-95-293

11. SUPPLEMENTARY NOTES

Rome Laboratory Project Engineer: James R. Hunter/OCPC/(315) 330-7045

12a. DISTRIBUTION/AVAILABILITY STATEMENT

Approved for public release; distribution unlimited.

12b. DISTRIBUTION CODE

13. ABSTRACT (Maximum 200 words)

This program has developed a hardware compressive fiber optic (FO) true time delay (TTD) system for broadband UHF and L band high performance Phased Array Antenna (PAA) applications. The TTD steering is based on a unique architecture that employs both electronic and FO programmable delay lines in conjunction with optical wavelength division multiplexing (WDM) to dramatically reduce system complexity, hardware, weight, volume, and cost. This report describes the development of the prototype transmit and receive WDM TTD systems and the results obtained from the antenna range demonstrations.

14. SUBJECT TERMS

Fiber optic true time delay, Optical beam steering, Photonic beam control, Optical control-phased array antenna, Optical true time shifter

15. NUMBER OF PAGES

136

16. PRICE CODE

17. SECURITY CLASSIFICATION OF REPORT	18. SECURITY CLASSIFICATION OF THIS PAGE	19. SECURITY CLASSIFICATION OF ABSTRACT	20. LIMITATION OF ABSTRACT
UNCLASSIFIED	UNCLASSIFIED	UNCLASSIFIED	UL

TABLE OF CONTENTS

LIST OF FIGURES

HARDWARE-COMPRESSIVE TRUE TIME DELAY STEERING SYSTEM FOR CONTROL OF PHASED ARRAY ANTENNAS

A. P. Goutzoulis, J. Zomp, D. K. Davies, I. Liberman, A. Johnson*, P. Hrycak*

Westinghouse Science and Technology Center, Pittsburgh, PA.

* Westinghouse Electronic System Group, Baltimore, MD.

1. INTRODUCTION

Future high-performance phased array antenna (PAA) radars and multi-function systems will be required to have large scan angles (e. g., ±65°), wide instantaneous bandwidths (100s of MHz to several GHz), center frequencies anywhere from the UHF to the X band, and multiple independent beam capability. The actual number of transmit-receive (T/R) modules depends on the system mission as well as on the operating frequency, and typically is in the 10^2 - 10^5 range for all airborne, ground based, and shipboard systems.

To satisfy the wide instantaneous bandwidth (BW) requirements of such PAAs, true time delay (TTD) frequency- independent beam steering techniques must be used, so that efficient vector summation (in the receive mode) or distribution (in the transmit mode) can be obtained independent of frequency. Fiber is an excellent medium for both TTD and signal distribution (i. e., manifolding). (i) It can store large BW analog signals (~ 100 GHz) for long times (10s of μs). (ii) It has low attenuation which is flat over radio frequencies up to 100 GHz. (iii) It has excellent transmission stability by virtue of the small ratio of signal BW to optical carrier frequency. (iv) It allows the remote processing of PAA signals and optical wavelength multiplexing to minimize the number of

lines in the PAA feed link. (v) It is a non-conducting dielectric and so does not disturb the RF field, is secure, and EMI immune. (vi) It is flexible, and has low mass and small volume, all of which are important attributes for airborne and spaceborne systems. The importance of the fiberoptic (FO) TTD has been widely recognized by both the radar and communications community. Independent demonstrations have already verified the viability of the FO TTD concept using both laboratory equipment[1,2] and an actual PAA[3]. Several developmental TTD systems have been implemented or are currently underway worldwide, using a variety of non-switched[4-8] or switch-based[9-26] FO or optical TTD techniques.

Westinghouse Electric Corporation has also been very active in developing FO-based TTD systems, and has long ago recognized both the need for TTD and the importance of the role of FO in its implementation. During the last 4 years, the Westinghouse Science and Technology Center in Pittsburgh, under a Rome Laboratory program entitled "Hardware-compressive true time delay steering system for control of phased array antennas" (Contract Number F30602-91-C-0111) has been developing a hardware compressive FO TTD system for broadband UHF- and L-band high-performance radar applications. The TTD steering system is based on a unique architecture which employs both electronic and FO programmable delay lines in conjunction with optical wavelength division multiplexing (WDM) to dramatically reduce system complexity, hardware, weight, volume, and cost.

In this final report, we describe the development of the prototype transmit (Tx) and receive (Rx) WDM TTD systems together with the results obtained from the antenna range demonstrations. In Section 2, we briefly describe the basics of TTD. In Section 3 we describe the binary fiberoptic delay lines (BIFODEL) which are required for the WDM TTD system. In Section 4 we describe the principles of phased array antenna partitioning based on which we developed the one-dimensional (1-D) WDM TTD architecture which we describe in Section 5. In Section 6 we describe the two-dimensional (2-D) WDM TTD architecture. In Section 7 we describe the hybrid WDM TTD architectures which use both

BIFODELs and electronic digital delay lines (DiBi). In Section 8 we discuss the dimensionality limits of the WDM TTD approach. In Section 9 we describe the design and development of the 16-element Tx hybrid WDM TTD system. Several important subsections are included in Section 9. In Section 9.1 we discuss delay calculation issues, in Section 9.2 we describe the DiBi development, in Section 9.3 we describe the BIFODEL development, in Section 9.4 we describe the Tx FO link design and development. This is followed by Section 9.5 (in which we describe the overall system integration), Section 9.6 (in which we briefly describe the computer interface), and Section 9.7 (here we describe the laboratory testing and evaluation results). In Section 10 we describe the antenna range demonstration of the Tx WDM TTD prototype system. In Section 11 we describe the development of the 8-element Rx hybrid WDM TTD prototype system. Several important subsections are included in this Section. Section 11.1 (in which we describe various Rx WDM TTD architectures), Section 11.2 (in which we describe an optimum, combined Tx-Rx hybrid WDM TTD system), Section 11.3 (in which we describe the development of high performance directly modulated Rx FO links), Sections 11.4 and 11.5 (where we describe the BIFODEL and DiBi selection respectively), Section 11.6 (here we describe the MUX/DMUX selection and temperature control), Section 11.7 (here we describe the use of an optical isolator to eliminate optical reflections), Section 11.8 (here we describe the electronic programmable attenuators we used), Section 11.9 (this sections contains a description of the taper we used), Section 11.10 (here we describe the receive WDM TTD system integration), Section 11.11 (here we describe the integration of the various power supplies), Section 11.12 (here we describe the receive WDM TTD system laboratory testing and evaluation), and Section 11.13 (here we discuss the system spurious free dynamic range (SFDR) and noise figure (NF)). In Section 12 we describe the results of the Rx WDM TTD prototype system demonstration in the Westinghouse antenna range in Baltimore, MD. Finally, in Section 13 we present our conclusions.

2. BASICS OF TRUE-TIME DELAY STEERING

The basics of the TTD concept are illustrated in Figure 2.1 for a the simple case of a K-element, receiving (Rx) linear PAA (the 2-D concept is very similar and analogous to that of Figure 2.1). For this antenna, the normalized vector summation, V, is given by:

$$V= \sum_{i=1}^{K} \sin \{2\pi f[t + (D_i/v_i) + (I_i/v_2)]\} = \sum_{i=1}^{K} \sin \{2\pi f[t + (T_1)_i + (T_2)_i \sin\theta]\} \quad (2.1)$$

where θ is the receiving angle, $I_i = d_i \sin \theta$, d_i, and D_i are the distances of the i-th antenna element from the wavefront, 1st element, and summing point, respectively, and v_1 and v_2 are the propagation velocities over D_i and I_i, respectively. When the path delays from the wavefront to the summing point via each antenna element are equal, the sine functions in the summation of Equation 2.1 will add in phase for all values of frequency, f, thereby forming a beam summation in the direction θ which is independent of frequency. This condition is given by:

$$(T_1)_i + (T_2)_i \sin \theta = \text{constant}. \quad (2.2)$$

In the Rx mode, the direction θ is varied by selecting the D_i paths so that Equation 2.2 is satisfied. Thus, for the propagation of a planar wavefront in the direction θ, the delay lengths D_i must satisfy the linear relationship:

$$D_{K-i} = (v_1/v_2)\, d_i \sin \theta. \quad (2.3)$$

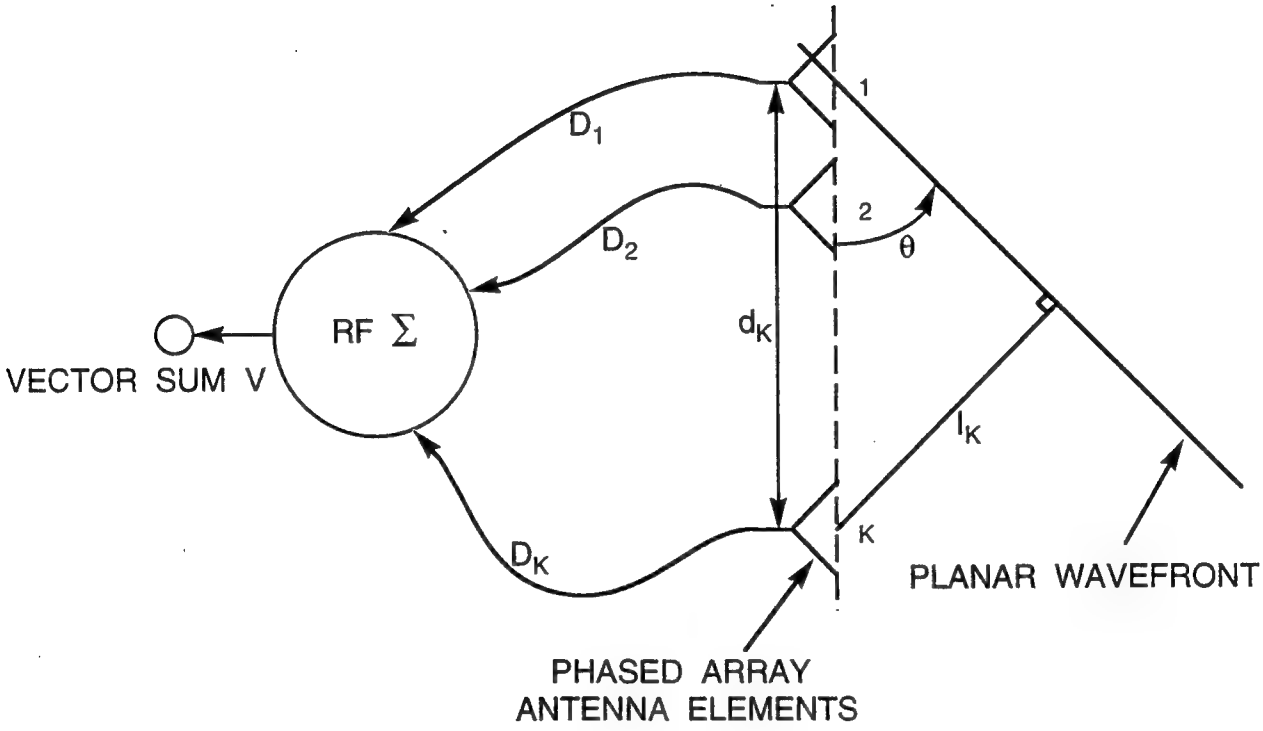

Figure 2.1 — Linear phase array antenna geometry.

In a 1-D PAA with K elements, the maximum time delay required by the i-th element is given by:

$$T_i = d_i \sin\theta_M / c \qquad (i = 1, 2, 3, \ldots, K), \tag{2.4}$$

where θ_M is the maximum scan angle and c is the speed of light. For a PAA with element-to-element spacing of $d = \lambda/2$, where λ is the wavelength of the RF radiation, the maximum possible delay T_{imax} is equal to:

$$T_{imax} = i \lambda \sin \theta_M / 2\, c. \tag{2.5}$$

Equation 2.5 indicates that the maximum delay required for a steering angle of θ_M is different for each of the K elements. This is also the case for the minimum delay corresponding to the antenna angular resolution θ_R:

$$T_{imin} = i \lambda \sin \theta_R / 2\, c. \tag{2.6}$$

Equations 2.5 and 2.6 determine the total number, R, of different delays required for steering the 1-D PAA antenna over θ_M with resolution θ_R. Similar equations can be derived for a 2-D TTD PAA for the x- and y- directions.

Note that virtually any photonic TTD concept can be arranged so that it generates fully symmetric $\pm T_{ij}$ delays, i. e., it can be made to operate over symmetric scan angles. The insertion of "negative" delays can be accomplished by time-biasing the antenna so that the zero delay position corresponds to the "negative" maximum scan angle. As an example consider an antenna operating over a scan angle of $\pm\theta_{sc}$ in conjunction with a TTD network which can provide a maximum delay corresponding to $\theta = \theta_{sc}$. To achieve this we must: (1) double the maximum delay to $\theta = 2\theta_{sc}$ and (2) time-bias the antenna such that when the variable TTD network provides zero delay, the antenna is steered at $\theta = -\theta_{sc}$.

Thus, when the TTD network provides exactly half of the maximum delay the antenna is steered at $\theta = 0°$, and when the maximum delay is provided the antenna is steered at $\theta = +\theta_{sc}$. The doubling of the delay corresponds to an extra bit of resolution whereas the time-bias of the antenna can be accomplished by inserting linearly-increasing but fixed time delays (e. g., fixed fiber lengths) into the paths of the various antenna elements (it is usually implemented at the photonic manifold level). Note that antenna biasing was employed in both the Tx and Rx WDM TTD prototypes we developed, and was found to be in excellent agreement with theory.

Equations 2.5 and 2.6 determine the total number, R, of different delays required for steering the antenna over θ_M with resolution θ_R. Since most PAAs have 10^3-10^5 elements, the number of the resulting delays, C, is enormous, and is approximately equal to K x R. For example, for a 10^3 element 1-D PAA operating at S-band (e. g., f = 3.5 GHz or λ = 85.7 mm) with d = 42.9 mm, $\theta_M = 90°$, and R = 1,024 (or 10 bits), a total of $C = 10^6$ different delays in the 0.44 ps-142.86 ns range are required. These numbers indicate not only the large delay complexity involved but also the large delay range required, conditions which become even more severe for larger PAAs. Large delay complexity results in large hardware complexity, i. e., switches and fiber segments necessary for the TTD implementation. Large hardware complexity implies not only high cost and difficulty in implementing and maintaining the TTD system, but also increased size and weight, parameters that must be minimized especially for airborne and spaceborne platforms.

The large hardware complexity issues can be better appreciated by considering one of the early, passive (i. e., no delay-switching capability) FO TTD implementations[1], a schematic of which is shown in Figure 2.2. In this system, the RF signal from a given antenna element is used to modulate a fiber-coupled laser diode (LD), the output of which is divided into R channels via the use of a FO 1:R divider. The length of each fiber is arranged so that it

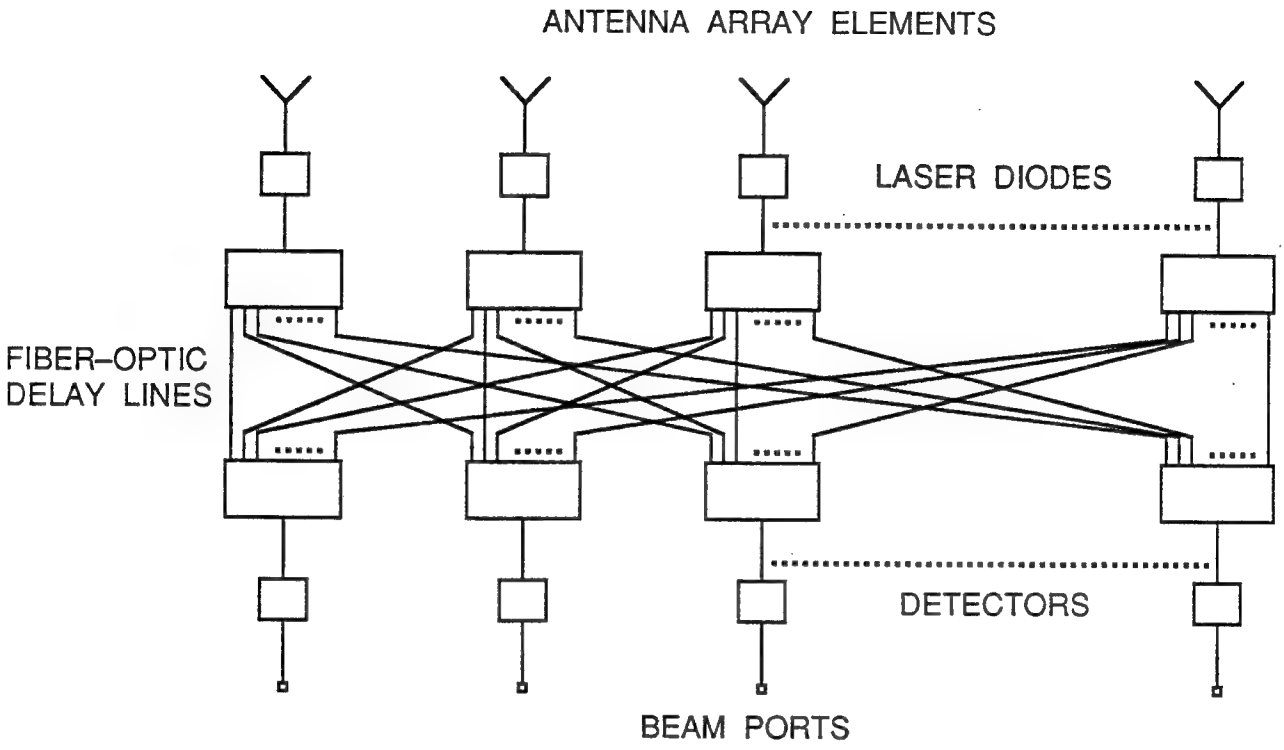

Figure 2.2 — Schematic of a passive FO TTD implementation comprising K elements and R beams.

corresponds to a specific angle θ_i, i = 1, 2, . . . , R. This is repeated for each of the K PAA elements with the understanding that for a given angle θ_i the length of the corresponding fiber varies linearly from element to element. The outputs from all fibers that correspond to the same θ_i are combined via a K:1 FO combiner. The combiner output is read-out by a detector which provides an output RF signal corresponding to that received from all PAA elements at angle θ_i. Thus, each of the R beam ports provides a simultaneous output of the signal received at each of the R discrete directions. From this brief description and with the aid of Figure 2.2, one can easily show that this passive FO TTD scheme is hardware intensive since it requires a total of K x R fibers.

From the above discussion we can conclude that straightforward implementations of FO TTD have large hardware complexities which makes them impractical. Therefore, it is essential that ingenious, hardware compressive, FO TTD architectures be employed for TTD steering. Such architectures must compress the hardware with respect to *both* the number of delays per PAA element and the number of elements per PAA. The development and demonstration of such hardware-compressive architectures is the subject of this work. In the next chapter we describe a hardware-efficient delay line architecture BIFODEL which compresses the overall hardware with respect to the number of delays.

3. BINARY FIBEROPTIC DELAY LINES (BIFODEL)

A thorough analysis of existing delay-compressive delay line architectures shows that the most efficient architecture is the binary fiber-optic delay line architecture, or BIFODEL, first suggested by Levine[10]. In the BIFODEL architecture (Figure 3.1.a), the optical signal is optionally routed through N fiber segments whose lengths increase successively by a power of 2. The required fiber segments are addressed using a set of N 2x2 optical switches. Since each switch allows the signal to either connect or bypass a fiber segment, a

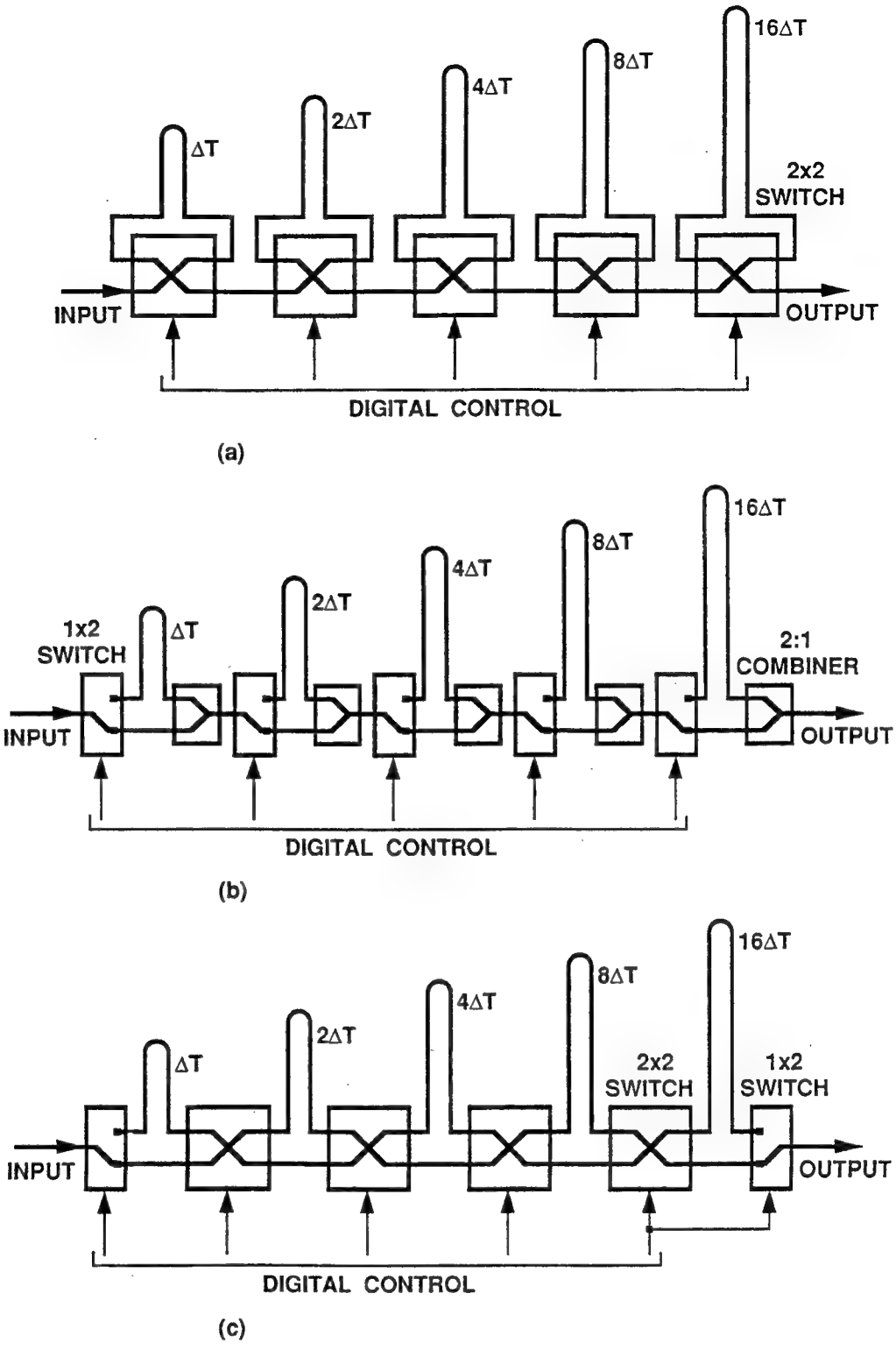

Figure 3.1 — Block diagrams for different binary fiber-optic delay line architectures (BIFODEL): (a) Design 1, (b) Design 2, and (c) Design 3.

delay T may be inserted which can take any value, in increments of ΔT, up to the maximum value, T_{max}, given by:

$$T_{max} = (2^0 + 2^1 + 2^2 + \ldots + 2^{N-1})\,\Delta T = (2^N - 1)\,\Delta T. \qquad (3.1)$$

For example, in order to introduce a delay of $53\Delta T$ using a 6-bit BIFODEL, the signal must be routed through the first, third, fifth, and sixth fiber segments. Note that the actual delays are implemented differentially, i. e., it is the difference between the delayed path and the undelayed path that sets the desired delay.

Since there exist $2^N - 1$ possible delay combinations, the number N of switches and delay segments for the BIFODELs of Figure 3.1 is given by

$$N = \log_2 R. \qquad (3.2)$$

This results in a very significant reduction of hardware; in fact, the BIFODEL architecture is the most efficient of all delay-compressive delay lines[17]. In practice, the actual BIFODEL complexity depends on the specific design implemented[22]. There are at least 3 different BIFODEL architectures for which the complexity (C), insertion loss (IL) and IL stability values are different. Figures 3.1a-3.1c show 3 different designs for N = 5. Design 1 (Figure 3.1a) requires the lowest component complexity of N 2x2 switches. However, it has a non-stable IL that varies between $(\log_2 R) \times IL_s$ and $2 \times (\log_2 R) \times IL_s$ as the BIFODEL program changes (IL_s is the switch IL). This is because, depending on the program, the signal might enter the same switch twice thereby increasing the IL. Design 2 (Figure 3.1b) uses N 1x2 switches as well as N 2:1 FO combiners. For this architecture:

$$IL = (\log_2 R) \times (IL_s + 3), \qquad (3.3)$$

where the 3 dB factor is due to the insertion loss of the 2:1 FO combiner. Assuming that all switches have the same IL_s value and that no significant attenuation changes occur as different length fiber segments are switched in, the loss is independent of the BIFODEL switch program, i. e., the loss is stable. Design 3 (Figure 3.1c) uses (N - 1) 2x2 switches and two 1x2 switches for a total switch complexity of ($\log_2 R + 1$). This design has a stable IL given by:

$$IL = (\log_2 R + 1) \times IL_s. \qquad (3.4)$$

Design 3 is the optimum configuration in terms of minimizing both complexity and loss. Table 3.1 shows a quantitative comparison of the performance of the 3 BIFODEL designs for $N = \log_2 R = 6$ and $IL_s = 1$ dB. The table shows that Design 3 is the best because it has minimum, stable loss and a very low complexity. The less complex Design 1 can be very lossy, and most importantly, its loss is not stable which means that significant correction must be made (up to 12 dB in the RF domain).

TABLE 3.1 - Comparison of the three BIFODEL designs for $N = 6$ and $IL_s = 1$ dB.

DESIGN #	IL (dB)	Stability (dB)	Complexity
1	6-12	±3	6
2	24	0	12
3	7	0	7

Using Design 3 as the optimum BIFODEL design for implementing the FO TTD K-element PAA (on a per element basis), we find that the switch (C_S) and fiber (C_F) complexities are:

$$C_S = (K - 1) \times (\log_2 R + 1), \tag{3.5}$$

$$C_F = (K - 1) \times \log_2 R. \tag{3.6}$$

From Equations 3.5-3.6 we find that for a 10^3 element PAA with R=10 bits, $C_S = 10.1 \times 10^3$, $C_F = 9.9 \times 10^3$, and IL = 11 dB. These complexities are lower by about 3 orders of magnitude than those of the non-compressive architectures; however, they are still large for most practical PAAs. In general, BIFODELs can be practical TTD devices so long as (1) the number of PAA elements is relatively small, e. g., a few tens, or (2) they are used in conjunction with antenna subarray techniques. Since most practical PAAs have at least several hundreds of elements, the latter rather than the former scenario is more realistic.

In order to avoid ambiguities as a result of signal splitting, the minimum programmability period, T_{pr}, defined as the time difference between the setup of two consecutive programs which occur at times $t = t_{i-1}$ and $t = t_i$, must satisfy

$$T_{pr} \geq T_s + T_{i-1}, \tag{3.7}$$

where T_s is the signal duration and T_{i-1} is the total delay introduced at time $t = t_{i-1}$. However, there are many signal-delay scenarios for which T_{pr} can be reduced. For example, consider the scenario where the signal is a pulsed waveform whose period T_p is compatible with T_{max} and whose pulsewidth T_w is less than $2^{N-1}\Delta T$. In this case, and under the assumption that two consecutive programs require the use of the longest delay segment available, T_{pr} need only satisfy

$$T_{pr} \geq T_w + T_{i-1} - 2^{N-1}\Delta T. \tag{3.8}$$

BIFODELs can be implemented with a variety of delay media and/or switches including combinations of fiber and/or free space and/or integrated

optical (IO) delays[16-24]. For example, a 3-bit IO BIFODEL has been demonstrated by Lagerstroem et al.[14] using Ti:$LiNbO_3$, and Sullivan et al.[20] have reported a 3-bit IO BIFODEL implemented on GaAs. As we will see, 6-bit BIFODELs based on Design 3 were implemented at the Westinghouse Science and Technology Center for the Tx-Rx WDM TTD prototype systems. These BIFODELs used piezomechanical switches with low loss (<1.0 dB), and low crosstalk (<-70 dB). The largest BIFODEL has the following delay bits: 97.8 ps, 195.5 ps, 391.0 ps, 782.0 ps, 1564.1 ps, and 3128.2 ps. The overall accuracy in these delays is ± 1.5 ps (independent of the actual delay value), and the measured SNR is 145 dB/Hz. Multi-channel, free-space BIFODELs have been demonstrated by Dolfi et al.[23] who used 2-D SLMs to achieve parallel switching. Goutzoulis et al.[16] have reported an electronically switched 7-bit BIFODEL using FO links for implementing the delays. The switching is performed with two back-to-back 1x2 GaAs FET switches, and the zero delay path is implemented with a microwave stripline. The overall BW is 0.5-1 GHz, the maximum delay is 5 μs, the resolution is 39 ns, and the measured SNR is 123 dB/Hz. Ng et al.[24] have proposed another type of hybrid BIFODEL where in each delay stage a different LD is used. The switching is performed in a way similar to that proposed by Levine[10].

In general, all-optical BIFODELs are preferable because: (1) they can be made bidirectional, and (2) they are transparent to microwave signals up to 100 GHz and therefore high fidelity microwave signal transmission is possible[18]. Furthermore, hybrid BIFODELs require RF amplifiers per bit of delay. These amplifiers must have enough gain to recover: (1) the FO splitting losses and (2) the electrical-to-optical and optical-to-electrical conversion losses. The presence of many cascaded electronic and optoelectronic components (especially LDs) may dramatically reduce the spurious-free DR of the system[16]. For delays of less than ~ 1 ns, IO approaches can result in smaller overall size and potentially lower cost. However, for longer delays fiber must be used (as is the case for free

space BIFODELs[23]) and IO switches are currently very lossy (about 3 dB/bit loss) and have high crosstalk (typical > -25 dB per switch).

4. PHASED ARRAY ANTENNA PARTITION PRINCIPLES

Delay and element hardware compressive TTD architectures for 1-D PAAs can be achieved by partitioning the K elements of a PAA into E sets of M elements, i. e., K = M x E, and exploiting the delay relationships among neighboring elements in the PAA. Using the indices $j = 1, 2, \ldots, E$, and $i = 1, 2, \ldots, M$, to represent the set and element location, respectively, the equivalence between the delay required by the k-th element, T_k, and that required by the ij-th element, T_{ji}, (which is at the same location as the k-th element) requires the following relationships:

$$j = \{(k - 1)/M\} + 1, \tag{4.1}$$

$$i = k - (j - 1)\, M, \tag{4.2}$$

where {(k - 1)/M} denotes the integer part of the quotient (k - 1)/M. Solving Equation 4.2 with respect to k, we see the following delay expression:

$$T_k = T_{ji} = T_i + (j - 1)\, T_M, \tag{4.3}$$

where T_i and T_M are the delays of the i-th and M-th elements of the 1st set which we will name the reference set (RS). Equation 4.3 shows that the delay required by the i-th element of the j-th set is equal to the delay of the i-th element of the RS plus a constant (or bias) delay which is equal to $(j - 1)\, T_M$. We note that the bias delay depends only on j and not on i, and thus it is common to all the elements of a given set. This situation is described graphically in Figure 4.1 which shows an E-way partitioned array with M = 4, where $T_{bj} = (j - 1)\, T_M$,

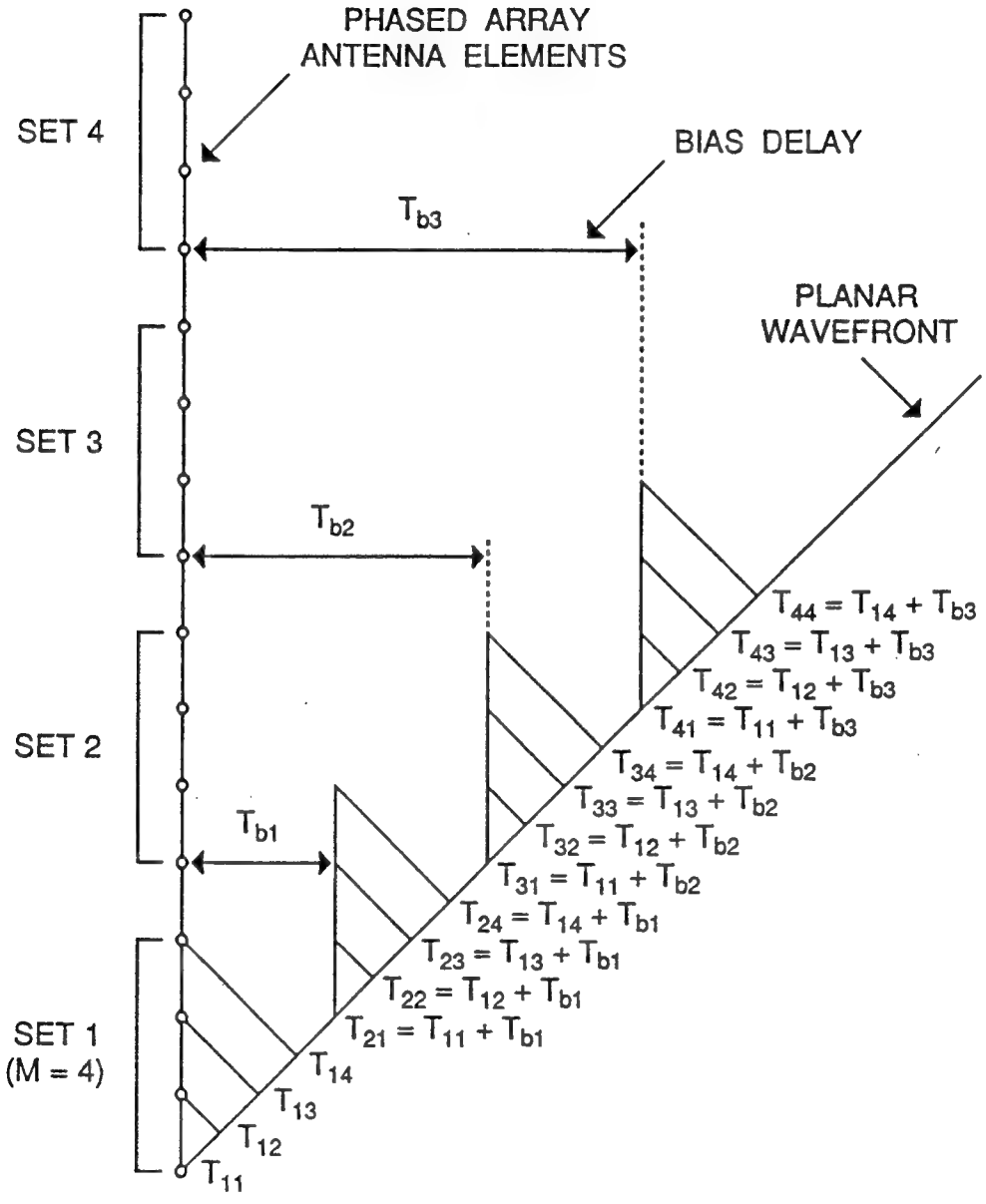

Figure 4.1 — Partitioning principles for a 1-D phased array antenna.

represents the bias delay necessary for the j-th set. Note that E different bias delay lines are required, each with a total of R different delays (i. e., the same number of delays as the delay lines of the RS). The bias delay resolution is equal to $(j-1)\,T_{Mmin}$, where T_{Mmin} is the delay resolution of the M-th element of the RS.

The importance of the PAA partitioning is that it results in very significant hardware reduction in both delay line type (i. e., delay lines with different resolution) and delay line quantity. Reduction in delay line type occurs because the total number of different types of delay lines can be as low as (M + E - 2), i. e., M-1 delay lines for the RS plus E-1 bias delay lines. Reduction in the total number of delay lines occurs because only one bias delay line is required per set and it is possible to cascade each of the M-1 delay lines of the RS to all E-1 bias delay lines and thereby address all the M x E elements of the PAA. In this case, (and for $M=E=\sqrt{K}$), we find that the total number of delay lines C_{DL} is equal to:

$$C_{DL}= 2(\sqrt{K}-1). \qquad (4.4)$$

Equation 4.4 demonstrates the very significant hardware savings possible using the partitioned PAA technique. Table 4.1 shows examples of hardware savings.

Table 4.1- Hardware savings for various PAAs and for $M=E=\sqrt{K}$

K	C_{DL}	Savings (%)
100	18	82.0
1,000	62	93.8
1,0000	198	98.0

5. 1-D ALL-OPTICAL WDM TTD ARCHITECTURE

The partitioned PAA concept can be uniquely implemented using optical WDM in conjunction with all-optical programmable delay lines and is reversible, i. e., the same hardware can be used for both the transmit and receive PAA modes.

In the transmit mode (Figure 5.1), M - 1 RS BIFODELs with outputs at wavelengths $\lambda_2, \ldots, \lambda_M$, are driven in parallel by the microwave radar signal. The M - 1 BIFODEL outputs along with a non-delayed output at wavelength λ_1 are multiplexed via a M-channel optical multiplexer (MUX), the output of which is divided into E channels via a 1:E channel optical divider. All but one of the divider outputs independently drive a bias BIFODEL, each of which is followed by an optical M-channel demultiplexer (DMUX). The divider output channel that does not drive a bias BIFODEL is also demultiplexed. Since the optical inputs to each bias BIFODEL contain M optical wavelengths, the DMUX output will also contain M wavelengths $\lambda_1, \lambda_2, \ldots, \lambda_M$. The outputs of the non-biased DMUX (extreme left in Figure 5.1) contain the M progressively delayed signals required for the RS (set 1 in Figure 4.1) which, as Figure 5.1 shows, requires no bias delay. The outputs of each of the remaining DMUXs contain a similar set of signals (but which are further delayed via the bias BIFODELs), and correspond to a different PAA set. Similar wavelength outputs drive similar location elements in each set. All BIFODELs must have $N = \log_2 R$ cascaded segments and different time resolution T_{imin}. The latter is determined by the location of the specific element, the antenna geometry, the radar characteristics, etc. Similar comments apply to the bias BIFODELs which have time resolutions, $(j - 1)T_{Mmin}$.

In the receive mode (Figure 5.2) the same architecture is used but in reverse. Here, the output of each PAA element drives a LD of a different wavelength. Elements with similar locations in different sets drive LDs of the same wavelength. For each PAA set, the LD outputs are multiplexed and drive

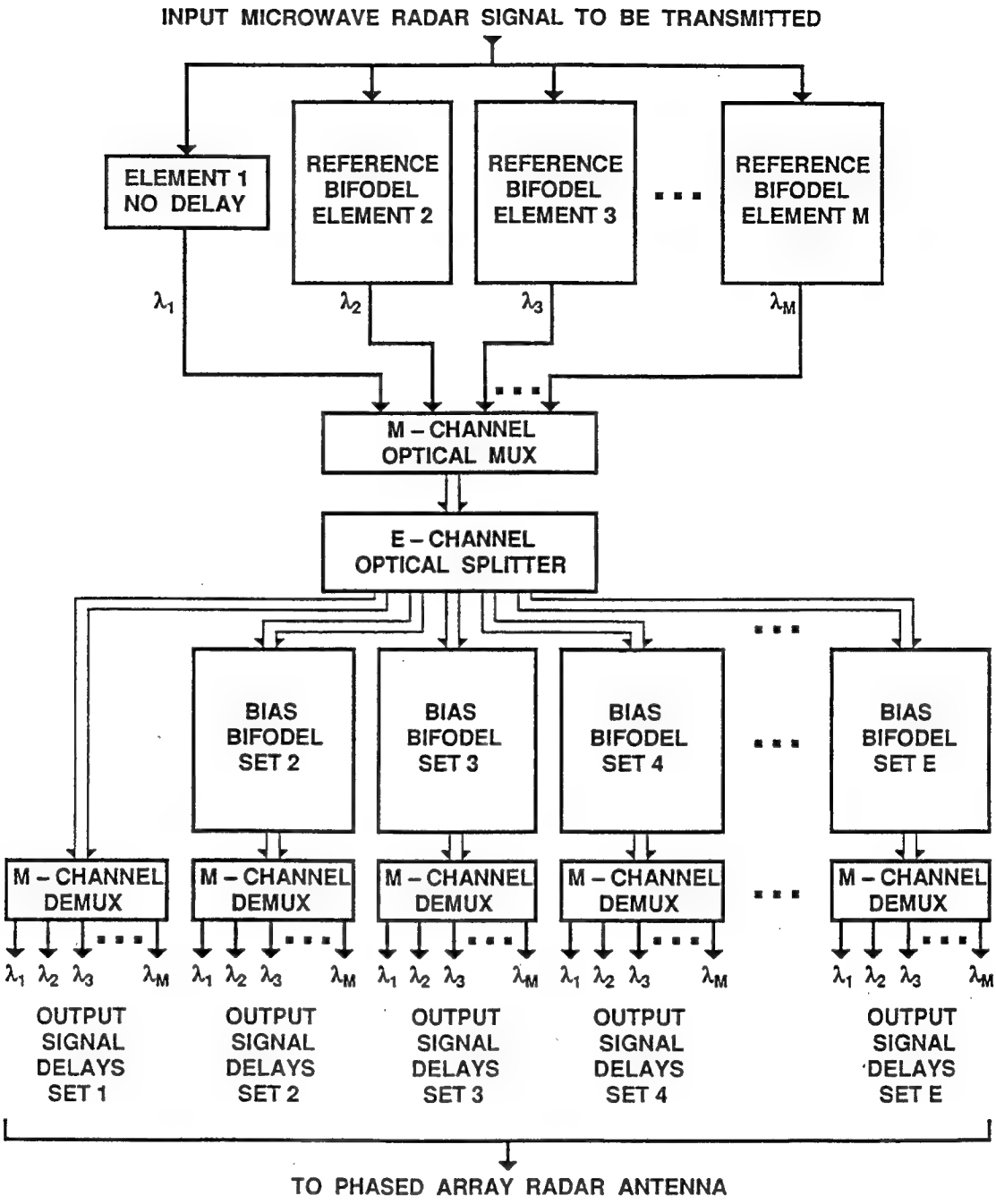

Figure 5.1 — Schematic of a BIFODEL-based delay-and element-compressive FO TTD architecture for transmitting 1-D PAAs using optical WDM.

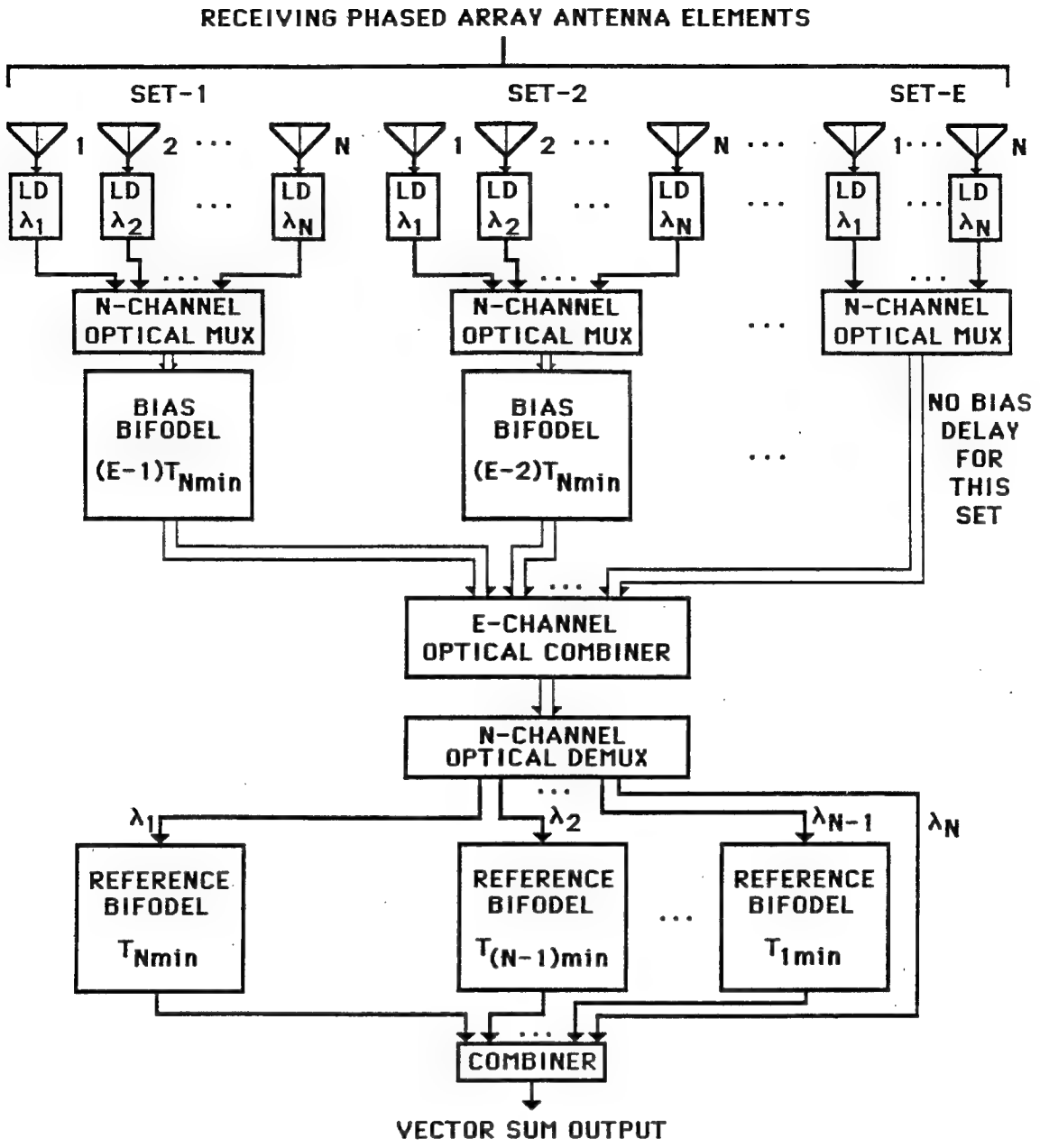

Figure 5.2 — Schematic of a BIFODEL-based delay-and element-compressive FO TTD architecture for receiving 1-D PAAs using optical WDM.

a bias BIFODEL. The bias BIFODELs eliminate the set-to-set bias delays, i. e., in Figure 4.1 all T_{bi} bias delays are removed, and the wavefront appears like a sawtooth having a "period" proportional to the width of a PAA set. The outputs of the bias BIFODELs are then combined via an E-channel optical combiner (i. e., a 1:E channel optical divider operating in reverse), the output of which is subsequently demultiplexed (i. e., via the M-channel MUX operating in reverse). Each of the DMUX outputs (which contains similar wavelengths) drives a RS BIFODEL. These RS BIFODELs eliminate the in-set delays, i. e., in Figure 4.1 all T_{ji} are now equal, and the wavefront is parallel to the antenna axis. The remaining step is to add the outputs of the reference BIFODELs via a combiner, the output of which provides the desired vector sum. The final summation can take place in either the optical or the RF domains (we discuss these issues in Section 11).

From the above discussion, and for the case where $M = E = \sqrt{K} = \sqrt{1024} = 32$, one can easily show that the total number of BIFODELs, C_{CDL}, is equal to:

$$C_{CDL} = 2\,(\sqrt{K} - 1) = 62. \qquad (5.1)$$

When the partitioned PAA concept is implemented with BIFODELs, the overall switch complexity, C_{CS}, or fiber (or IO waveguide delays) complexity, C_{CF}, as a function of the resolution R=10 bit and the number of elements K=1,024 (again for $M = E = \sqrt{K} = 32$) is given by:

$$C_{CS} = C_{CF} = (\log_2 R) \times 2\,(\sqrt{K} - 1) = 620. \qquad (5.2)$$

When these complexity figures are compared with the complexity figures of the delay-compressive (i. e., one BIFODEL per PAA element), 10^4, and non-compressive, 10^6, architectures, one immediately understands the power of the WDM TTD architecture. This comparison clearly demonstrates the dramatic

hardware complexity reduction (2-3 orders of magnitude) that is possible using antenna partitioning in conjunction with BIFODELs. These dramatic hardware savings are extremely important for airborne system applications (such as AWACS) since they translate to dramatic savings in size, weight, power consumption and cost. Note that these kind of savings are not possible with any known electronic TTD technique since such techniques cannot offer WDM.

6. 2-D ALL-OPTICAL WDM TTD ARCHITECTURE

The WDM TTD concept can also be applied to 2-D PAAs but without the necessity for antenna partitioning. The basic idea[19] is to use two sets of optical delay lines, one set with $K_x - 1$ delay lines for TTD control along the horizontal direction (called H-control) and another set with $K_y - 1$ delay lines for TTD control along the vertical direction (called V-control). The two delay line sets are interconnected such that all the delays from the H-control are combined with all delays from the V-control thereby creating a total of $K_x \times K_y$ different delay combinations. These different delays are separated via the use of both WDM and spatial coding.

The concept is illustrated in the 3x3 BIFODEL-based transmit example shown in Figure 6.1 (the receive mode can be implemented in a similar manner). For simplicity, we will use K_x and K_y delay lines rather than $K_x - 1$ and $K_y - 1$ required by an actual system. In a 2-D PAA the direction of the beam in the transmit (or receive) mode can be uniquely described by the two angular components: one along x (i. e., θ_x) and one along y (i. e., θ_y). The beam can be steered to the desired direction if independent control exists along x and y. Control along θ_x (H-control) is established using K_x different BIFODELs (3 for the 3x3 example of Figure 6.1). These BIFODELs are different because they address different elements along x, each of which requires its own delay range. All these

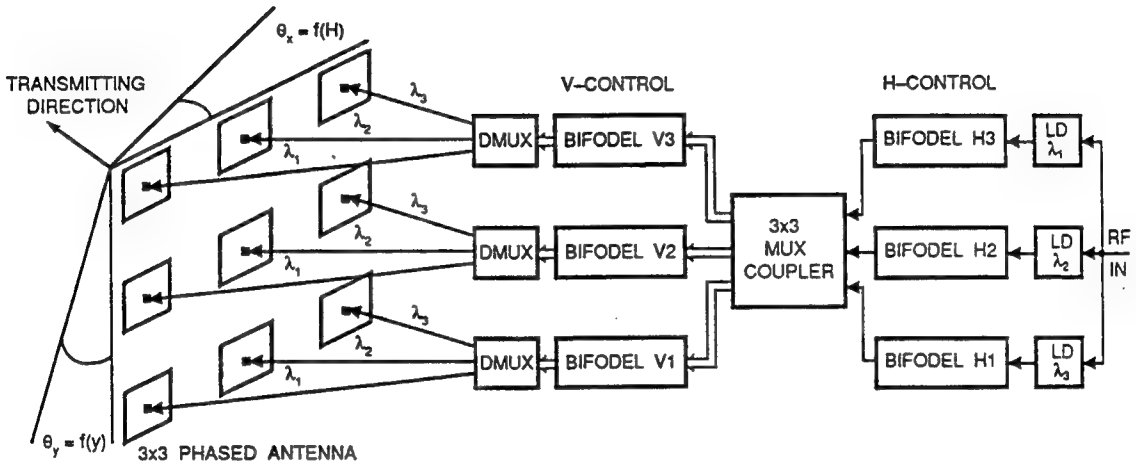

Figure 6.1 — Schematic of a BIFODEL-based delay-and element-compressive FO TTD architecture for a transmitting 2-D PAAs using optical WDM.

BIFODELs have the same number of segments, $N_x = \log_2 R_x$, which is determined by the angular resolution along x. The RF signal to be transmitted drives K_x LDs at wavelengths λ_i, i = 1, 2, . . . , K_x (λ_1, λ_2, λ_3 for the example of Figure 6.1). Next, a MUX is used to combine the outputs of the H-control BIFODELs. The output from the MUX drives a K_y channel optical divider the outputs of which drive the K_y V-control BIFODELs. (In Figure 6.1, the MUX and 1:K_y division operations are accomplished by the block entitled "3x3 MUX COUPLER"). Note that each of the V-control BIFODELs is different because it addresses different elements along y, each of which requires its own delay range. All V-control BIFODELs have the same number of segments, $N_y = \log_2 R_y$, which depends on the desired angular resolution along y. Unlike the 1-D PAA case, N_x and N_y may be different if so desired. The last step involves the separation of the K_x different wavelengths at the output of each V-control BIFODEL via a 1:K_x DMUX.

Since we have a total of K_y DMUXs each of which has K_x outputs, we have the necessary K_y x K_x different optical signals for driving the K_x x K_y PAA elements. Each optical signal has a unique delay T_{ij}, where the subscripts i and j depend on the location of the H- and V- control BIFODEL respectively, and they correspond to the desired θ_x and θ_y angles. Different programs are used for the H- and V-control BIFODELs in order to independently control the θ_x and θ_y angles. However, as in the case of the 1-D WDM TTD concept, the 2-D system can also operate over symmetric scan angles via time-biasing, with the understanding that the time-bias now extends to two dimensions.

The 2-D WDM TTD system has the advantage (similar to the 1-D WDM TTD system) of very low BIFODEL complexity C_{2CDL} given by:

$$C_{2CDL} = K_x + K_y - 2. \qquad (6.1)$$

Equation 6.1 should be compared with the delay line complexity, C_{2NDL}, required by the delay-compressive 2-D architecture which is equal to $(K_x - 1) \times (K_y - 1)$. The savings are similar to those described in the previous section.

It is of interest to note that the 2-D WDM TTD system allows the formation of multiple beams at different frequencies steered in different directions. Multiple simultaneous beams at different directions require the simultaneous use of different delay combinations, which is obviously not possible with BIFODELs that employ 2-state switches. The straightforward solution is to double the hardware for two beams or quadruple it for four beams. However, less hardware is required if we partition the 2-D PAA. Figure 6.2 shows an example of a 16x16 element partitioned array for generating 4 independent beams in both frequency and direction. The idea is to use the same number of H-control BIFODELs (i. e., 16 for our scenario) and double the number of the V-control BIFODELs every time we need to double the number of independent beams. For the four beam example, we use four sets of four H-control BIFODELs (for a H-control total of 16) in conjunction with four sets of sixteen V-control BIFODELs (for a V-control total of 64). In this case, the array is divided into four 4 x 16 fully independent sections. Using this technique, we find that the BIFODEL complexity, C_m, is given by:

$$C_m = (K_x - 1) + m\,(K_y - 1), \qquad (6.2)$$

where m is the number of independent beams. Equation 6.2 shows that the beam complexity factor, m, multiplies only $K_y - 1$ and not $K_x + K_y - 2$ which would be the case for the straightforward implementation. For example, a 256 element antenna would require a total of 75 delay lines for 4 independent beams.

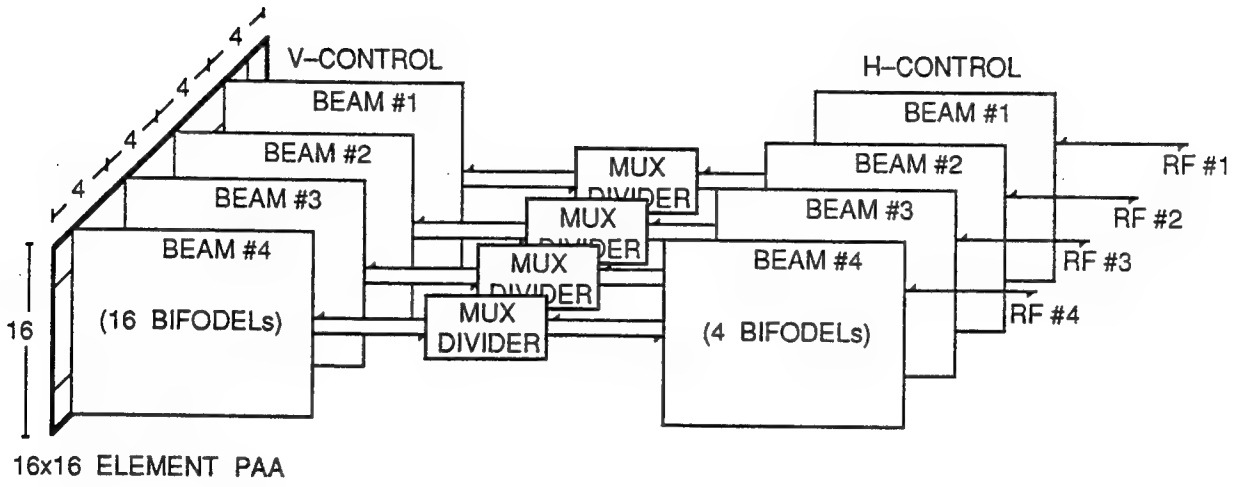

Figure 6.2 — Partitioning technique for a 2-D phased array antenna with independent multi-beam formation.

7. HYBRID ELECTRONIC-FIBEROPTIC WDM TTD ARCHITECTURES

The all-optical architectures we described in the previous sections are well suited for various PAA applications for both 1-D and 2-D antenna geometries. However, they can be optimized considerably depending on the actual PAA application. Since we are interested mainly in PAA surveillance scenarios (which typically reside in the L and/or S frequency bands) we consider 2 such scenarios: (1) 10.6 m long L-band (f = 1.4 GHz) 1-D PAA with K = 100 elements, and (2) 12.7 m long S-band (f = 3.0 GHz) 1-D PAA with K = 256 elements. Assuming that the PAAs are partitioned with $N = E = \sqrt{K}$ we find that the maximum RS delays occur for element #10 and #16, respectively, for the two different scenarios. For a maximum scan angle of ±45° in conjunction with a 6-bit BIFODEL, one can easily show that the delays for each of the BIFODEL bits are:

Example #1: 73, 147, 293, 586, 1173, and 2346 ps.

Example #2: 57, 114, 228, 456, 912, and 1824 ps.

For both the L- and S-band PAA examples, the RS delays are small enough to be well within the transmission capabilities of microstrips (or striplines) without serious differential attenuation and/or delay (or phase) dispersion effects as a function of frequency. For example, using ARLON Isoclad-917 31-mil board with a dielectric constant $\varepsilon = 2.17$, delay lines with over 2 ns delay can be fabricated which have a differential attenuation of ~ 0.7 dB and ±2 ps delay dispersion over the 0.5 - 4 GHz band. Furthermore, one can use simple coaxial ultra-low loss cable (e. g., GORE 0.12") for ~ 3 ns delay lines with better than 0.5 dB differential attenuation and ±1 ps dispersion over the 0.5 - 4 GHz band. In addition, low-cost ($2-$20) 1x2 GaAs FET switches are available that operate well over the S-band with very low insertion loss (< 0.5 dB) and a

response which is flat (to better than ±0.05 dB) over the 0.5 - 3.5 GHz band. From these data, we conclude that for many typical L- and S- band PAA applications, the reference BIFODELs can be implemented using all-electronic techniques, i. e., electronic binary delay lines (DiBi) are possible. We emphasize that this is not necessarily the case for all PAA scenarios because, for large PAAs at higher frequencies (e.g., X-band), the board and/or cable attenuation and/or dispersion is unacceptable.

Figure 7.1 shows a block diagram of a 6-bit DiBi architecture which uses two back-to-back 1x2 switches to implement a 2x2 switch. We emphasize that the actual delay per segment is a "relative" rather than an "absolute" delay, i. e., it is the difference between the two switched paths that gives the desired delay. This allows great flexibility in setting and tuning the actual delays as we will see in more detail later. Furthermore, the DiBi is fully reversible, i. e., the signal can propagate from either end. This is very important in that it allows the same DiBi to be used for both the transmit and receive PAA mode. The advantages of DiBis over BIFODELs for implementing the RS portion of the system include: (1) much lower cost (~ 2 orders of magnitude less per delay line, the main difference being the switch cost), (2) the potential for certain PAA scenarios to implement the RS delays in IC form using GaAs MMIC and/or wafer-scale integration techniques (indeed a 5-bit 2 - 20 GHz GaAs IC DiBi has been demonstrated[27-28] with a total delay of 317 ps), and (3) much smaller size - DiBis are inherently 2-D devices whereas fiberoptic BIFODELs are 3-D devices (for example, the IC DiBi of Ref. 28 has dimensions 2.7x3.4 mm^2).

Use of DiBis for the RS delays and BIFODELs for the bias delays results in a hybrid WDM TTD architecture, an example of which is shown in Figure 7.2 for the case of a 16 element transmitting 1-D PAA. Such a hybrid architecture has significant advantages over an all-optical approach: (1) it uses fiber optics only where standard low-cost microwave electronic techniques cannot perform, and (2) it preserves the unique features of optics: (a) WDM for implementing the

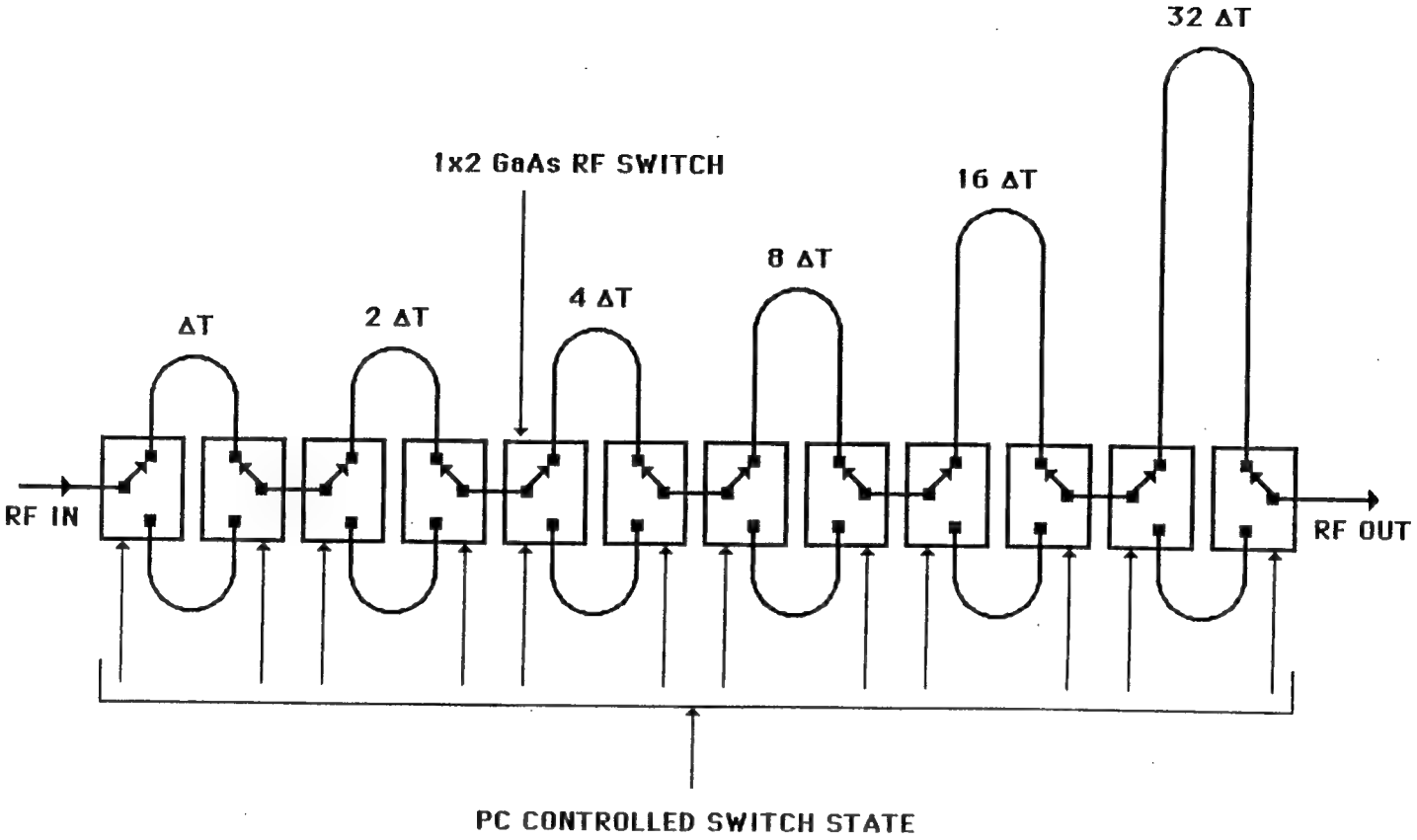

Figure 7.1 — Block diagram of a 6-bit electronic binary delay line (DiBi)

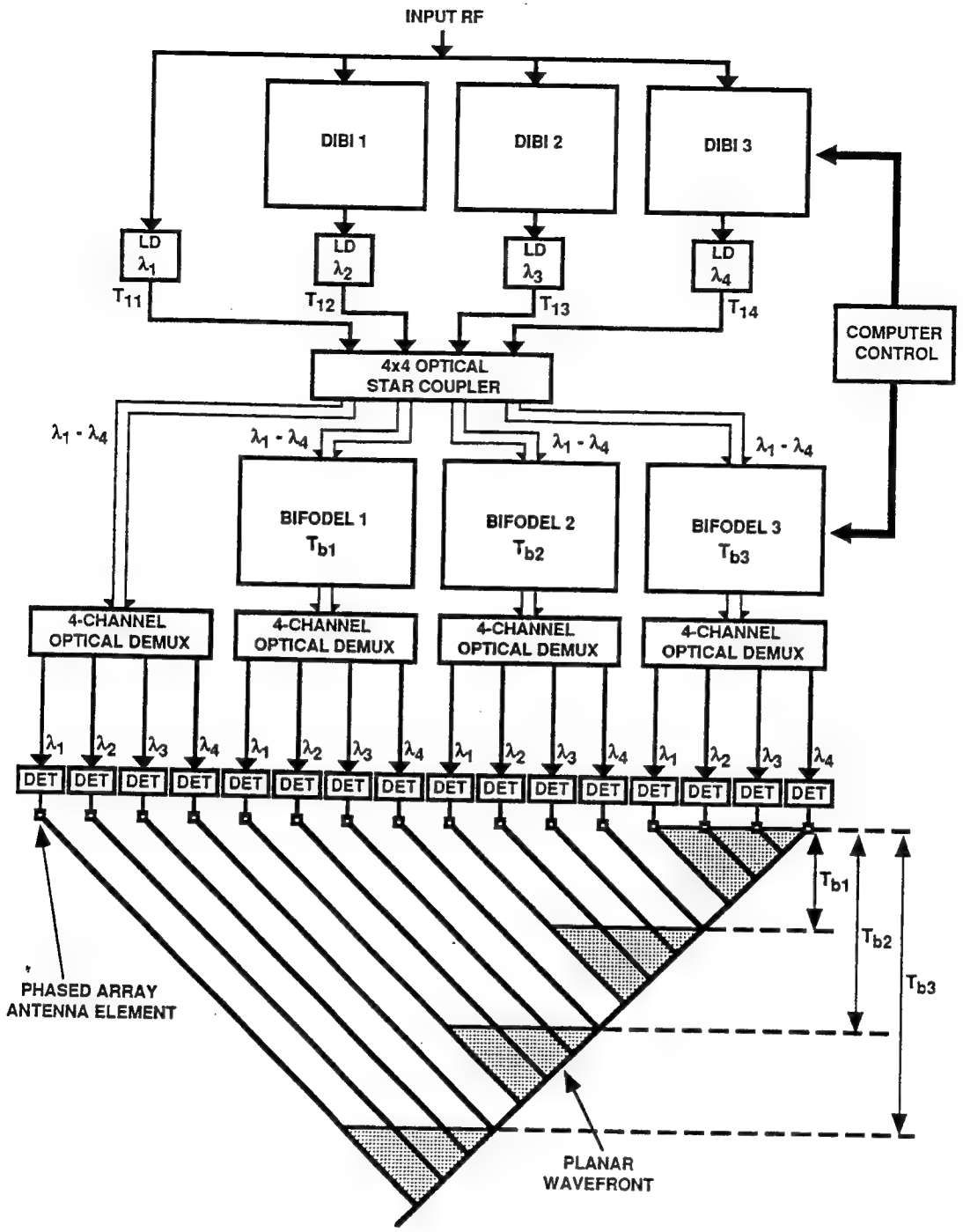

Figure 7.2 — Block diagram of a 16-element 1-D hybrid WDM TTD architecture.

hardware compression architecture, and (b) use of optical fiber for implementing long delays. However, we point out that it is not necessary to implement all the bits of the RS delay lines in the electronic domain; we can implement as many bits as possible in the electronic domain and then revert to fiberoptic delays prior to WDM. This allows the hybrid scheme to be used for very large PAAs for which the sole use of DiBis in the RS level may not be possible. Finally, we note that since both the DiBis and BIFODELs are reversible, the hybrid architecture is also reversible.

The hybrid WDM TTD concept can also be applied to 2-D PAA. In this case the H-control BIFODELs will be substituted by low-cost DiBis. Each DiBi will be followed by a laser diode of the appropriate wavelength, which will be followed by the MUX coupler, the V-control BIFODELs, etc. We emphasize that the DiBis must be used along the smallest antenna dimension, which in most cases is dedicated to elevation.

8. DIMENSIONALITY LIMITS OF THE WDM TTD ARCHITECTURES

In general, the limits in the dimensionality (i.e., maximum number of channels) of the WDM TTD architectures are set by the Rx system. Recall that for the Rx system, PAA elements of similar location within different sets must have the same wavelength so that they can all be compensated simultaneously by the same RS delay line. Since the output of the delay line leads to a single detector, care must be taken so that small differences among the "similar" wavelengths do not result in in-band beat notes, produced by the mixing of the various wavelengths, at the square-law detector. Given that frequency locking of the various wavelengths to within a few Hz is virtually impossible, we must make sure that any beat notes fall well outside the RF band of the system. One can show[29] that for the simple case of 2 unmodulated LDs at optical frequencies f_{o1} and f_{o2}, the beat power spectral density $S_b(f)$ is given by:

$$S_b(f) = 0.25\, E^2_{o1}\, E^2_{o2}\, [d(f + f_{o1} - f_{o2}) + d(f - f_{o1} + f_{o2})], \qquad (8.1)$$

where E_{o1} and E_{o2} are the amplitudes of the two LD optical fields. The term of interest is the first term within the bracket of Equation 8.1 and corresponds to the difference beat note between f_{o1} and f_{o2}. Thus, we conclude that the separation between "similar" wavelength LDs must be at least equal to the RF BW of the PAA system, otherwise the beat notes will fall within the band. In practice, the separation must be kept even wider (e. g., 2x - 3x that of the RF BW) in order to avoid beat note movement within the band because of temperature changes, LD aging, etc.

To help understand the above issues, let us calculate the separation requirements for the example of 4x4 Rx system. For this case, we can use 16 LDs over the 1270 - 1340 nm band with maximum LD-to-LD separation $\Delta\lambda = 4.66$ nm, which corresponds to a difference beat note spacing of 864 GHz and obviously does not present any real problem. The results of this type of analysis for other PAA systems are shown in Table 8.1.

TABLE 8.1 - Laser diode wavelength separation and beat frequencies for various PAAs.

PAA Elements	LDs Required	LD separation (nm)	Beat Frequency (GHz)
16 (4x4)	16	4.66	864
64 (8x8)	64	1.11	206
256 (16x16)	256	0.27	51
1024 (32x32)	1024	0.07	13

From Table 8.1 we see that for systems up to 8x8 elements, the beat notes represent no problem even if the full 2-18 GHz RF band is to be implemented

with the same WDM TTD network. For higher order systems, there is a constraint in the overall usable RF BW of the TTD network. For example, for the 32x32 case and assuming a separation of 3xBW, the resulting RF BW is no more than 4.3 GHz. In addition, as the wavelength separation of LDs is reduced, the full spectral width of the LDs at power levels much lower than -3 dB (e. g., -40 dB optical) becomes important because any given LD power at this level beats with that of the neighboring LD (at a similar low power level) and the difference will appear within the RF BW. However, these spurious signals will be at much lower power levels compared with the level of the signal of interest, e. g., -40 dB optical sidebands produce noise beats at a level of -80 dB in the RF domain, a level which is acceptably low for many PAA applications. At the -40 dB level, the full spectral width of currently available DFB LDs is less than 0.5 nm so that systems up to 12x12 are easily accommodated; however, higher order systems with high dynamic range requirements, become more difficult to implement even if the LD separation requirement can be satisfied. Note however, that if necessary, the 1500 nm band can also be employed in order to increase the overall system dimensionality.

9. DEVELOPMENT OF A 16-ELEMENT Tx HYBRID WDM TTD SYSTEM

In the first phase of the program we developed a 16-element Tx hybrid WDM TTD system with the following specifications: BW covering the 0.7 to 1.4 GHz band, scan angle ±45° with delay resolution of 6 bits or angular resolution of 1.31° (calculated by dividing the maximum delay that corresponds to 45° by 2^5-1 and then finding the angle that corresponds to the resulting minimum delay, i.e., $\sin^{-1}[(\sin 45°)/(2^5-1)]=1.31°$), reconfiguration time of the order of ms, rms phase error of < 5°over the full band, and element-to-element amplitude uniformity of better than ±0.75 dB.

In the following sections we describe step-by-step the overall system design, the design and development of the DiBis, the design and development of

the FO links, the design and development of the BIFODELs, and the integration of the full hybrid WDM TTD system.

9.1 Delay Calculation

Linear PAAs operating over a wide band have a typical element spacing of $\lambda_{min}/2$, where λ_{min} is the wavelength corresponding to the highest frequency. Thus, a 16- element linear PAA operating over the 0.7 - 1.4 GHz band has an element spacing of 10.707 cm and a total length of 1.606 m. The maximum delay required to steer the antenna over an angle θ is given by

$$T_{kmax} = k \lambda_{min} \sin \theta / 2 c, \qquad (9.1)$$

where k = 0, 1, 2, . . . , K - 1 is the element number. We define a negative (positive) scan angle when the antenna looks to the left (right) of the boresight. For our present scenario (where K = 16 and $\theta = \pm 45°$), the maximum delays required for the angle +45° with respect to elements k = 0, 1, 2, . . . ,14, 15 are 0, 252.37 ps, 504.73 ps, . . . , 3533.13 ps, 3785.50 ps, respectively, whereas for the angle -45° the delays are 0, -252.37 ps, -504.73 ps, . . . , -3533.13 ps, and -3785.50 ps. To implement the negative delays (and still cover a symmetric ±45° scan angle) we "time-bias" the antenna as described in Section 2. This can be accomplished by inserting a linearly-varying but fixed time-bias into the various elements. Thus, for elements k = 0, 1, . . . , 14, 15 the fixed delays are 3785.50 ps, 3533.13, ps, . . . , 252.37 ps, and 0 ps, respectively.

We can now calculate the actual delays for the various bits of the RS DiBis and the bias BIFODELs. Since we have a total of 6 bits (or 64 combinations including 0) per delay line, we can cover the ±45° scan angle with a resolution of 1.31°. Thus, we assign the first 31 positions (numbered 0 - 30 in decimal notation or 000000 - 011110 in binary notation) to cover the -45° to -1.31° angles, position number 31 (011111) to steer at 0.0°, and positions 32 - 62 (100000 - 111110) to

steer over the +1.31° to +45° range. (Note that although position number 63 (111111) corresponds to an angle of +46.31° the antenna can still respond).

To calculate the RS DiBi delays (notation T^r_{ji} where r denotes RS, j is the DiBi number and i is the DiBi segment), we use the above information and the fact that the delays of the first 4 PAA elements (0 - 3) determine the delays of the RS DiBis. For $\theta = 45°$, the maximum delays for elements 0, 1, 2, and 3 are 0.0 ps, 252.37 ps, 504.73 ps, and 757.1 ps, respectively. Thus, the smallest non-zero delay segment is equal to the maximum delay required divided by the number of switch positions (for our case 31) available to cover the positive scan angle. The delays of the remaining segments can then be calculated from

$$T^r_{ji} = 2^{i-1} T^r_{j1}, \qquad (j = 1, 2, \ldots, N - 1, \text{ and } i = 2, 3, \ldots, R), \tag{9.2}$$

where T^r_{j1} is given by:

$$T^r_{j1} = T_{jmax}/(2^{R-1} - 1), \qquad (j = k = 1, 2, \ldots, N - 1), \tag{9.3}$$

and R is the antenna resolution in bits that corresponds to the full scan angle. The delays of the three bias BIFODELs (notation T^b_{ji}) are now easily calculated by noticing that the delays of the 1st bias BIFODEL are equal to the delays of the 5th element (i. e., k = 4), those of the 2nd are equal to the delays of the 9th element (i. e., k = 8), and those of the 3rd are equal to the delays of the 13th element (i. e., k = 12). This is valid provided $\sqrt{K} = E = N$. The bias delays are given by

$$T^b_{ji} = 2^{i-1} T^b_{j1}, \qquad (j = 1, 2, \ldots, E - 1, \text{ and } i = 2, 3, \ldots, R), \tag{9.4}$$

where T^b_{j1} is given by

$$T^{b}_{j1} = T_{kmax}/(2^{R-1} - 1), \qquad (j = 1, 2, \ldots, E - 1 \text{ and } k = E\,j). \qquad (9.5)$$

Using Equations 9.1-9.5 we can now calculate the delays for the various segments of the RS and bias delay lines. The results are shown in Table 9.1.

TABLE 9.1 - Segment delays (in ps) for the RS and bias BIFODELs.

Segment	T^{r}_{1i}	T^{r}_{2i}	T^{r}_{3i}	T^{b}_{1i}	T^{b}_{2i}	T^{b}_{3i}
1	8.15	16.29	24.44	32.59	65.17	97.76
2	16.29	32.59	48.88	65.17	130.34	195.51
3	32.59	65.17	97.76	130.34	260.68	391.03
4	65.17	130.34	195.51	260.68	521.37	782.05
5	130.34	260.68	391.03	521.37	1042.74	1564.11
6	260.68	521.37	782.05	1042.74	2085.48	3128.21

Finally, since we are dealing with a system which must provide high-accuracy non-dispersive delays, we must examine the role of fiber dispersion in producing differential delays. This is because the inputs to the bias BIFODELs consist of all the different wavelengths, and the fiber itself introduces small but nevertheless differential delays for the various wavelengths. State-of-the-art single mode fibers operating over the 1270-1340 nm band exhibit typical dispersion in the range 4 - 6 ps/nm.km. Using an average figure of 5 ps/nm.km for a 70 nm band, we find that the worst-case dispersion is ~0.35 ps/m. For the prototype we are developing, the total length of the longest bias BIFODEL is ~1.2 m (i. e., ~ 6 ns) for which the worst case dispersion is about 0.4 ps, and is negligibly small. If we perform the same calculations for the two examples of Section 7, we find that the worst-case dispersion-induced differential delays are: (1) for the L-band PAA: ±1.61 ps (the longest BIFODEL length is 9.2 m), and (2) for the S-band PAA: ±2.01 ps (the longest BIFODEL length is 11.5 m). Once

again we find that these differential delays are very small and have no significant effect on the PAA performance.

9.2 Digital Binary Delay (DiBi) Line Development

In designing the DiBi, much attention must be paid to the transmission line (microstrip in our case) material. Ideally the microstrip must have the following characteristics: (1) low differential attenuation over the band of interest so that the overall passband is as flat as possible (this is very important for broadband TTD because otherwise the precise element-to-element matching is extremely difficult), (2) low dielectric constant ε_r so that the delay accuracy is as high as possible, and (3) low phase dispersion as a function of length and frequency. Requirement 2 is dictated by the fact that the speed of propagation (Up) in the microstrip material is given by:

$$U_p = c / \sqrt{\varepsilon_{ef}}, \tag{9.6}$$

where ε_{ef} is the effective dielectric constant given by

$$\varepsilon_{ef} = 0.5 (\varepsilon_r + 1) + 0.5 (\varepsilon_r - 1) [1 + 12 h / W]^{-0.5}, \tag{9.7}$$

where h is the thickness of the dielectric surface, W is the width of the microstrip, and where $W/h \geq 1$. Thus, it is obvious that the "faster" the material, the longer the distance per unit of time, and thus the better the accuracy in determining the exact length of the segments. Requirement 3 simply expresses the need for the TTD to be independent of frequency. Note that at low frequencies (i. e., a few GHz) the effective dielectric constant is for all practical purposes independent of frequency. However, as the frequency increases both ε_{ef} as well as the characteristic impedance (Z_0) of the microstrip line begins to change (due to the propagation of hybrid modes) making the transmission line

dispersive[30]. The frequency dependence of ε_{ef} describes the influence of dispersion on the phase velocity, whereas the frequency dependence of the effective width describes the influence of the dispersion on Z_0. Note that frequency dispersion can be a serious factor limiting the extension of the hybrid system to frequency bands significantly higher than S. Fortunately, for frequencies in the L- and S-bands and with good board fabrication, the changes in ε_{ef} and Z_0 with frequency are very small. The frequency below which dispersion effects may be neglected is given by the relation

$$f_0\,(\text{GHz}) = 0.3\,\sqrt{[Z_0 \,/\, \{h\sqrt{(\varepsilon_r - 1)}\}]}, \qquad (9.8)$$

where h is given in cm.

With the above in mind, we have acquired and tested various board materials in order to identify the material that best satisfies the above requirements. For all acquired board materials, we designed (using CAD software) and fabricated various delay segments which we then evaluated on a network analyzer. Our search showed that the ARLON Isoclad-917 board provides excellent results, and for $Z_0 = 50\ \Omega$, the attenuation is less than 0.5 dB for a 1.2 ns delay, and the worst case peak-to-peak delay dispersion is less than ±3 ps.

The next step is to identify a suitable, low cost switch which will allow us to implement a miniaturized, low cost DiBi. The switch requirements are: (1) flat frequency response over the desired band, (2) low insertion loss, (3) low crosstalk, and (4) low phase dispersion. Once again we have performed a market search which identified several low-cost ($25 - $40) 1x2 FET switches that satisfied our requirements. Typical data obtained are: (1) ±0.5 dB frequency response from DC - 3 GHz with low ripple (< 0.05 dB), (2) isolation of better than 40 dB over the 0.7 - 1.4 GHz band (in practice, this translates to better than 80 dB because we use two 1x2 switches per segment), (3) insertion loss of < 0.5 dB per

1x2 switch (or < 1 dB per 2x2 switch), (4) 1 dB compression point of +23 to +30 dBm, (5) peak-to-peak phase dispersion of ±1° over the 0.7 - 1.4 GHz band, (6) reconfiguration speed of < 6 ns, and (7) typical dimensions of 5x5x1 mm^3. Once the board and switches were identified, we proceeded with the development of the DiBis, which were fabricated in house, using well established microwave and electronic fabrication techniques. The resulting DiBis (Figure 9.1) are of low cost (< $250 for a 6-bit DiBi), and bidirectional. A total of 4 DiBis were fabricated. Three DiBis were used to produce the delays for RS elements 2, 3, and 4. The 4th DiBi contains a "zero-delay" path board for the first PAA element. This DiBi is permanently programmed for zero delay (i. e., with a switch setting of 000000). We use this approach in order to match as much as possible the amplitude and delay dispersion responses with those of the other three DiBis. The integrated DiBi system has been tested and evaluated extensively.

Figure 9.2 shows the amplitude responses (for the 000000, 010101, 101010, and 111111 paths) of the largest DiBi over the 0.7 - 1.4 GHz band, and shows that the 0.5 dB BW for each response is 700 MHz. The four responses match each other to about ±0.25 dB peak-to-peak and better than 0.1 dB rms. Similar matched response is obtained for the paths of the other DiBis and from DiBi to DiBi. These DiBis are high speed delay lines, and their program can be changed every 15 ns. The DiBis are housed in aluminum enclosures of dimensions 4.5x4.75x0.75 in^3 and fitted with a 25-pin connector for the computer and power feeds.

The DiBi phase deviation from linearity has been measured for each bit of each DiBi. Figure 9.3 shows the phase deviation for the largest delay segment (bit # 6) of the largest DiBi (#3). It can be seen that a peak-to-peak deviation of under 2° has been achieved. For smaller delay segments, the phase error was typically <0.3° over the full band. These are excellent results and show the capabilities of low cost all-electronic delay lines implemented with COTS components.

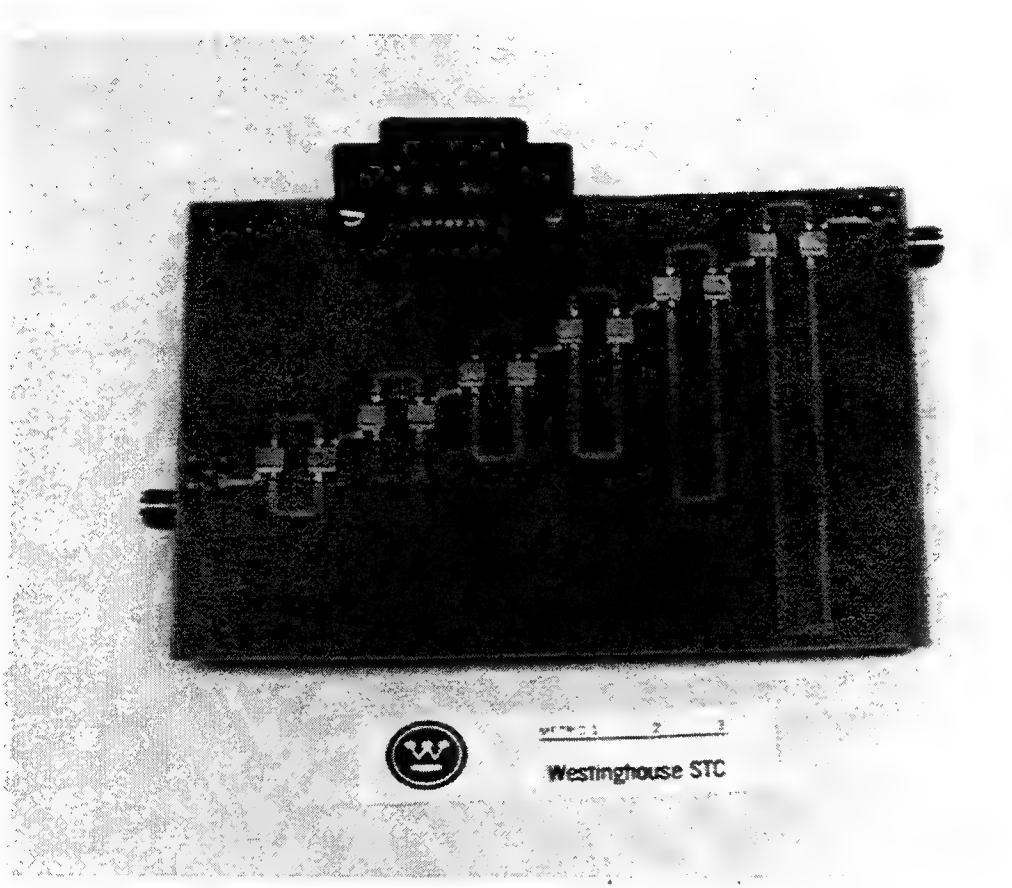

Figure 9.1 — Photograph of the largest prototype 6-bit DiBi.

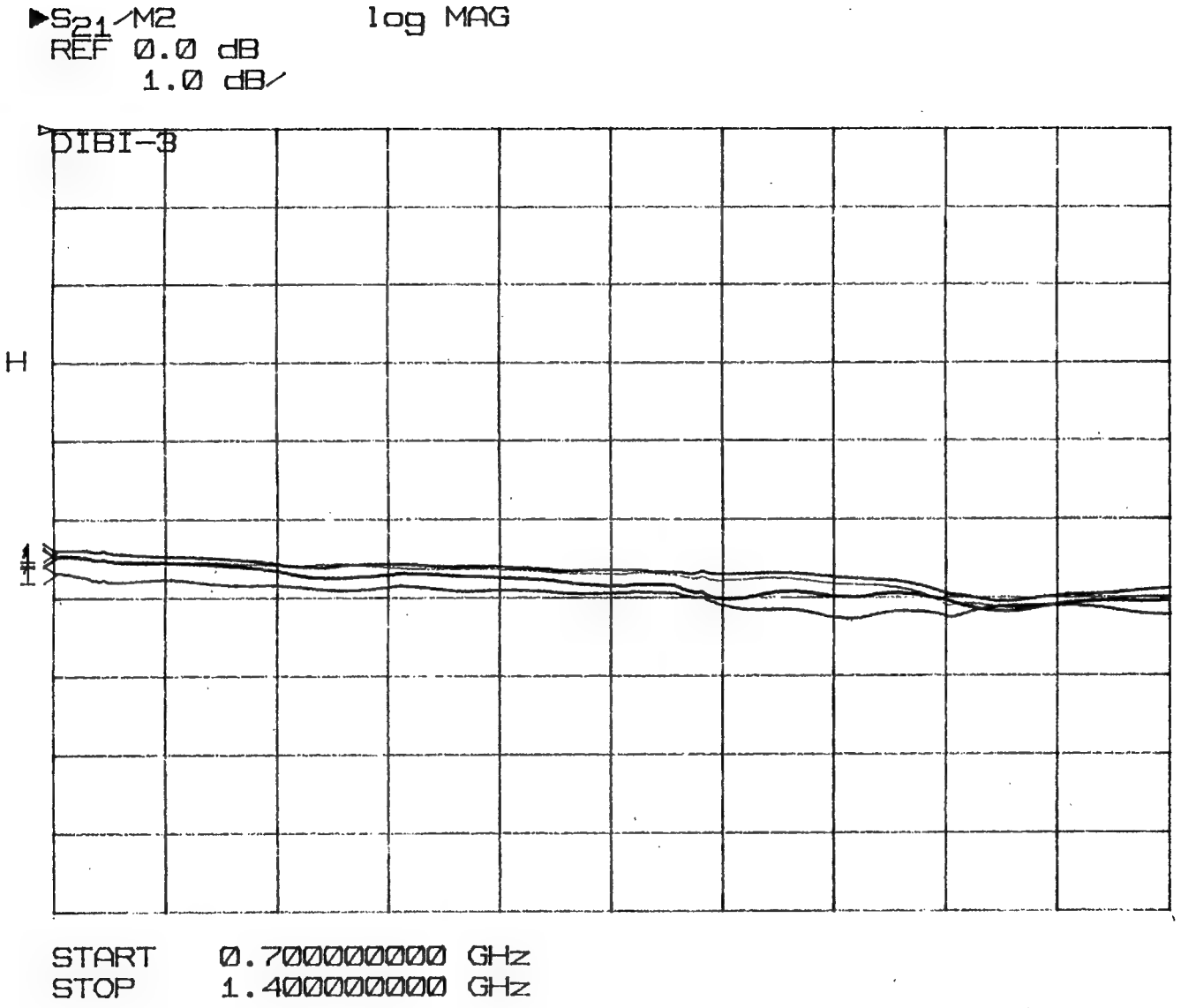

Figure 9.2 — Frequency response of the largest DiBi for the 000000, 010101, 101010, and 111111 delay paths.

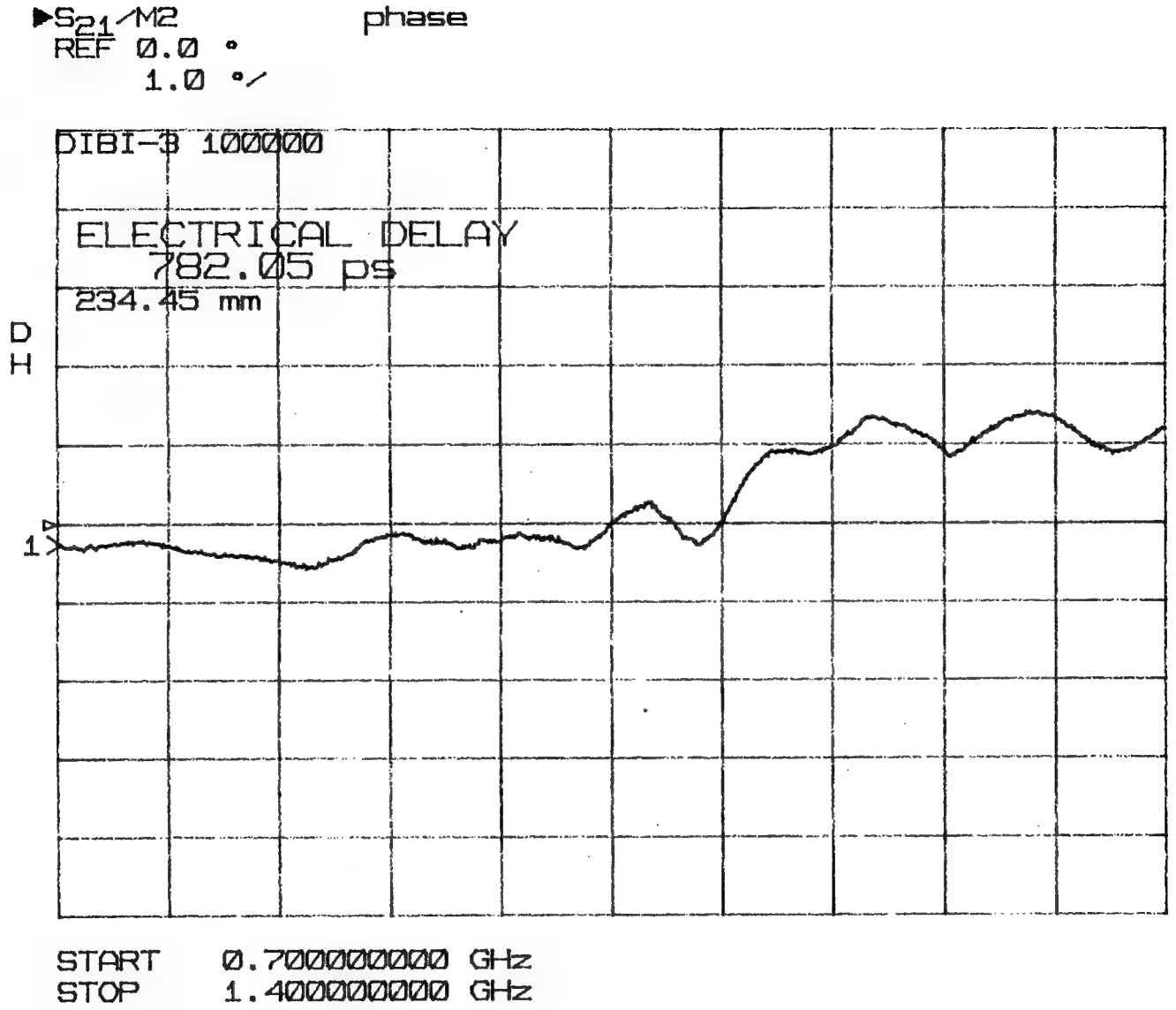

Figure 9.3 — Phase response of the largest delay segment of the largest DiBi (#3) over the 0.7-1.4 GHz band. (A peak-to-peak deviation of <2° is achieved.)

The DiBi delays have been measured for all 6 bit combinations and compared with the design data. Figure 9.4 shows the results for an input tone of 1 GHz as a function of the steering angle, with a resolution of 1.31°. It can be seen that there is excellent agreement between the design and measured data for all 3 DiBis. The difference between the design and measured data is plotted in greater detail in Figure 9.5 for all 3 DiBis. The worst case delay deviation from the design values is < ±4 ps peak-to-peak (or < ±2° of phase at 1400 MHz) and is sufficient for many high performance radar applications. We have measured the delay error for all DiBi bits, and have found that it is of uniform distribution with a zero mean and a standard deviation of 1.45 ps (or 0.72° at 1400 MHz). Furthermore, the delay error is independent of the delay range (Figure 9.5), a result of the in-house developed technique for delay measurement.

All DiBis have excellent SNR and spurious-free dynamic range (SFDR). Figure 9.6 shows a plot of the measured and calculated SNR and SFDR performance for the largest DiBi in the 111111 program mode; excellent agreement is found between the calculated and measured response. The SNR is well above 177 dB/Hz and the SFDR is about 135 dB-$Hz^{2/3}$. The insertion loss is -6 dB and the noise figure (NF) is 6 dB (this is due to the signal loss rather than noise introduction by the DiBi). Similar, path-independent performance is found for the other DiBis regardless of the direction of signal propagation. Measurement of the crosstalk between different delay paths is not a trivial task. Using a time-domain technique with a sensitivity of about -65 dB, the measured DiBi crosstalk is found to be less than the measurement limit. The theoretical crosstalk is estimated to be about -90 dB, and is due mostly to the switch crosstalk.

9.3 Binary Fiberoptic Delay Line (BIFODEL) Development

The BIFODEL design we adopted was Design-3 (see Figure 3.1) because it has the smallest possible stability loss figure and requires a low component

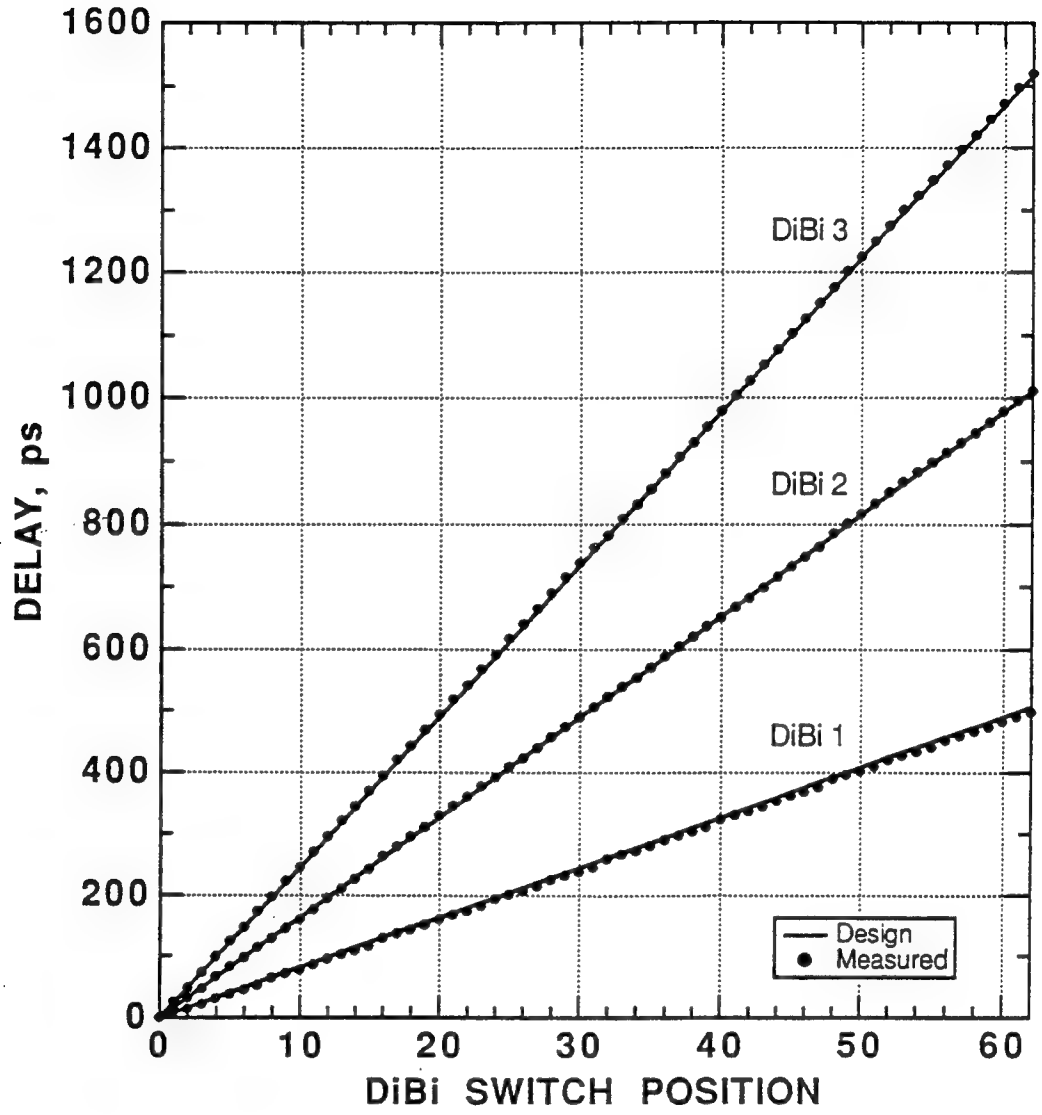

Figure 9.4 — Measured and calculated delays for the DiBis' as functions of the steering angle with 1.31° resolution.

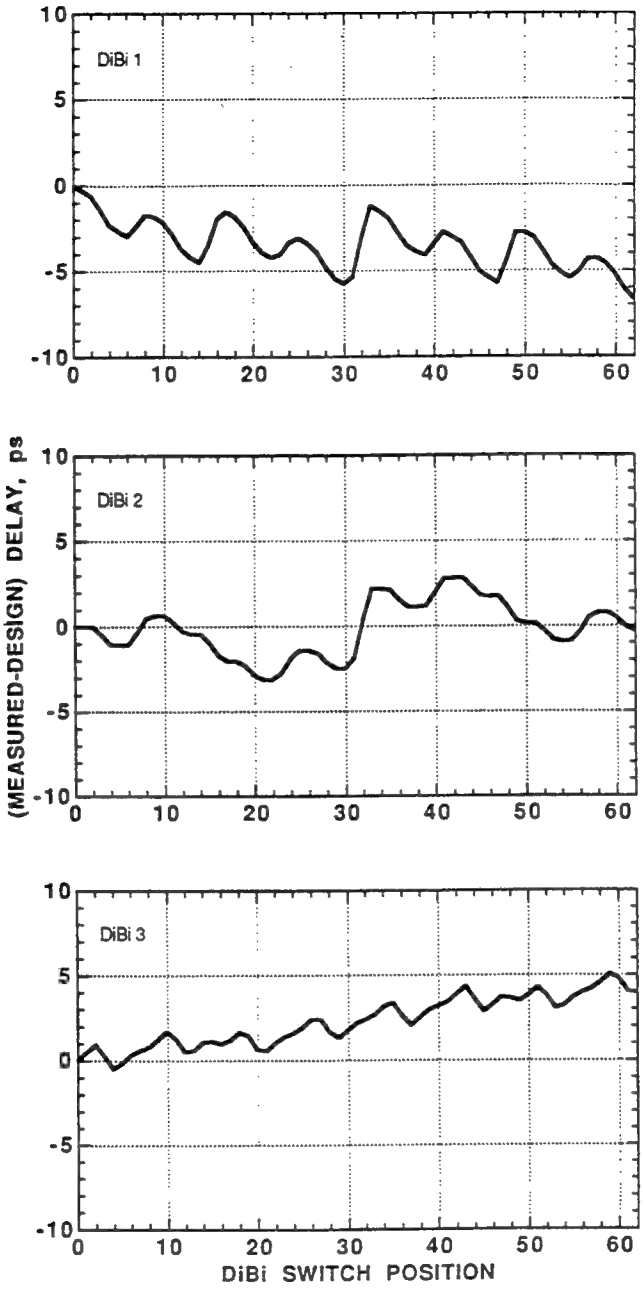

Figure 9.5 — Deviation of the measured DiBi delays from the design values as a function of the switch position.

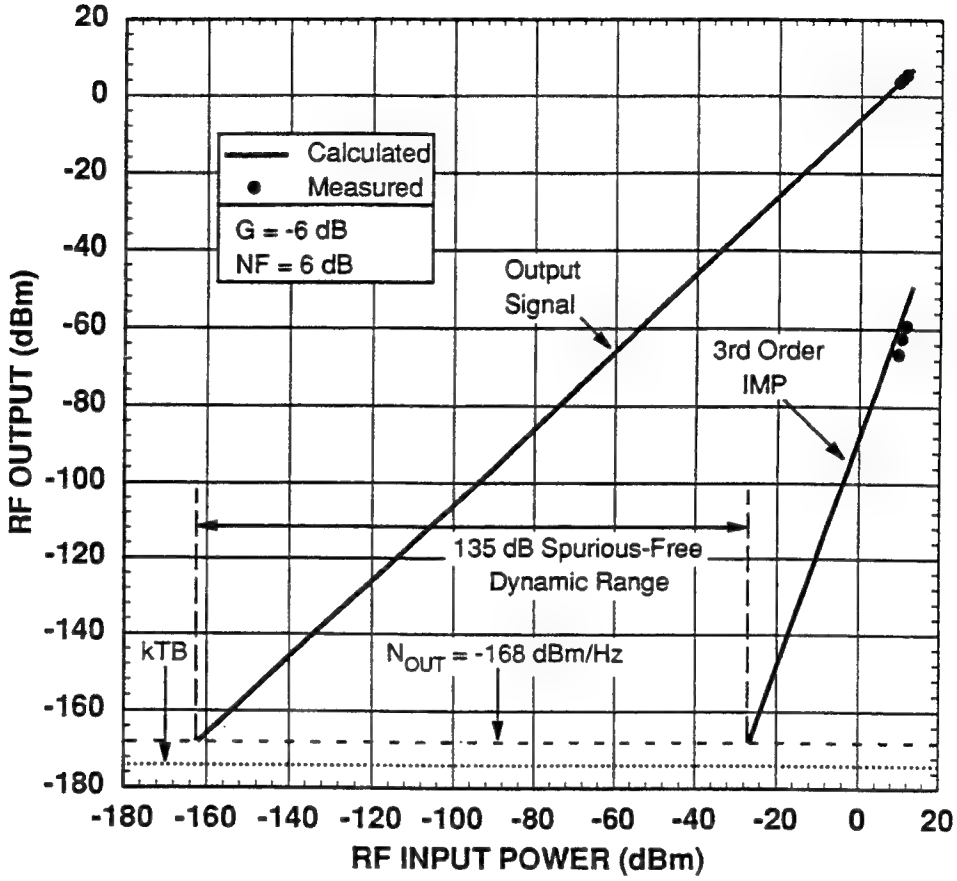

Figure 9.6 — Typical SNR and SFDR of the DiBi.

complexity: N - 1 (i. e., 5) 2x2 switches and two 1x2 switches, where N is the number of BIFODEL bits. There are several key specifications which the switches must satisfy that are determined mainly by system requirements and include: (1) 2x2 configuration, (2) low insertion loss (e. g., 1 dB or better), (3) > 50 dB optical crosstalk, (4) switching speed of 10s of μs or better (although several applications exist where ms response is acceptable), (5) small size and low power consumption, and (6) low cost. In addition, it is desirable to have switches with several parallel 2x2 configurations so that with one switch we can implement all the BIFODELs in parallel. Parallel switching is possible because, at any given time, the same binary program is needed for all BIFODELs (and DiBis). Several technologically different types of switch exist that could conceivably be used for the BIFODELs. In general, the performance of these switches varies significantly and most of them are not yet developed to the point that they can be used in current systems. For example, 2x2 ferroelectric liquid crystal switches (FLC) have been demonstrated with rise times of 150 μs (i. e., switching times of ~ 400 μs); however, their insertion loss is currently ~ 3 dB and their crosstalk about -27 dB. Furthermore, various types of 2x2 integrated optical switches are commercially available from several vendors with typical switching speeds of ~ 1 ns; however, their insertion loss is high, e.g., 3 - 6 dB (optical) and their crosstalk (-20 to -30 dB, optical) is unacceptable. For our prototype, we decided to use commercially available piezomechanical switches which have been optimized for BIFODEL use and which have the following performance characteristics: insertion loss of < 1 dB, optical crosstalk of < -60 dB, and optical rise time of < 1 ms. These switches were satisfactory for our purposes.

The switches we used were made by JDS FITEL over a period of 2 years. Initially, JDS implemented the switches using a moving prism, but such switches were not acceptable because of the differential delays involved between the "through" and "cross" states. This forced JDS to use a moving double-sided mirror approach, an operation that took about 2 years to complete. However, at

the end, these switches did not have the "differential delay" problem, and in general they had the following performance characteristics: insertion loss of < 1 dB (~ 0.7 dB average), optical crosstalk of < -65 dB (or -130 dB RF), and optical rise time of about 1 ms which allows switching speeds as low as 5-10 ms. For each switch we also performed two key tests:

Test-1: Drive the switch with a square wave (4.5-6 V) and reduce the pulsewidth to identify the highest possible speed. Repeat this for all I/O combinations.

Test-2: Perform a stress test: excite the switch with a 150 ms pulse train for about $4\text{-}5\text{x}10^5$ cycles and see if the performance has changed.

By using Test-1 we found that the best switches could operate at about 5 ms pulses (200 Hz) but we thought it was safer to use 10 ms square train to find whether there are non-uniformities including: "rabbit-ears", "up-down hills", "breathing", etc. Most switches were capable of working rather reliably to about 10 ms. The ones that we identified as "bad" we returned to JDS and "new" improved were send back to us. With Test-2 we identified switches that could not work for long periods. These were also returned to JDS. After about 2 years of switch iterative testing, we ended up with most switches working "well".

Having determined that the switches work well, we proceeded with the fabrication of BIFODELs. Initially we fabricated a BIFODEL where the switches were set vertically (Figure 9.7) but aftre some tests we found that the switches "preferred" to be horizontal. We then proceeded with the horizontal implementation (Figure 9.8, black trays). Each BIFODEL is packaged on a 10x14 in^2 plexiglass board which also houses the DEMUX and a 25-pin connector for the computer control and power feeds. The overall dimensions of the BIFODEL are determined by the number and dimensions of the switches, and by the minimum bend radius of the fiber pigtails necessary to avoid loss of light between switches. The fibers for the various delay segments are placed in

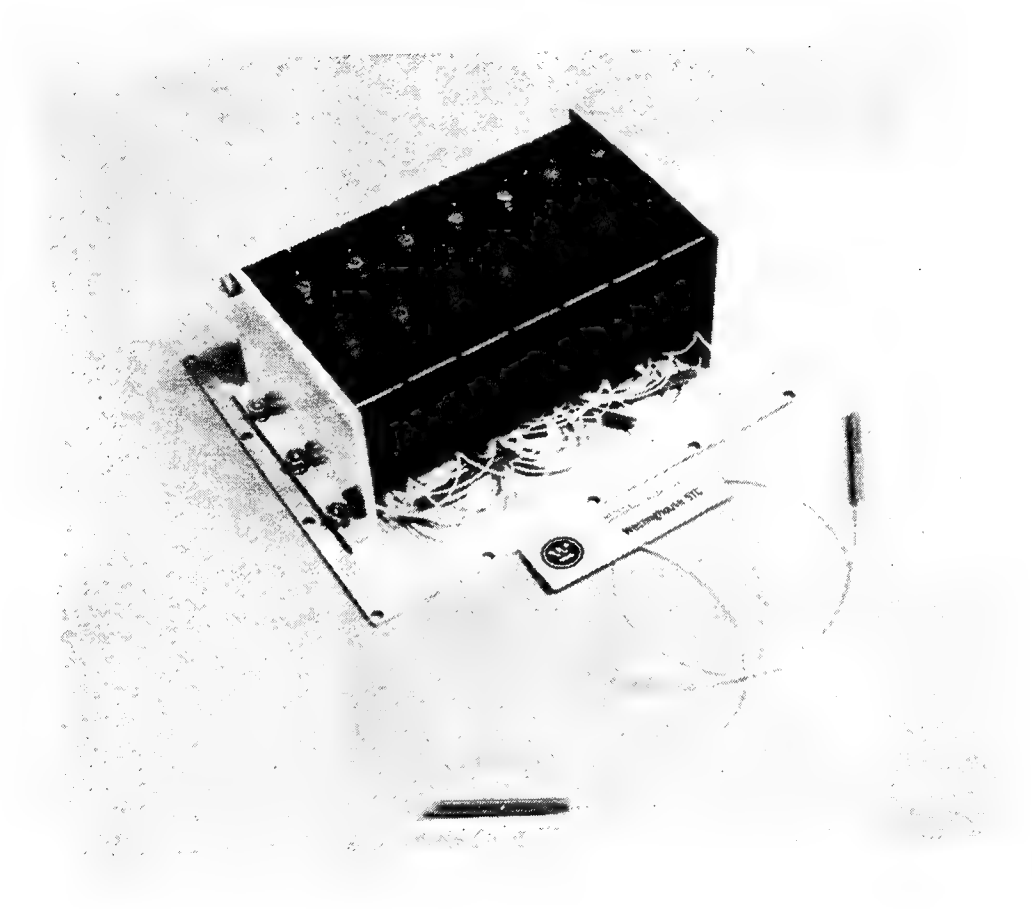

Figure 9.7 — Photograph of the early BIFODEL version employing vertically-oriented switches.

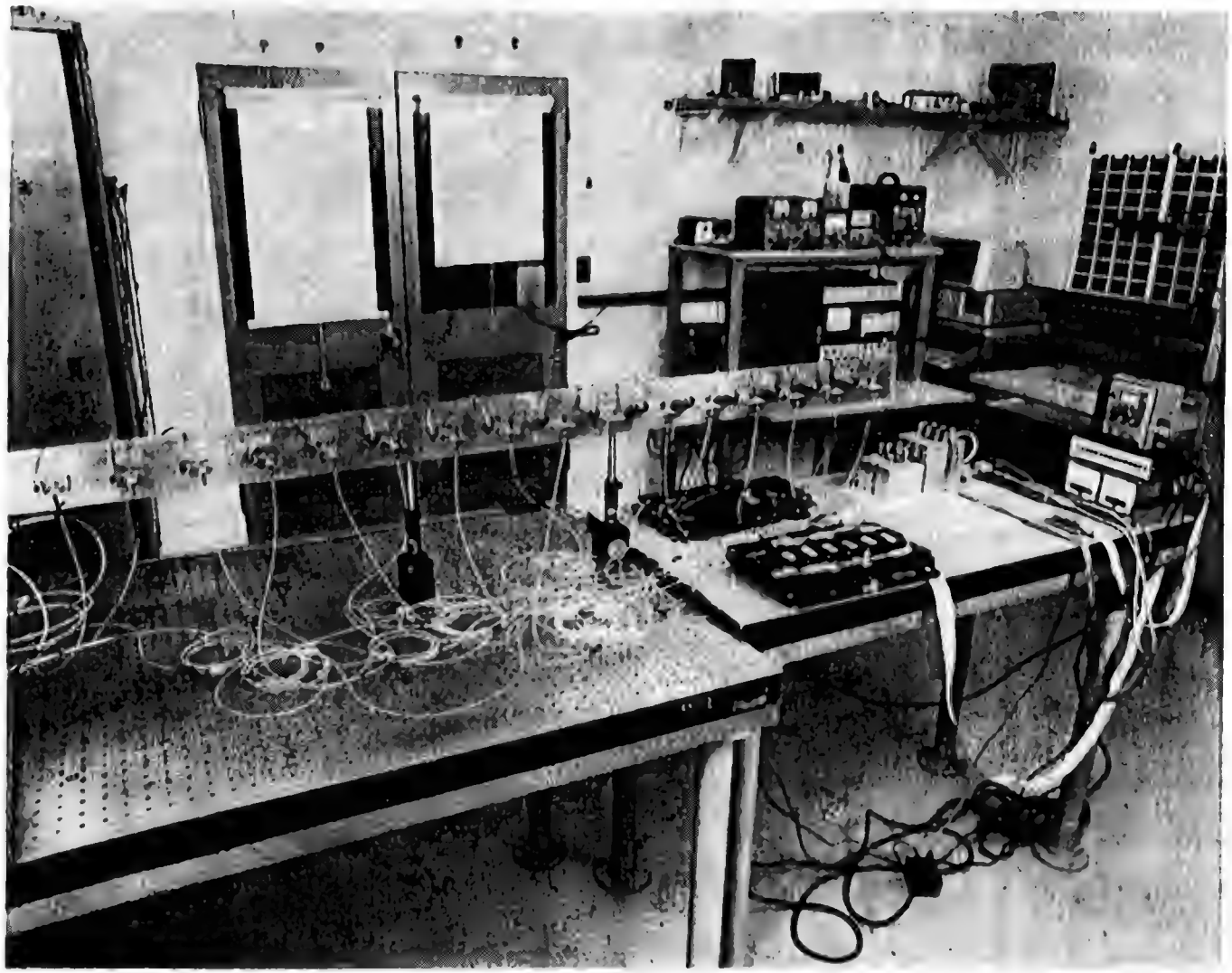

Figure 9.8 — Photograph of the laboratory version of the prototype Tx system showing BIFODEL trays with horizontally-oriented switches.

between two layers of soft foam material which provides mechanical stability and protection. No signal fluctuations due to fiber or switch vibration were observed.

All BIFODELs have been tested bidirectionally for hundreds of hours, and no deterioration in performance has been observed. The delays are set differentially, and measured using the same delay measurement technique as used for the DiBis. Overall, the time delay performance is very similar to that of the DiBis. Figure 9.9 shows the results for an input tone of 1 GHz as a function of steering angle, with a resolution of 1.31°. It can be seen that, similar to the DiBis, excellent agreement is found between the design and measured data for all 3 BIFODELs. The difference between the design and measured data is plotted in greater detail in Figure 9.10 for all 3 BIFODELs. The worst case measured delay deviation from the design value is < ±2.5 ps peak-to-peak or < ±1.25° of phase at 1400 MHz. We have also measured the delay error for all BIFODEL bits, and have found that it is of uniform distribution with a zero mean and a standard deviation of 1.42 ps or 0.71° at 1400 MHz (similar to that found for the DiBis). The delay error is also found to be independent of the delay range (Figure 9.10) and is attributed to the in-house developed delay measurement technique. We have not observed any crosstalk greater than the measurement limit of -65 dB (RF), which is to be expected since the switches we used have a theoretical crosstalk level of better than -130 dB RF.

Overall, the time delay performance of the BIFODELs is found to be very similar to that of the DiBis, which is an interesting result in view of the fact that completely different technologies are involved. Both devices are bidirectional but the BIFODEL requires much larger volume. However, the BIFODEL can operate with much larger delays (e. g., 100s of μs) and is transparent to microwaves whereas the DiBi is limited to a few ns and a few GHz of bandwidth. On the other hand, the DiBi can be switched in 15 ns whereas the BIFODEL has ms-type response. The most striking difference between the two

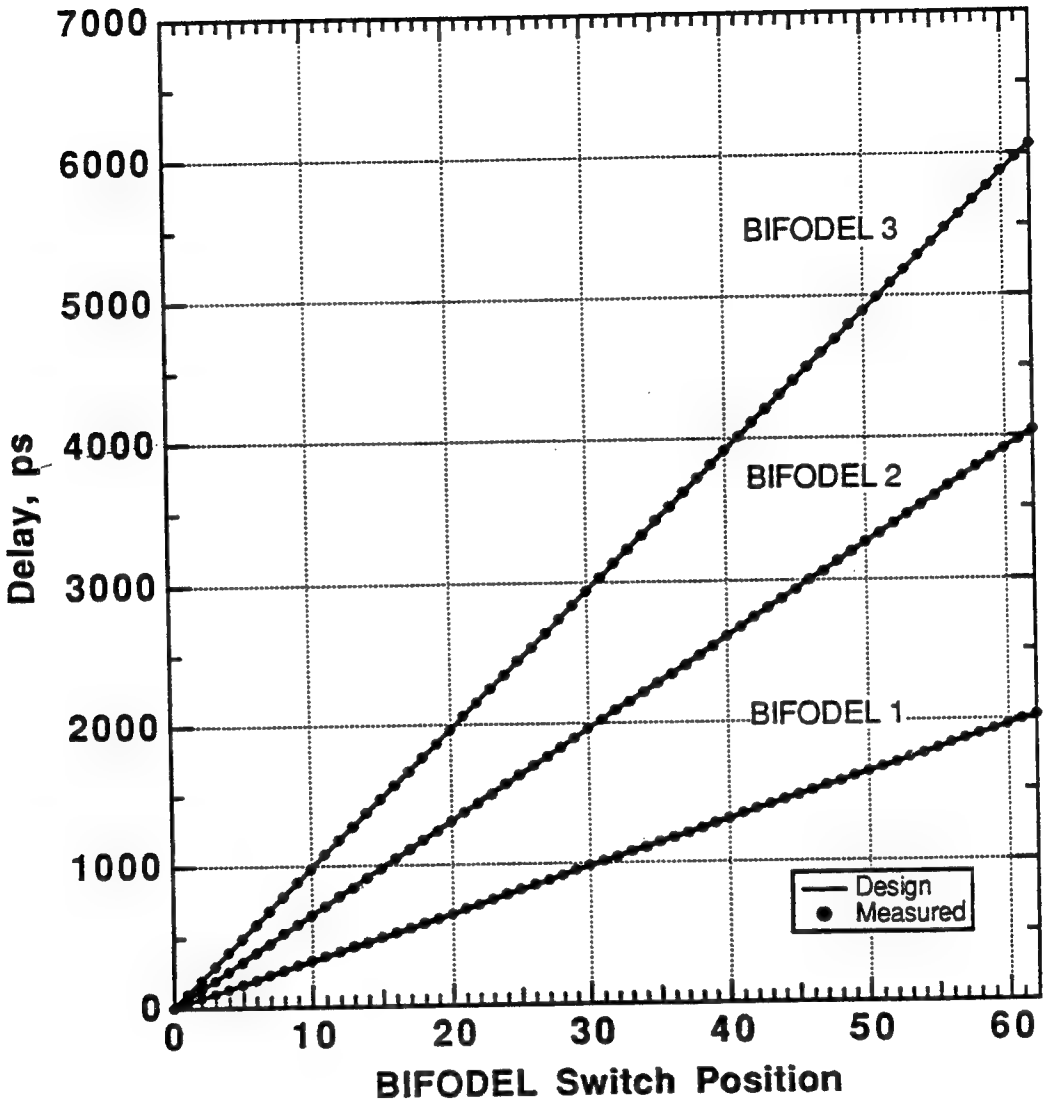

Figure 9.9 — Measured and calculated delays for the BIFODELs as functions of the steering angle with 1.31° resolution.

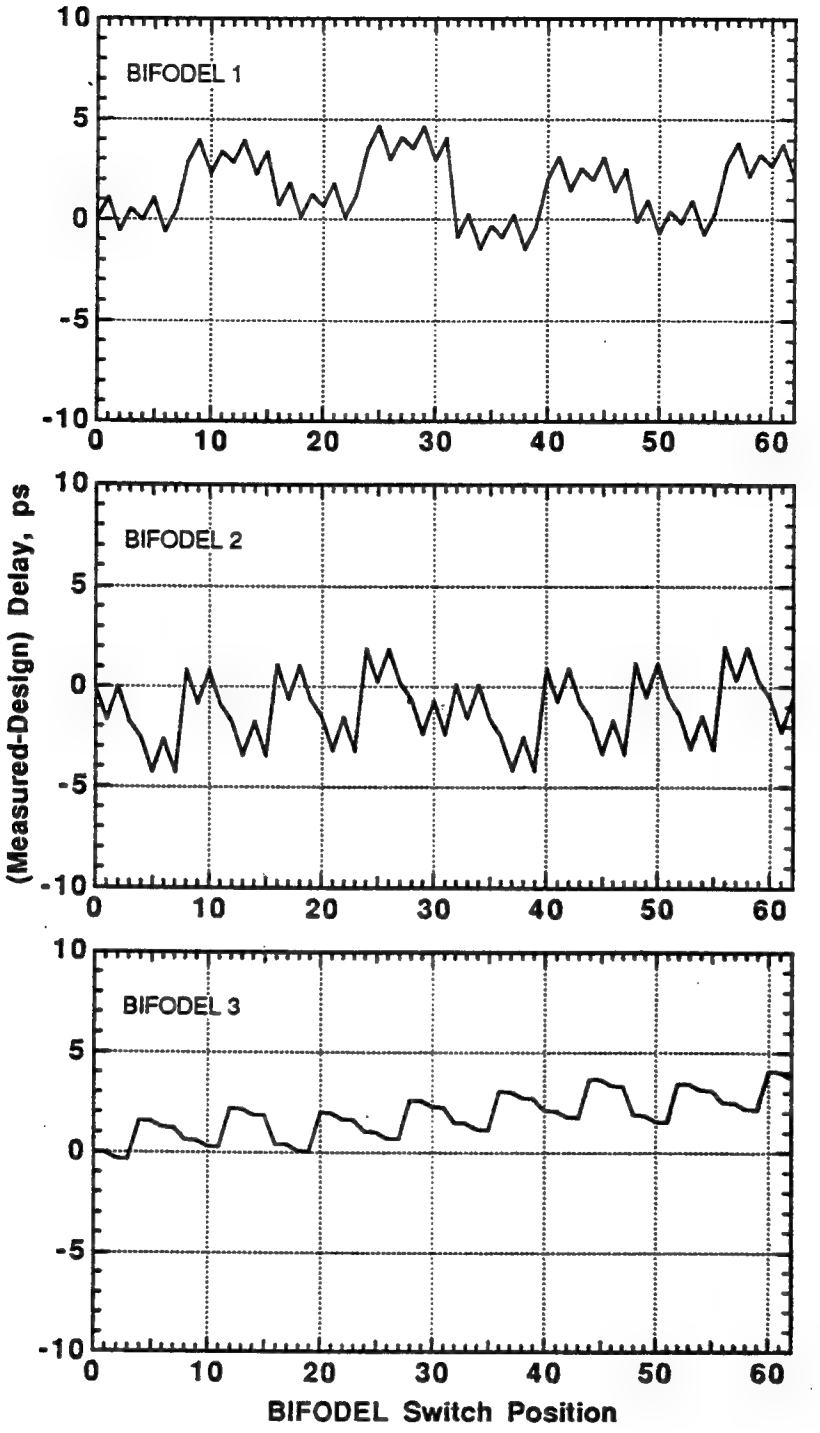

Figure 9.10 — Deviation of the measured BIFODEL delays from the design values as a function of the switch position.

devices is their cost: < $250 for each DiBi and > $7,500 for each BIFODEL, the main difference being the cost of the switches.

9.4 Fiberoptic Link Design and Fabrication

To provide the 4 different wavelengths required by the 16-element transmit system we used commercially available distributed feedback (DFB) LDs in the 1300 nm range. In general, we have found that the performance of FO links may be the limiting factor in the overall TTD system. Developing a high performance fiberoptic link for TTD applications is not an easy task because for most DFB LDs the amplitude response usually varies by about ±1.5 dB over the band of interest. The detector response is usually better but in many cases the LD-detector combination corrupts the LD response even more. To solve this problem we performed the following tasks: (1) identified LDs with the flattest possible amplitude response, (2) matched and corrected the LD response with an appropriate detector response, and (3) designed the appropriate input and output impedance matching networks in order to flatten the response even more. For task 1, we tested various DFB LDs from different manufacturers, selected the ones with the best response, and then carried out further testing in combination with different pin and APD detectors. The optimum combination was then subjected to various types of matching networks.

In general, the narrow spectral widths of the DFB LDs enable the practical LD-to-LD wavelength spacing to be as close as 1 nm, since MUX/DMUX devices having compatible resolution are also commercially available. COTS DFB LDs have typical output power levels of 2 mW and are packaged with integral optical isolators, coolers, feedback detectors, etc. The wavelength stability of these LDs is typically 0.2 nm/°C, and since temperature regulation of better than 0.01°C is easily achievable, wavelength stability of better than 0.002 nm is easily maintained. For our prototype system we chose to maximize the LD-to-LD spacing in order to reduce the cost of the DMUX. Using a

combination of LD selection and temperature tuning we have been able to maximize the LD separation. The resulting 4 wavelengths are 1301.0, 1308.7, 1314.3, and 1321.6 nm.

Each LD is incorporated in a module (Figure 9.11) constructed on a single circuit board using both through hole and surface mount technology. The populated board is housed in a shielded aluminum enclosure of dimensions 4x2x0.5 in^3. Each LD module contains: (i) a power regulator, (ii) a circuit that provides "soft-start" for the LD and which limits the current to a safe level, (iii) a bias supply which is regulated by a closed loop amplifier fed by a signal derived from the integral pin diode of the LD package, (iv) a thermistor and a closed over-damped loop to control the integral LD thermoelectric cooler to a few millidegrees, and (v) a microstrip matching network for the LD designed to flatten the response of the LD-detector (DET) combination.

Figure 9.12 shows an example of the amplitude and delay dispersion characteristics for one of the FO links. It can be seen that the amplitude response is flat to within ±0.25 dB over the 0.6 - 1.6 GHz band and to within ±0.2 dB over the 0.7 - 1.4 GHz band. The insertion loss of the link is about -23 dB and is in good agreement with the theoretical figure predicted using the component parameters selected for the SNR analysis[22]. Figure 9.12 also shows that the delay dispersion is flat to within ±4 ps over the 0.6 - 1.6 GHz band and to better than ±3 ps over the 0.7 - 1.4 GHz band. Similar performance has been measured for the other 3 FO links. These are important results because they demonstrate that optimized FO links can achieve performance comparable to that of the DiBis. When the same DET is used, the responses of the 4 FO links are matched to within ±0.25 dB over the full 0.7-1.4 GHz band. In practice, however, this matched performance deteriorates somewhat because: (i) different DETs are used for the 16 output ports, and (ii) we have incorporated a gain block of about 60 dB at the output of each detector. The amplification was necessary in order to provide about +18 dBm of transmit power per element at the antenna range since the available PAA had no T/R modules at the time of the demonstration.

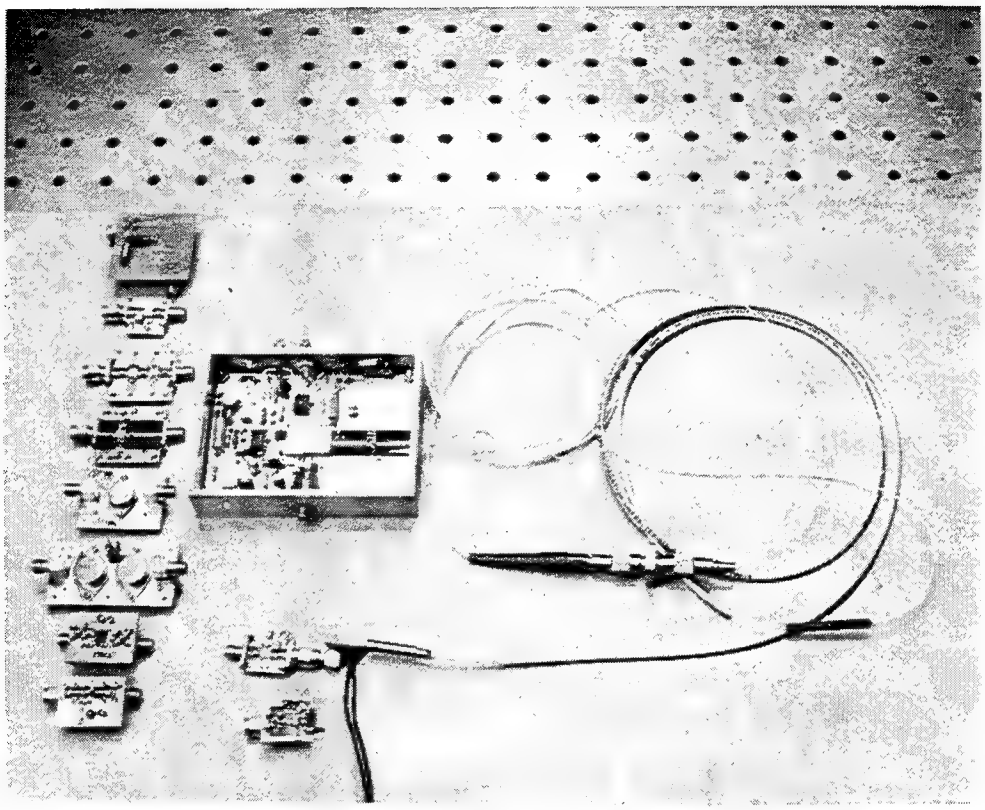

Figure 9.11 — Photograph of the transmit LD module with several experimental output amplifiers.

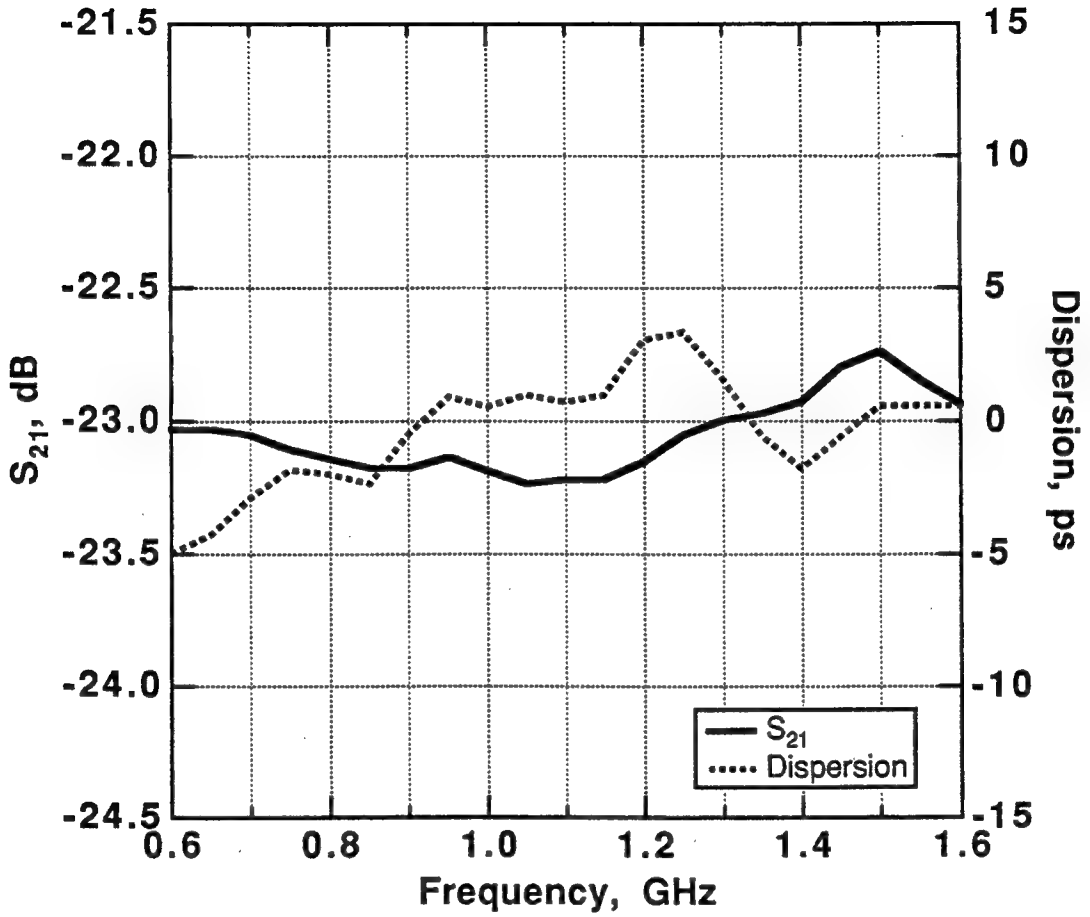

Figure 9.12 — Typical amplitude and delay dispersion characteristics as function of the frequency for the DFB LD-pin diode detector combination.

The requirements of the FO receiver are demanding both electrically and physically because each assembly is required to: (i) be lightweight and small enough to be located on and supported by each PAA element input SMA connector, and (ii) withstand diverse environmental conditions during the antenna range demonstration. In addition to the broadband gain and output power requirements, the receiver module is required to have a ripple of < 0.5 dB in the passband, and a means for adjusting the gain over a ±2 dB range (without altering the overall delay) in order to equalize the gains of the 16 receiver modules.

The receiver modules have been built on DiBi-compatible board material measuring 2.5x1.5 in^2 using surface mount and microstrip technology in conjunction with standard microwave CAD/CAM techniques and careful component selection. The commercially available pin diode DET is connected to the amplifier section at a 90° angle to facilitate the interface with the PAA. The amplifier section consists of two GaAs amplifiers having a combined gain of 40 dB followed by a Si amplifier with 20 dB of gain and a 1-dB compression point of +25 dBm. The Si amplifier has a 2-dB tilt in the passband favoring the low frequencies, and has been corrected by selecting an appropriate input coupling capacitor. Numerous other adjustments have been made to achieve the required gain flatness and we have used printed inductors and paid detailed attention to component placement, shielding, and decoupling. The small gain adjustment is realized by adjusting the bias of the GaAs devices over a range of ±2.5 V without affecting the gain flatness or the overall delay. Figure 9.13 shows the frequency and phase response of the 60 dB gain block when a 61 dB calibrated attenuator is connected at its output. This shows that the frequency response is flat to 0.7 dB over the 0.7 - 1.4 GHz range of interest. This excellent performance is compatible with that of the DiBis and the FO links, and does not degrade the overall system frequency response. The phase response, measured after subtracting the device delay, is flat to within ±5° which is worse than the phase response of the DiBi by a factor of 2.5X. Therefore, the phase response of

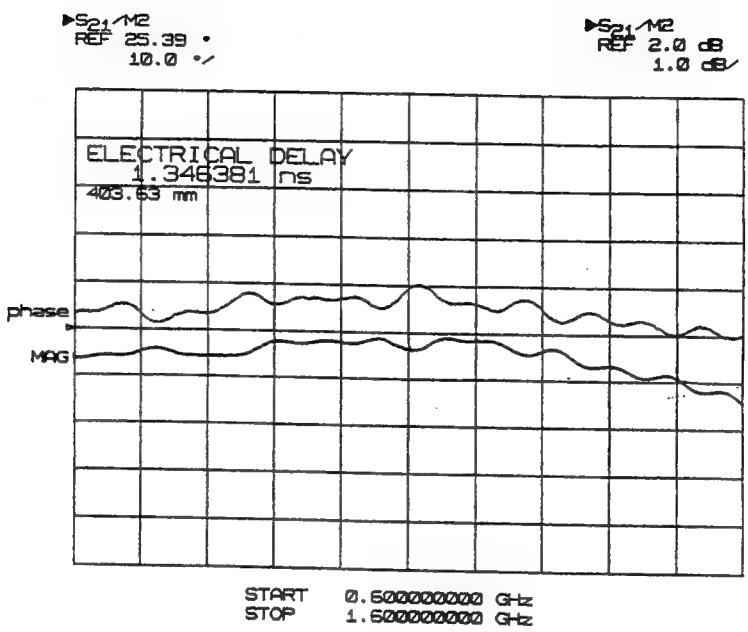

Figure 9.13 — Frequency and phase response of the 60-dB gain block used at each output port.

the output module is the limiting factor in the system phase response. To match the overall frequency response of the 16 receiver modules, we have tuned the response of each amplifier taking into account the specific DET and LD used. By incorporating this individual tuning we have been able to match the frequency and phase response of the majority of the output modules (13 of 16) to within 0.5 dB and 3°, peak-to-peak, respectively. The worst case amplitude and phase deviations measured were 1.0 dB and 6° respectively.

9.5 System Integration

The prototype TTD system was assembled in three packages, (i) the delay generation system, (ii) the FO feed together with the DET-gain block module for each element, and (iii) the computer control and power supply. This arrangement allowed the maximum flexibility in the installation of the complete system for field testing at the antenna range. Figure 9.14 shows a photograph of the delay generation system, the FO feed, and the 16 output modules of the packaged TTD system. The delay generation system is mounted on an aluminum base with plexiglass sides and top to minimize weight; the package has a footprint of 15x13.75 in^2 and is 6.37 in high. With reference to Figure 9.14, the inputs to the packaged system are located on the lower left and comprise the ribbon cable feeds from the computer controller, the cable feed from the power supply, and the RF signal to be transmitted from the antenna. The output from the package (middle right) comprises the FO feed for the 16 output modules.

The input signal to the TTD system is fed to a high-performance 0.35 - 2.1 GHz 1:4 RF divider, the outputs from which drive the 3 DiBis and the zero path module (lower left in Figure 9.14). Over the 0.7 - 1.4 GHz band, the frequency and phase response of the divider are flat to ±0.05 dB and ±0.1°, respectively. The frequency and phase response of the 4 output channels are matched to within 0.05 dB and 0.5°, respectively.

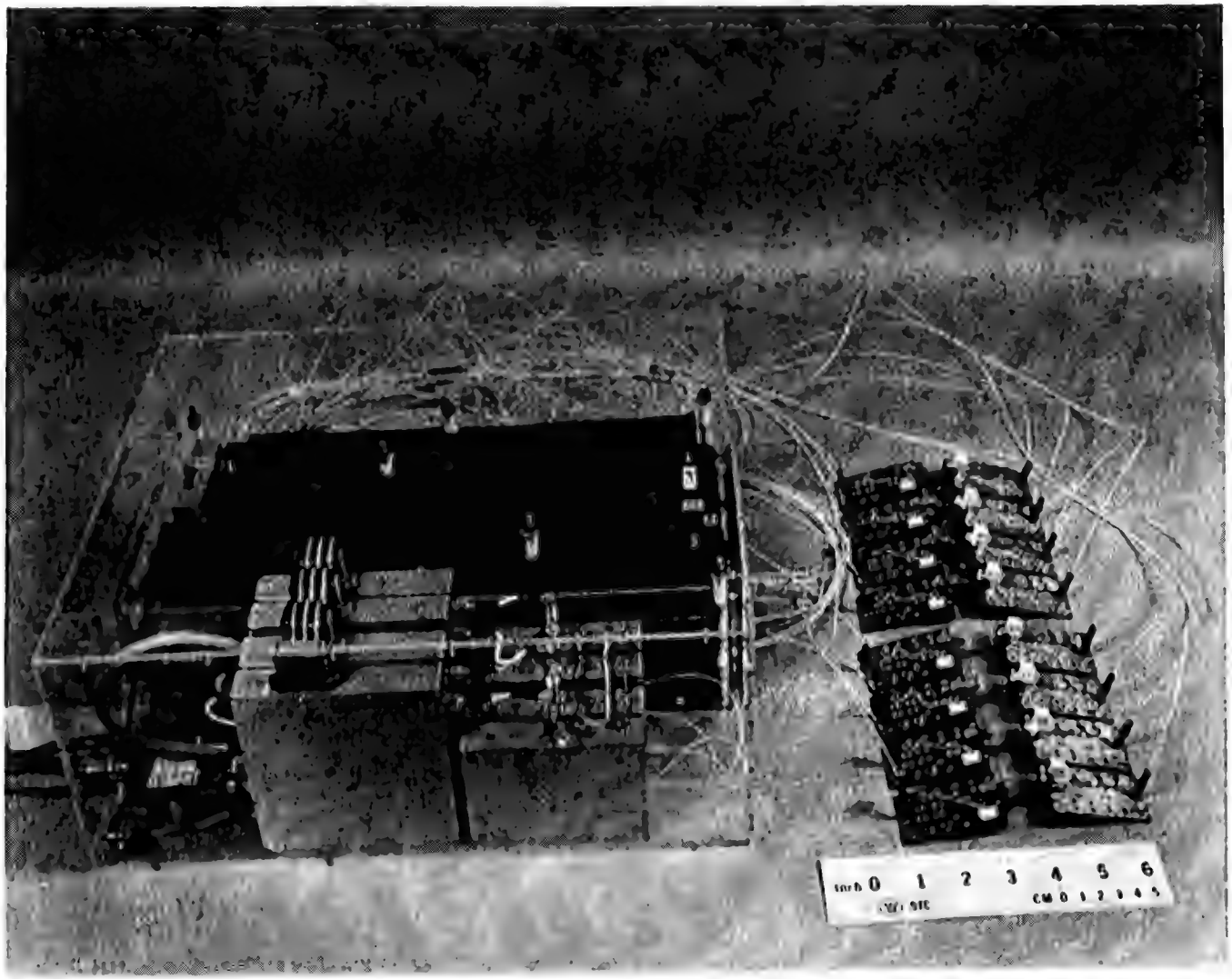

Figure 9.14 — Prototype transmit 16-element WDM TTD system with the 16 output receivers, each of which include a detector and 60-db gain block.

The outputs from the DiBi modules (middle left in Figure 9.14) are connected to the LD modules via delay-equalized cables (lower middle in Figure 9.14). We use a small attenuator (in the 0.5 - 3.5 dB range) at the input of each LD module to equalize the 4 DiBi-LD pairs. This allows us to eliminate amplitude differences resulting from the different slope efficiencies of the 4 LDs, and match the 4 DiBi-LD pairs to within 0.5 dB.

To sum and broadcast the outputs from the 4 LDs to the BIFODELs, we use a commercial 4x4 wavelength-independent coupler (WIC series H made by Gould Electronics) which performs the combined functions of a 4-channel MUX and 1-to-4 divider. The motivation for this choice was the lower cost of the WIC and its lower excess loss (0.25 dB versus 4 dB for the MUX-divider combination). However, although this device is appropriate for a Tx system, it cannot be used for the Rx TTD mode since it does not act as a DMUX in the reverse direction.

The 4 outputs of the WIC were reasonably equalized. To test them, we connected the 4 LDs and measured the output RF at each output (using the same detector and equal RF power at the input of each LD). The results are shown in Table 9.2 (f=fused, nf=not fused):

TABLE 9.2 - WIC output power levels (in dB RF) for equal input power

Wavelength	Output-1	Output-2	Output-3	Output-4
1301.0	-29.4 (f)	-28.0 (nf)	-29.2 (nf)	-28.8 (nf)
1308.7	-28.8 (f)	-32.8 (nf)	-30.4 (nf)	-30.8 (nf)
1314.3	-28.8 (f)	-31.4 (nf)	-27.6 (nf)	-31.2 (nf)
1321.6	-29.2 (f)	-29.2 (nf)	-30.8 (nf)	-27.2 (nf)

To minimize the output variation, we identified the strongest WIC outputs and connected them to the weakest BIFODELs. The WIC coupler was

placed in a flexible tube and located in the space between the center two DiBi and LD modules (part of the tube can be seen above the 1:4 RF divider in the lower left of Figure 9.14).

The optical signals from the BIFODELs (which are stacked vertically as shown in the upper part of Figure 9.14), are demultiplexed via four identical single-mode fiber, diffraction grating-based, DMUX devices which were custom-made by ISA Jobin-Yvon (one such device can be seen at the top left of Figure 9.14). These devices are bidirectional (i. e., they can perform the DMUX function for the transmit mode and the MUX function for the receive mode), and have a 90% optical bandwidth of 0.48 nm, an insertion loss (IL) in the 2.8 - 3.5 dB range, and a specified optical crosstalk level of < -30 dB. We tested these devices extensively and found that their overall operation is sufficient for various TTD system applications. All 4 devices have passbands that are centered to better than ±0.05 nm from the design wavelengths. The crosstalk level is measured to be less than -75 dBc (RF); however, we believe that most of this measured crosstalk is due to RF pick-up rather than optical leakage. Each of the devices has a similar IL (to within 1 dB) whether operated as a DMUX or as a MUX. However, the IL is dependent on temperature and to ensure a loss of less than 0.5 dB, the temperature must be kept to within 2° - 3°C of room temperature (as we will see latter, this problem was eliminated for the Rx operation via the use of heaters). Thus, for a TTD system in the field, the MUX/DMUX must be kept in a protected environment within the TTD system package rather than on the PAA which is subject to wide temperature variations. Consequently, $\sqrt{K}$ fibers are necessary for connecting the TTD system to the $\sqrt{K}$ PAA elements. On the other hand, if the MUX is located on the PAA, only 1 fiber is necessary per $\sqrt{K}$ elements.

The fiber outputs from each DMUX are cut to appropriately different lengths prior to fusing to the DET fiber pigtails so as to provide the fixed time-bias for symmetric steering of the TTD system and to accommodate the feed

manifold length ~ 3 m. Accurate measurement of the total delay between the system input and each output module enables any relative delays present in the DiBis, BIFODELs, LD modules, DMUXs, output modules, interconnecting cables, etc., to be eliminated during manifold fabrication. Each output module consists of a DET, a 60 dB gain block, and a fixed element-dependent attenuator to provide a 28-dB Chebychev taper over the 16 elements.

9.6 Computer Interface

The integrated system is computer controlled with a fast parallel I/O board having direct memory access (DMA) capability. The menu-driven software is written in Pascal and allows for entering: (i) a fixed steering angle, or (ii) a swept steering program with control of start and stop angles over the ±45° range, step resolution, sweep rate, and number of sweep repetitions. Six bits of the I/O board are used for the control word for the 6 GaAs switches of the DiBis. This word is simultaneously written to all DiBis and to a PROM look-up table which provides the 7-bit word for the 7 optical switches of the BIFODELs.

9.7 Laboratory Testing and Evaluation

The integrated TTD system has been subjected to several tests in order to evaluate the system performance prior to the antenna range experiments. The system has been operated for over 250 hours under laboratory conditions over the 18° - 28°C temperature range without failure. The best performance is achieved over the 22° - 26°C range where the DMUXs are optimized.

The overall delay generation has been verified by accurately measuring the relative output delays for each of the 16 output elements and for each steering angle. The total delay error per element depends mainly on the errors associated with: (i) DiBis, (ii) LD modules, (iii) BIFODELs, and (iv) output modules, and varies as a function of: (i) switch position (because the DiBi and BIFODEL errors are switch position- dependent), and (ii) RF frequency (because

the DiBi, LD module, and output module errors are frequency dependent). A complete system characterization therefore requires measurements of the delay errors for each switch position and for each input frequency or frequency combinations, obviously a very tedious task. In practice however, a good indication of overall system performance can be achieved by measuring the delays for: (i) several discrete RF frequencies over the 0.35 - 2.1 GHz band, and (ii) basebanded pulses. We have performed several such experiments and have found very good agreement between the design and the measured delay data. In Figure 9.15, we show an example of the design and the measured non-biased delays for the 16 output elements as a function of the 6-bit (63 combinations) switch position. These data are found to be identical for any frequency taken every 50 MHz in the 0.7 - 1.4 GHz band. These data are also similar to those obtained by propagating pulses of 500 ps half-width. We have also measured the rms time error over the 16 output channels. The worst case performance has a $\sigma = 9.8$ ps over the full band (i. e., $\sigma = 4.8°$ at 1.4 GHz), whereas the best case performance has a $\sigma = 4.03$ ps over the full band (i. e., $\sigma = 2.0°$ at 1.4 GHz). These standard deviations clearly demonstrate that sufficient system-level time delay performance is possible without error correction.

The 3-dB frequency response of the full system (i. e., any of the 16 output ports) covers the 0.35 - 2.1 GHz band, with the lower frequency being limited by the 1:4 RF divider and the upper frequency being limited by the DET and the output amplifiers. Over the 0.6 - 1.5 GHz band the overall response of any of the 16 output elements is flat to ±0.5 dB, with the response profile being determined by the product of the responses of: (i) DiBi, (ii) LD module, and (iii) output module. The ±0.5 dB flatness is achieved as a result of: (i) having optimized the responses of the DiBis, LDs, and output modules, and (ii) having tuned each output module. The average gain of the 16 elements is matched to better than 0.25 dB via bias control of the output GaAs amplifiers. The gain of the output modules varies by ±0.5 dB over the 22° - 26°C temperature range.

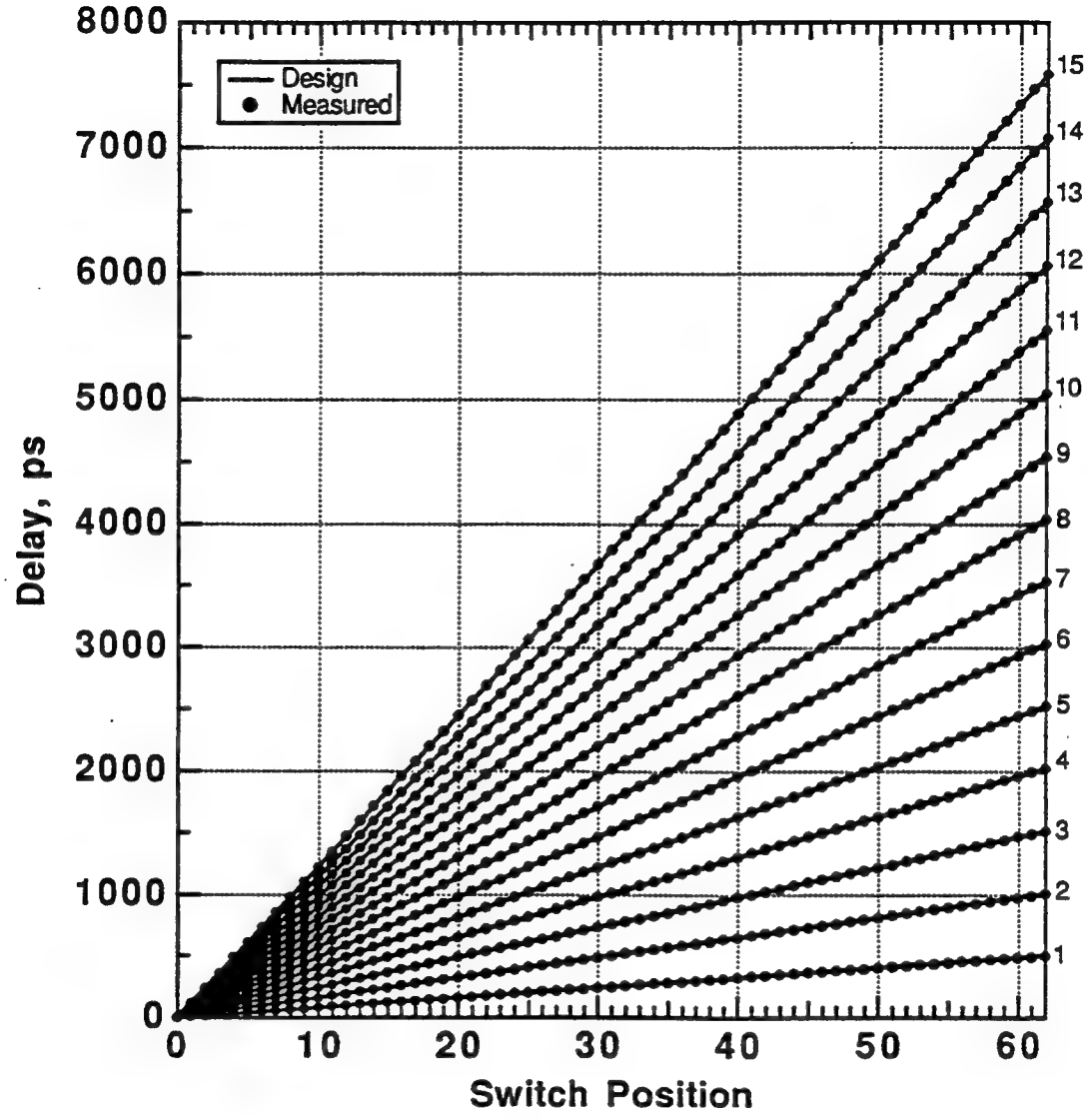

Figure 9.15 — Measured and calculated delays for each of the 16 output elements of the integrated Tx WDM TTD system as functions of the steering angle with 1.31° resolution.

The system losses can be analyzed at two levels: (1) the DiBis and (2) the full fiberoptic circuitry needed for the control of a single PAA element. The DiBi loss is relatively low, about 1.0 dB per bit, for a total of ~ 6 dB per DiBi. This loss can be easily recovered at the output of each DiBi via the use of a small amplifier prior to driving the fiberoptic link. On the other hand, a simple analysis to estimate the overall loss of the fiberoptic part shows that the total optical insertion loss IL_O is given by:

$$IL_O\,(dB) = (N + 1)\,IL_S + (N + 2)\,IL_C + IL_{MS} + IL_{D'} \tag{9.10}$$

where N is the number of BIFODEL bits, IL_S is the insertion loss per switch, IL_C is the loss per fiberoptic connection, IL_{MS} is the loss of the MUX/splitter, IL_D is the insertion loss of the DMUX (all the ILs are expressed in dB). To evaluate Equation 9.10 for the prototype system we used the advertised specifications of the various components: (1) the WIC has an excess loss of 1 dB and total insertion loss per channel of IL_{MS} = 7 dB, (2) the 2x2 switches had a loss of 1 dB, (3) each fiber connection was made by fusion splicing and had IL_C = 0.1 dB, and (4) the DMUX loss was 3.5 dB. Using these component characteristics we find that IL_O = 18.3 dB which is a very moderate figure considering the complex function performed and especially the fact that it includes a 6 dB loss due to the 1:4 power split at the WIC. However, this energy is not lost since it drives 4 elements. Also much of the system optical loss can be recovered in either the RF or optical domain via the use of amplifiers.

The system SNR depends on both the optical loss and the electronic-optic-electronic conversion loss. One can show[16] that for a sinusoidal input, in a directly modulated LD fiberoptic link utilizing a pin output detector, the output SNR is given by:

$$SNR = \frac{0.5(grmP_o)^2}{RIN\ BW(grP_o)^2 + 2eBW(grP_o + I_D) + kT\ BW\ (R_L)^{-1}} \tag{9.11}$$

where g is the link loss (g = 0.0148 for IL_o = -18.3 dB), P_o is the LD optical bias power level (typically P_o = 2 mW for CATV DFB LDs), r is the detector responsivity (typically r = 0.7 mA/mW at 1300 nm), m is the modulation index (m = 0.397 for an input RF power of +8 dBm, a LD efficiency of 0.1 mW/mA, a LD input impedance of 50 Ω, and P_o = 2 mW), RIN is the LD relative intensity noise (typically RIN = -155 dB/Hz for DFB LDs or 3.16×10^{-16}/Hz), e is the electronic charge (1.6×10^{-19} C), I_D is the detector dark current (typically a few nA), k is Boltzmann's constant, T is the operating temperature (300°K) and R_L is the detector load impedance (R_L = 50 Ω). Evaluating Equation 9.11 using these characteristic values with IL_o = -18.3 dB, we find that SNR = 115.8 dB/Hz. This SNR figure is thermal-noise limited and thus a significant improvement can be achieved if the output detector drives a transimpedance amplifier (TRAM), e. g., for a conservative transimpedance figure of 1000 Ω, the SNR improves by 13 dB to about 128.8 dB/Hz. Further improvement is possible if optical amplification is used which, if sufficiently large, can make the output SNR RIN-noise limited and > 145 dB/Hz. These SNR values are satisfactory for many PAA applications. Note that the measured SNRs of the four FO links (each link consisting of a LD module and a DET) are 144.3, 150.1, 150.2, and 152.2 dB/Hz, the limiting factors being the LD RIN levels. The measured average optical loss of the system was about 14 dB. These results lead to a best case system SNR of 124 dB/Hz and a worse case of 116 dB/Hz. Note that we evaluated the possibility of a TRAM, and have found that, for BWs up to 1.5 GHz, the best commercially available TRAM has an output SNR of about 145 dB/Hz. We have also found that matching the response of the output TRAMs is a more difficult task than matching conventional voltage amplifiers. We point out that the above performance applies to a transmit system where the power of each LD is divided into $\sqrt{K}$ channels. For the Rx TTD system this is not the case; the LD signal is not divided and the RF signals from all the LDs are coherently added so that significant improvements are possible. For example, if we were to use the

prototype system for the receive mode, we would have a 6 dB improvement in optical IL, i. e., a 12 dB improvement in the SNR, and a further 12 dB improvement from the coherent addition of the 16 optical channels.

10. Tx WDM TTD SYSTEM ANTENNA RANGE DEMONSTRATION

10.1 Phased Array Antenna Description and Antenna Range Set-Up

The PAA used for the TTD demonstration was developed by Westinghouse and consists of 16 columns (three views of the PAA are shown in Figures 10.1, 10.2, and 10.3). Each column contains two radiating elements with an integrated 3.0 dB coupler. The radiating elements are vertically polarized, reduced depth notch radiators. Typical notch radiators are at least one wavelength deep (about 9.8 in at 1.2 GHz). Although standard notch radiators can operate over a broad band, they are impractical for many applications because of their depth. The notch radiators of this PAA are compact, 0.3λ deep (< 3.0 in), and simultaneously broadband: 850 - 1400 MHz (1 dB BW) or 700 - 1500 MHz (3 dB BW). The antenna has a scan angle of ±60°, and the VSWR is < 2:1 across the 700 - 1500 MHz band, and < 5:1 across the 600 - 1500 MHz band. The PAA is extremely manufacturable, and it can be integrated directly into a vertical beamforming column.

The antenna range used for the testing is set-up for antenna manifold and antenna element development. The transmit antenna is mounted on a pedestal at a height of 12 feet above ground. The pedestal, which is mounted on top of an 8 foot wooden scaffold, consists of a 3-axis positioner which can turn the antenna ±180° horizontally and vertically (Figure 10.1). The Tx WDM TTD prototype system was placed inside a conventional food cooler (Figure 10.2) to protect it from rain. The cooler and the associated electronics were placed on the surface of the wooden scaffold. The fiberoptic manifold and the receive modules were connected directly to the input SMA connectors of the 16 PAA elements (Figure 10.3). A reference notch element mounted centrally on top of the 16-element

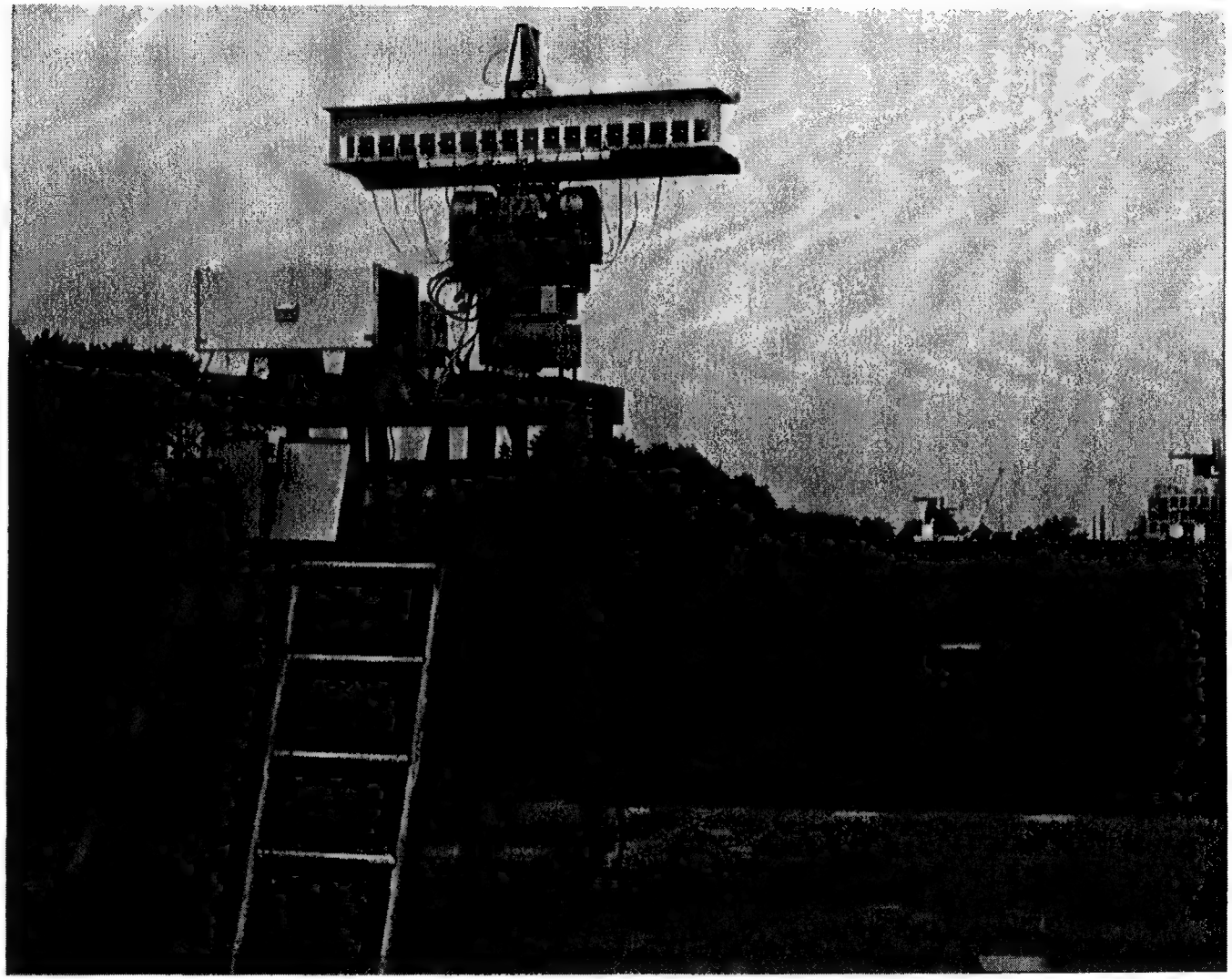

Figure 10.1 — Antenna-range setup that shows the 16-element TTD-driven PAA mounted on a three-axis rotary positioner and the 4 element matching receiver (middle right).

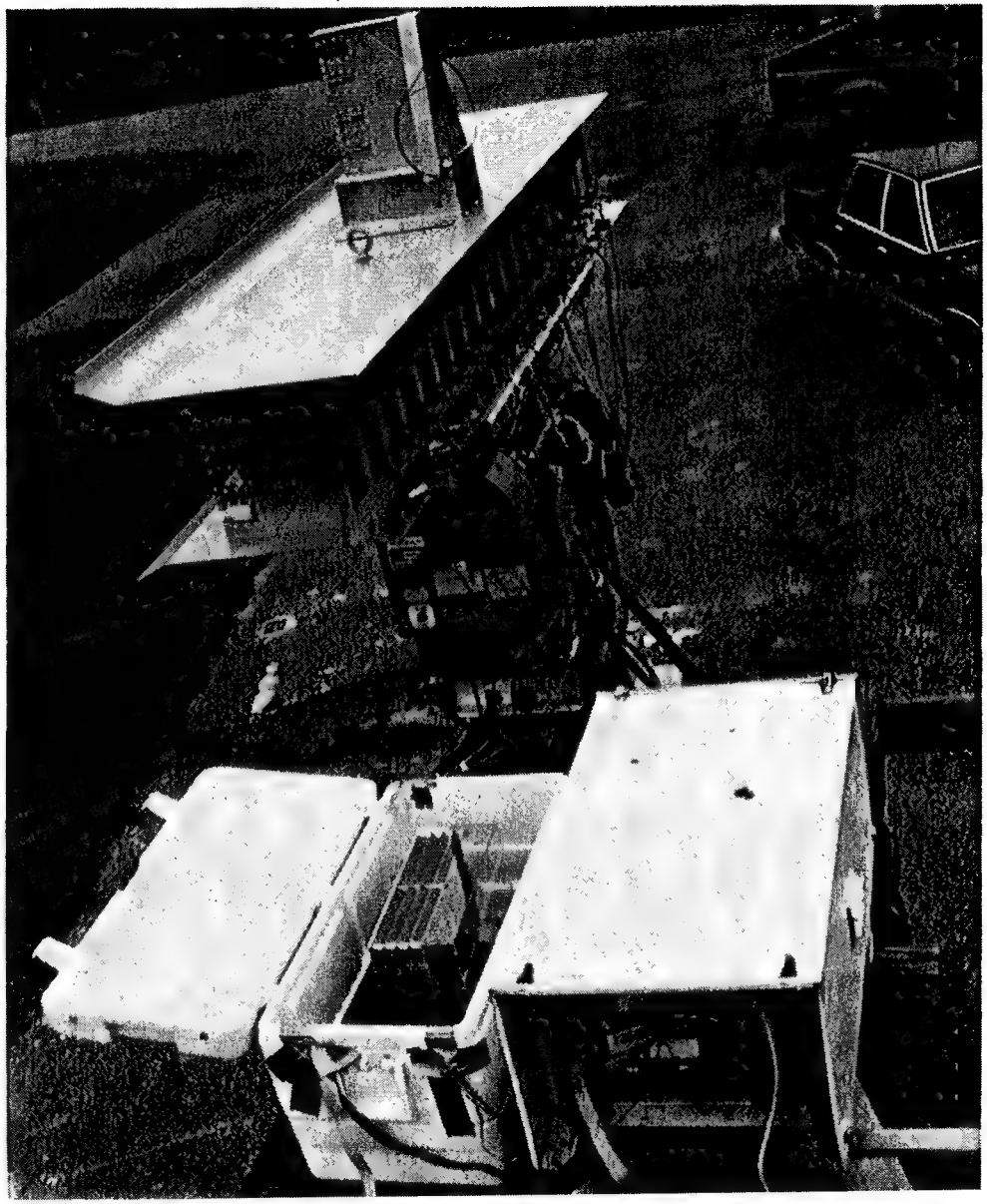

Figure 10.2 — Experimental PAA driven by the photonic Tx WDM TTD system.

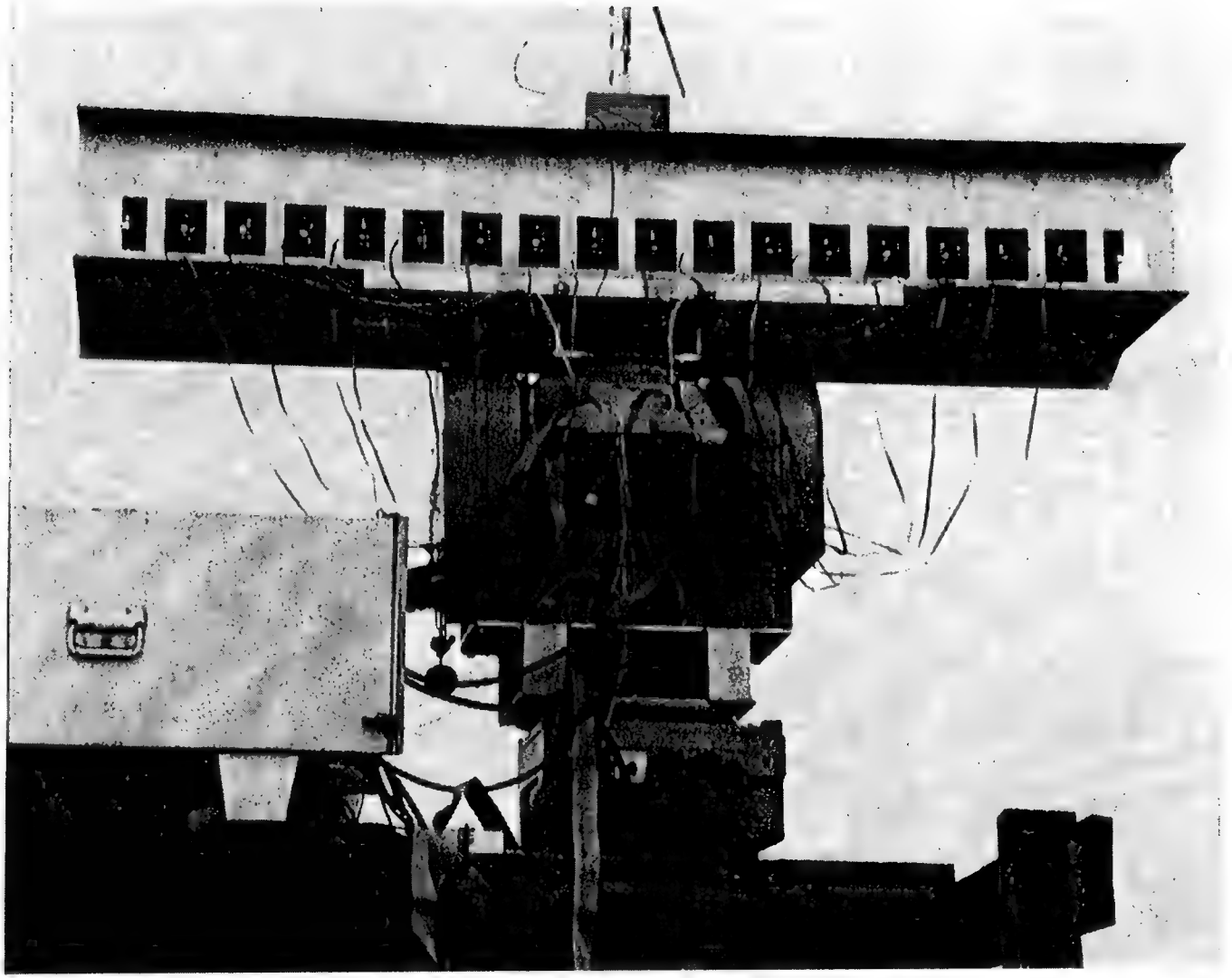

Figure 10.3 — Close-up view of the PAA and the photonic manifold

PAA (Figures 10.1, 10.2, 10.3) provides phase and amplitude references for the diagnostic software. A length of coaxial cable was added in order to phase the reference element to the array.

Figure 10.4 shows a block diagram of the overall system set-up, whereas Figure 10.5 shows a photograph of the control room electronics. Note that since the far-field pattern ($2D^2/\lambda_{RF}$, where D is the PAA length and λ_{RF} is the center wavelength of the RF signal) of the antenna is approximately 40 feet, the receive antenna should be located at some point greater than 40 feet from the antenna in order to observe the sidelobe structure (Figure 10.4). A 2x4 notch element PAA (similar to the 2x16 element used with the TTD system) was used as a receive antenna and was located 192 feet down range from the antenna at a height of 43 in above ground to satisfy the maximum lobe ground effect equation. The 43 in height is optimum for operation over the 0.7 - 1.5 GHz band. To minimize reflections from the side of the range, the output of the receive antenna was connected to a 4:1 power combiner having a 30-dB sidelobe taper. The receive antenna was connected via a 230 feet, 21 dB loss coaxial cable to the receive electronics located in the control room (Figure 10.5).

The following procedure was followed for recording an antenna pattern: (i) the TTD system switches were set to the desired steering angle, (ii) a CW signal in the 0.6 - 1.5 GHz band was generated in the control room and fed to the input of the TTD system, (iii) the transmit antenna was mechanically rotated horizontally by ±80°, and (iv) the signal from the receive antenna was recorded as a function of the transmit antenna rotation angle. (Unfortunately, the antenna range electronics at the time of the demonstration, could not accommodate the transmission of broadband pulses or simultaneous CW frequencies). For each antenna pattern, a computer tuning program (MTUNE) was used to measure the amplitude and phase distribution over the 16 elements. MTUNE has been used for ultra-low sidelobe antennas to -55 dB, and captures the angle in sine space at which the pattern amplitude and phase is measured. These pattern data are

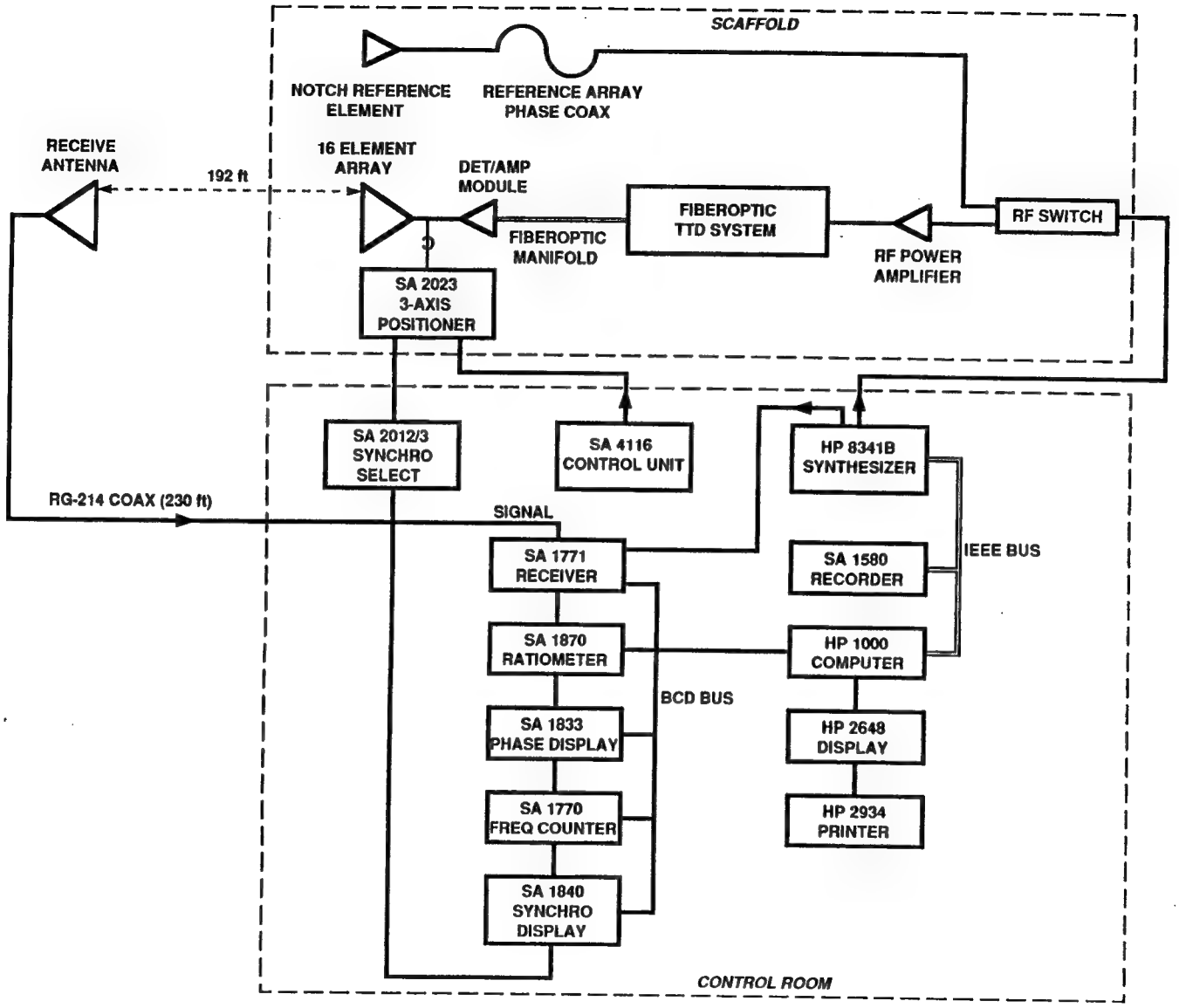

Figure 10.4 — Block diagram of the overall system set-up including the devices in the scaffold and the control room.

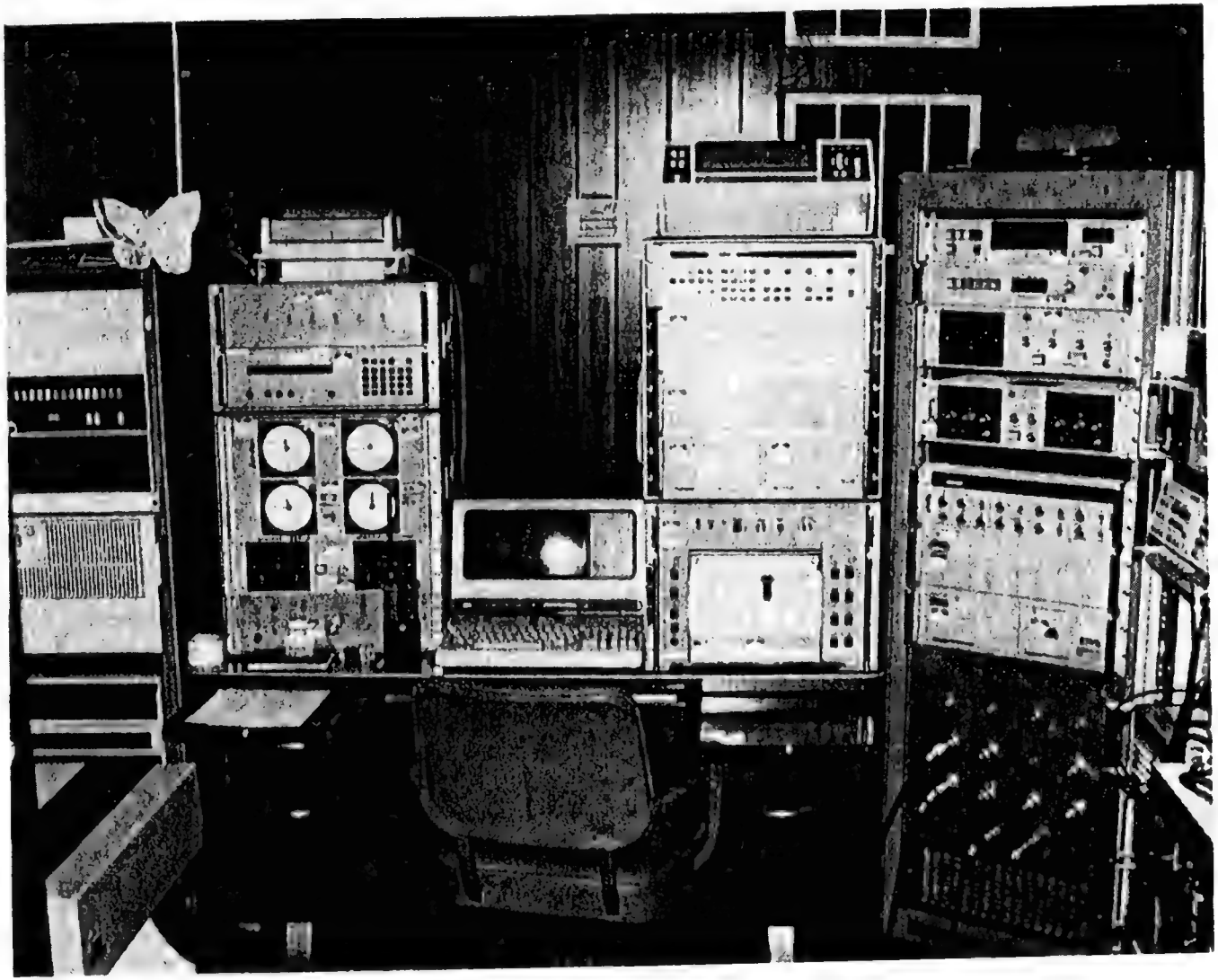

Figure 10.5 — Photograph of the control room electronics.

reverse transformed back to the aperture and a distribution is computed. From this, an error plot of the amplitude/phase compared to the theoretical distribution is generated. Each recorded pattern has an accompanying plot showing errors in the array. Sixty four data points over ±80° were recorded on each antenna pattern taken. The use of MTUNE proved extremely valuable since it helped identify various problems at the antenna-receiver module interface, e. g., module mismatches due to humidity, shorted output amplifiers, mutual coupling between antenna elements, etc.

10.2 Demonstration Results

The prototype Tx WDM TTD system was tested successfully at the antenna range over a period of two weeks under various temperature and humidity conditions. No effects attributable to humidity variations were observed; however, ±1.3 dB gain variations were observed as the temperature varied, probably due to changes in the response of the DMUX devices with temperature.

The main test involved the demonstration of the antenna beam stability as a function of frequency, which is the main characteristic of the TTD operation. For this purpose we: (i) steered the antenna at a specific angle, (ii) changed the RF input frequency to the TTD system in discrete steps over the antenna BW, and (iii) for each angle-frequency combination we recorded the resulting antenna pattern over a ±80° scan. Figure 10.6 shows examples of some of the recorded squint-free antenna patterns obtained. Twelve superimposed antenna patterns are shown for 3 different steering settings, -43°, 0°, and +45°, and for frequencies of 600, 900, 1200, and 1500 MHz. These specific angle and frequency settings were chosen because they cover the full scan range of the TTD prototype system and the maximum possible BW of the antenna. As Figure 10.6 shows, in all cases stable, squint-free antenna patterns were recorded regardless of the operating frequency, which unambiguously demonstrates the TTD nature of the

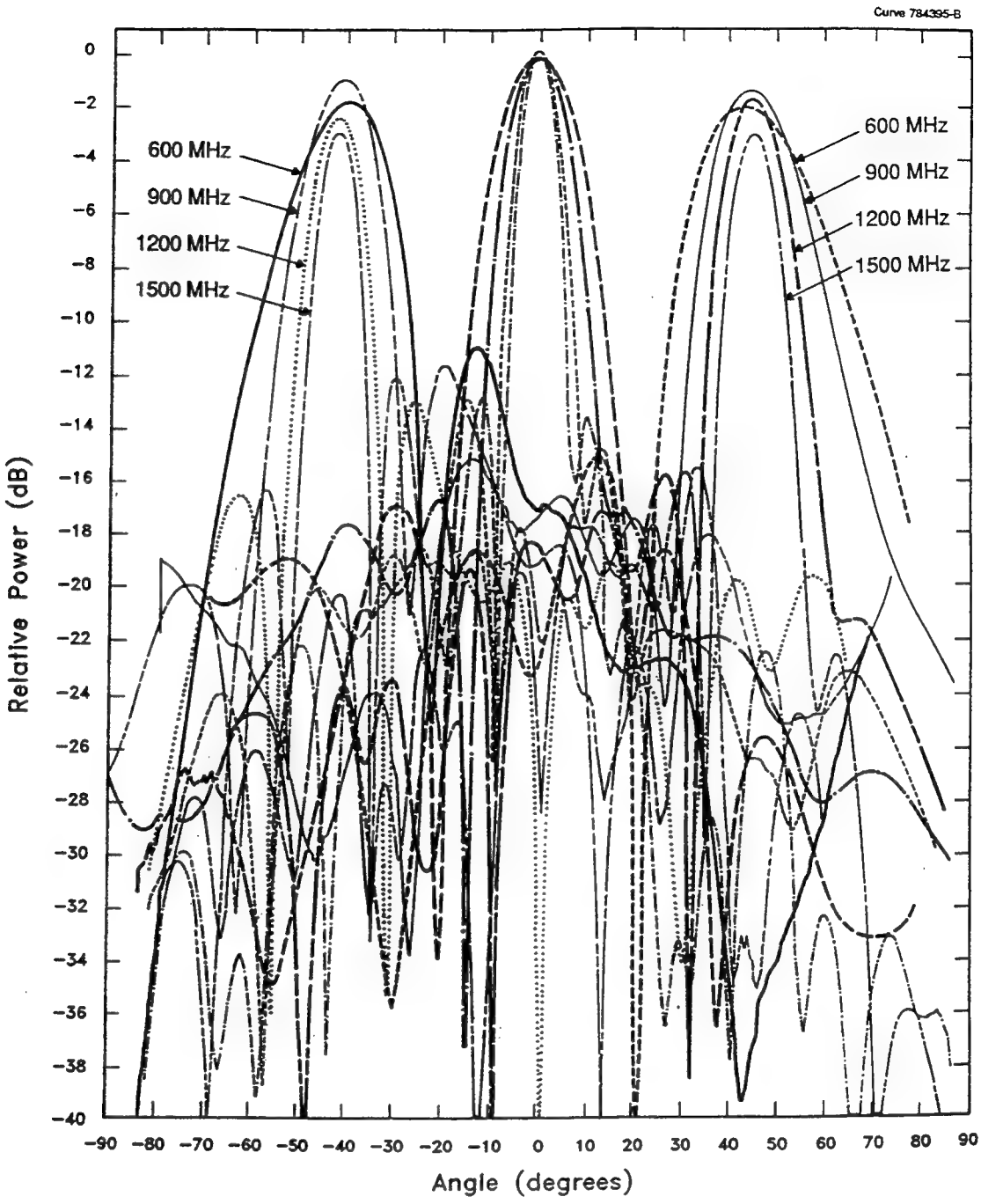

Figure 10.6 — Squint-free antenna patterns for steering at the -43°, 0°, and +45° angles and for frequencies of 600, 900, 1200, and 1500 MHz.

prototype system; such patterns are not possible with phase steering. We have obtained similar results over the full range of steering angle covered by the TTD system and for any frequency covered by the BW of the antenna. It can be seen in Figure 10.6 that the -43° and +45° patterns at 600 MHz are slightly different from the programmed angles (by -3° and -2.5°, respectively). This is because, at 600 MHz, the 16 antenna elements are not well matched (the antenna VSWR is about 5:1) and therefore the beam cannot be steered with precision. Also, we note that the ±1.5 dB antenna pattern gain variations, at the -43° and +45° angles, are due to the characteristics of the element patterns rather than the TTD system. Also, the 600 - 1500 MHz BW results are limited by the antenna bandwidth and not by the TTD system BW which is 0.35 - 2.1 GHz.

As described earlier, the gain of the 16 output modules was controlled to provide a 28-dB Chebychev taper. However, as the data of Figure 10.6 indicate, the sidelobes were observed to be significantly higher, at an average level of -18 dB. To identify the source of this problem we ran the MTUNE diagnostic program which showed that significant amplitude and phase distortion existed, especially between the middle elements of the array, e. g., errors up to ±4 dB in amplitude and ±40° in phase were indicated in the middle 6 elements. This was a puzzling result given that no such errors were measured in the laboratory, and various experiments were performed to identify the source of the problem. The most successful of these experiments involved the use of a directional coupler at the output of the 9th output module (while still connected to the antenna) to measure the amplitude and phase of the return signal. By measuring these quantities alternately either with all elements switched on or with nearest neighbors switched-off, we were able to determine whether the problem was caused by the TTD system or by the antenna itself. A series of such measurements proved that the problem was caused by mutual coupling between antenna elements and the absence of RF isolators between the antenna elements and the output modules. For example, the amplitude and the phase of the 9th

element changed by 4 dB and +35° (as calculated by the MTUNE program) , respectively when elements #8 and #10 were switched off.

Since no matched broadband RF isolators were available at the time of the demonstration, we explored other ways in order to obtain some idea about the sidelobe levels due to the TTD system itself. Specifically, we switched off all the even numbered PAA elements in order to double the element spacing and reduce the mutual coupling, accordingly. Using this 8-element PAA arrangement we recorded various antenna patterns with input frequencies restricted to the 600 - 700 MHz frequency band, over which range the element spacing is still $\lambda_{RF}/2$. An example of such a pattern is shown in Figure 10.7 where we show the theoretical and experimental patterns for an input frequency of 700 MHz. We note that the 28-dB Chebychev taper designed for the 16 elements was still present for the data of Figure 10.7, and affects the pattern resulting from the 8 antenna elements differently than a true 8-element 28 dB Chebychev taper. As Figure 10.7 shows, the measured sidelobes are within 1.8 dB of the theoretical sidelobes (calculated using the appropriate components of the 16-element 28-dB Chebychev taper) which proves that no serious errors were produced by the TTD system. Similar behavior was observed for various steering angles and frequencies in the 600 - 700 MHz range. Furthermore, during these measurements we frequently observed deep, e. g., < -40 dB, nulls in the antenna patterns. In view of the small antenna size used in these experiments, such deep nulls are associated with small time errors, which is consistent with the results obtained in the laboratory time error tests.

Another interesting experiment we performed was related to the angular resolution of the TTD system. For these experiments we used the even-numbered elements of the 16-element antenna with a fixed input RF frequency of 700 MHz, and we recorded a total of 63 patterns; one for each binary combination of the 6-bit switches. Examples of such patterns are shown in Figure 10.8, which demonstrate the quantized (in binary form) resolution of the

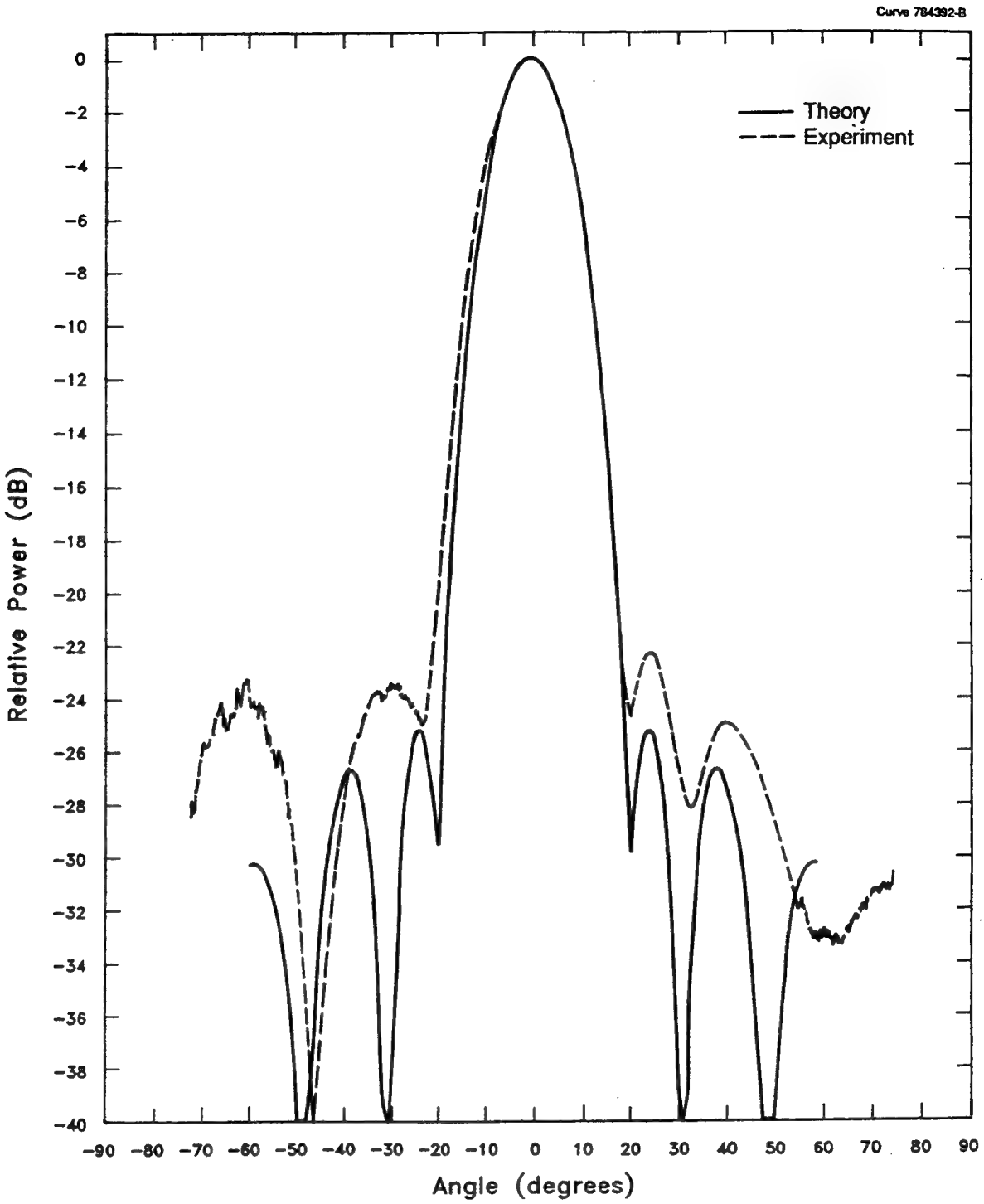

Figure 10.7 — Theoretical and experimental antenna patterns for 8 antenna elements (odd numbers) and for a frequency of 700 MHz.

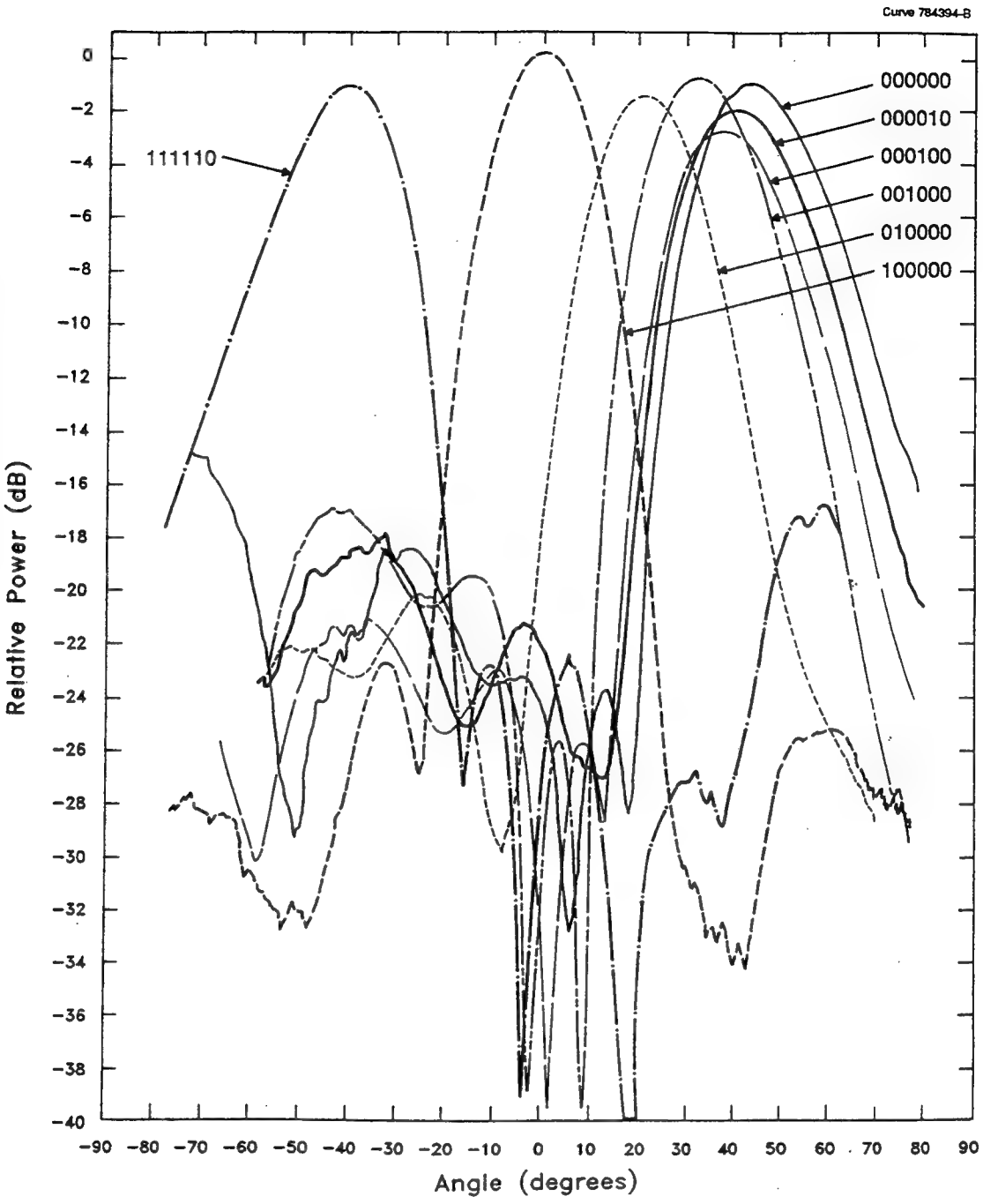

Figure 10.8 — Antenna patterns as functions of DiBi and BIFODEL switch settings that cover the -42°-to-+45° angular range for a frequency of 700 MHz.

antenna. For example, the steering angle sequentially doubles as the TTD program is switched in turn from 000100 to 001000 to 001000 to 010000. These experiments verify the expected system resolution (1.31°) and the scan angle range (±45°) of the system.

11. DEVELOPMENT OF AN 8-ELEMENT Rx HYBRID WDM TTD SYSTEM

In the second phase of the program, we developed an 8-element Rx hybrid WDM TTD system with specifications similar to those of the 16-element Tx WDM TTD system. In the following Sections we describe the overall system design, test, and demonstration.

11.1 Receive WDM TTD Architectures

In general, there are two basic architectures for implementing a Rx hybrid WDM TTD system and employ either: (i) optical, or (ii) RF summation. Figure 11.1 shows a schematic of 16-element Rx WDM TTD system that employs optical summation. This system is the "reverse" analog of the Tx WDM TTD system. Here, the output of each antenna element drives a LD of a different wavelength. For 1-D antennas, elements with similar locations in different sets of the antenna array drive LDs of the same wavelength (for 2-D antennas elements with the same location within different columns drive LDs of the same wavelength). For each array set, the LD outputs are optically multiplexed, and the resulting optical signal drives either a BIFODEL or a no-bias delay path. The outputs of the 3 BIFODELs and the no-bias delay path are then added via a 4:1 fiberoptic combiner. The output of the 4:1 combiner is subsequently demultiplexed by an 4:1 optical DMUX. At the output of each DMUX channel, a detector, "adds" the modulation of the 4 optical signals present in that channel, and produces a single, coherently-added RF output, which drives a DiBi. The next step is to add the outputs of the DiBis via a 4-channel RF combiner, the output of which provides the desired vector sum (i.e., coherently received RF

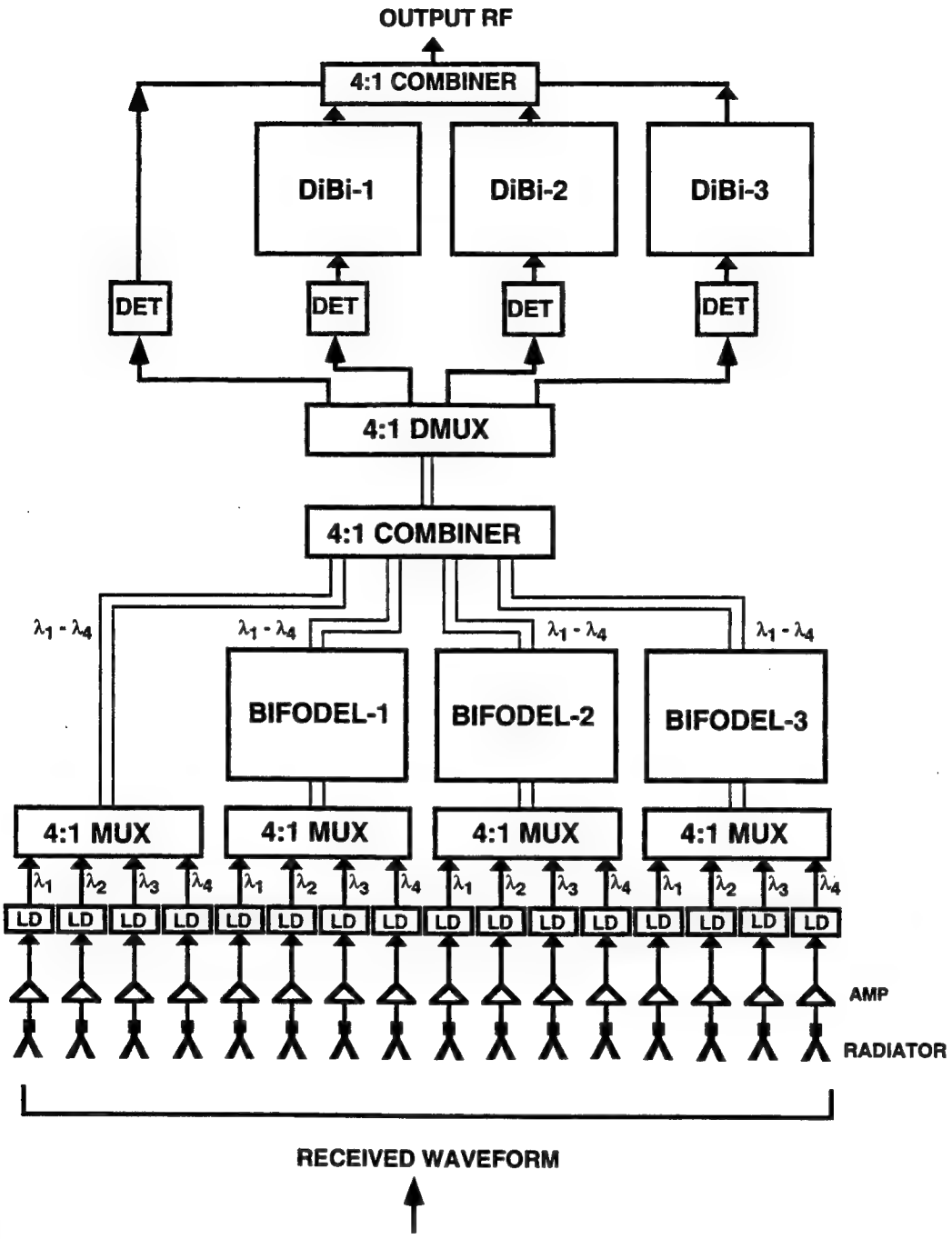

Figure 11.1 — Schematic of a 16-element hybrid WDM Rx TTD system employing optical summation.

signal from all 16 channels). We note that for the case of 1-D arrays the BIFODELs eliminate the set-to-set relative delays whereas the DiBis eliminate the in-set delays. For the case of 2-D arrays, the BIFODELs eliminate the delays along the horizontal (vertical) axis whereas the DiBis eliminate the vertical (horizontal) delays.

The problem in the architecture of Figure 11.1 is the insertion loss of the 4:1 FO combiner. Commercially available, single mode, 4:1 FO combiners (dividers) are "symmetric" devices and thus their combination loss is equal to their splitting loss. This is due to inherent mismatches in the mode field diameters (or alternatively to numerical aperture mismatches) between the input and output fibers. These losses may be severe since they increase as the square of the number of combined channels because of the square-law relation between optical intensity and RF signal power (i.e., the dB-expressed loss in the optical domain doubles in the electronic domain). In Table 11.1 we give examples of an E:1 FO combiner loss for different values of E.

TABLE 11.1 - Examples of optical and RF loss for an E:1 channel FO combiner

E	Optical Loss (dB)	RF Loss (dB)
2	3	6
4	6	12
8	9	18
16	12	24
32	15	30

As Table 11.1 shows, for most "real world" applications involving PAA with over 64 elements (i.e., E≥8), the FO combiner loss is significant and for all practical purposes unacceptable. This is because high loss at the Rx mode results in a high noise figure (NF) which reduces the system sensitivity or equivalently, it increases the T_x output power requirements. In general, the FO combiner loss

may be recovered with the use of an optical amplifier between the FO combiner and the DMUX. A better approach involves the use of an asymmetric FO combiner and a multi-mode DMUX. Here, we can take advantage of the short distance (a few meters) involved between BIFODELs and DiBis and use a special kind of asymmetric FO combiner which is nearly lossless.

The basic idea behind the asymmetric combiner is: use single mode fibers to bring the signals from each BIFODEL, bundle these fibers together and couple them into a wider diameter short piece (e.g., 1-2 meters) of multi-mode fiber. Then use a multi-mode DMUX in conjunction with a DET of active area diameter compatible with that of the multi-mode fiber core (note that at the same time, the DET used must have small enough diameter so that its RC constant allows it to respond to the desired RF). Also note that for tens of meters of 50/125 μm multimode fibers, the modal noise is virtually absent for frequencies well beyond C-band (i.e., 8 GHz). For this technique it is mandatory to reduce the diameter of the input fibers of the bundle, so that the end active areas of the coupling partners are matched. The degree of the reduction depends on the core of the output multi-mode fiber used. This in turn depends on the DET diameter we use. A good method for controlling the cross sectional area of a fiber is that of wet chemical etching by hydrofluoric acid (HF). Before etching, the fiber is first prepared by stripping several cm of the buffer coating from the fiber, cleaving the stripped portion of the fiber, and finally scrupulously cleaning the stripped portion with acetone. The fiber is then mounted vertically in a fixture attached to a micrometer drive such that the fiber can be mechanically lowered into a beaker containing concentrated HF. The fiber mounting fixture is such that several fibers may be etched simultaneously. Upon completion of the etching process, the reduced fibers are bundled together via the use of a thin layer of glue, and the resulting fiber bundle is fine-polished via the use of standard FO polishing equipment. Polishing assures that all fiber ends are at the same plane and that no differential lengths or gaps exist between the various members of the bundle. The polished fiber bundle is then attached to the output fiber by: (1)

direct fusion via the use of a slightly modified commercially-available fiber fusion equipment, or (2) butt-coupling in conjunction with the use of UV-cement, or (3) lens coupling in conjunction with miniaturized SELFOC lenses, etc.

A hybrid Rx WDM TTD architecture uses RF coherent summation in place of the optical summation. A schematic of this approach is shown in Figure 11.2 for the case of 8 receiving elements. In this architecture, the E:1 optical combiner is completely eliminated and is substituted by an RF network that performs the addition. Here, the signals exiting from the BIFODELs and the no bias delay path are demultiplexed. The demultiplexed signals are then *individually* detected by a set of detectors the outputs of which are then added via K different E:1 RF combiners (where K is equal to the numbers of antenna elements). For the example of Figure 11.2 M is equal to 4 and E is equal to 2. The outputs of the RF combiners drive the DiBis.

A brief comparison of the two low-loss hybrid Rx WDM TTD approaches is as follows:

(1) The asymmetric optical combiner technique does not require extra fiberoptic or electronic hardware and is thus preferable. It will be adequate for array antenna operation from the UHF to 8-GHz. However, for frequencies above 8 GHz and large TTD networks, it starts losing its effectiveness. This is because the required DET sizes will be much smaller than the mutlimode fiber's cross-section, thereby increasing the system loss.

(2) The RF-summation is hardware-intensive. For small TTD networks, e.g., 4x4 or 6x6, the required extra hardware may be acceptable. For larger networks the extra hardware will not be acceptable. In these cases however, we can combine the asymmetric optical combiner and RF summation and extent the overall TTD dimension. Note that this approach has no frequency limits since commercially-available DETs and RF-combiners can operate well into the mm-wave ranges. An advantage of this approach is the fact that we have access in

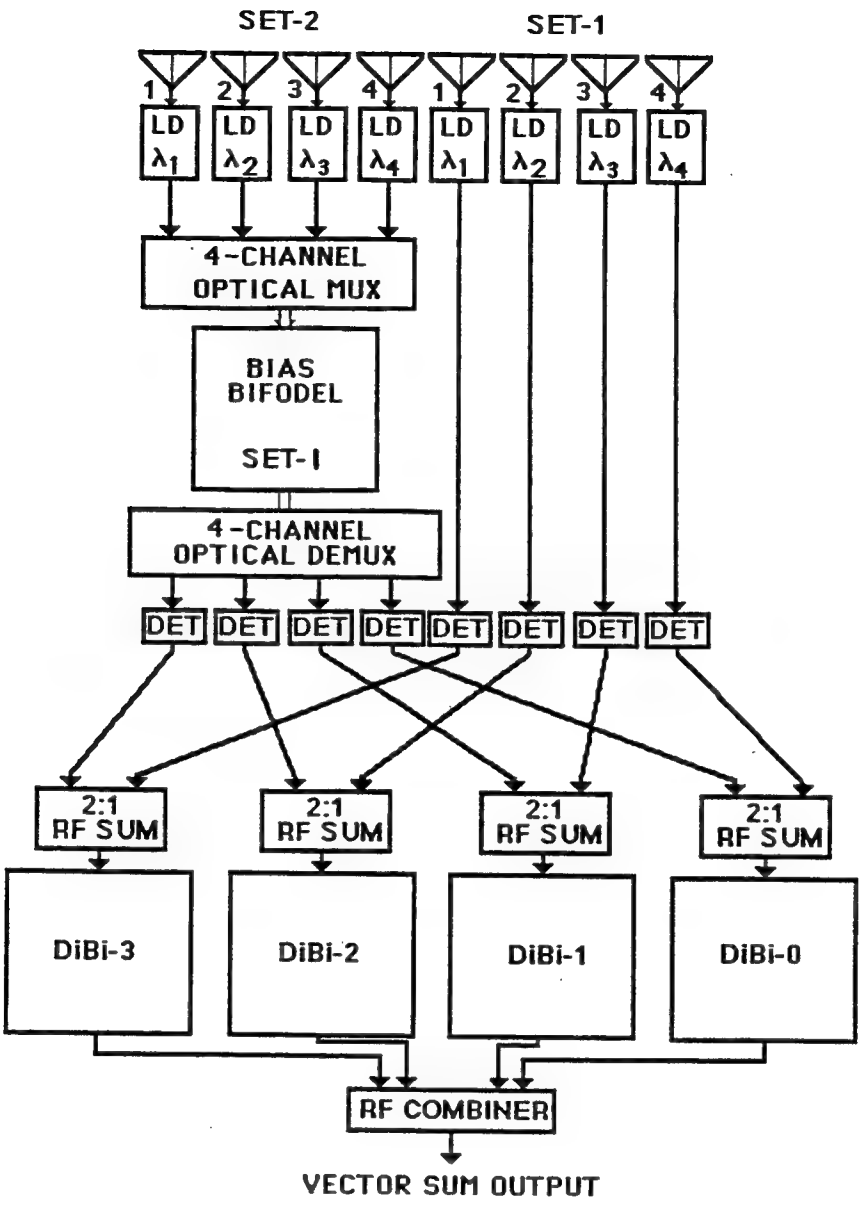

Figure 11.2 — Schematic of an 8-element hybrid WDM Rx TTD system employing RF summation.

each Rx channel and therefore we can perform functions such as (1) delay and amplitude corrections, and (2) adaptive beamforming.

For the current program, the decision was made jointly between Westinghouse STC and Rome Laboratory to use the RF summation approach. The main reason for this decision was the significantly lower cost involved as well as the much smaller time period required for its implementation.

11.2 Combined Tx-Rx hybrid WDM TTD Architecture With Optical Addition

As mentioned earlier, the asymmetric combiner-based Rx architecture is hardware efficient and therefore it is of interest to see how it could be combined with a Tx WDM TTD architecture in order to take advantage of "common" hardware. An example of such a combined system is shown in Figure 11.3 for the case of a PAA with 16 elements. It can be seen that two different switchable networks are used between the DiBis and BIFODELs. For the Tx mode, a 4x4 wavelength-independent star coupler is used (i.e., a 4x4 WIC). For the Rx mode a 4:1 asymmetric combiner in conjunction with a 1:4 multi-mode DMUX are employed. The two networks are switched depending on whether the PAA is in the Tx or Rx mode. Note that the switching is performed in the optical domain, prior to the BIFODELs, and via 4 1x2 optical switches. However, a second set of K optical switches is needed (for a K-element PAA) in order to switch the DET and LD of each PAA element into the TTD network. Also a set of $\sqrt{K}$ 1x2 RF switches is required to switch the DET-LD to the DiBis.

As Figure 11.3 shows, the key components of the system (DiBis, BIFODEL, and output-input MUX/DMUX devices) are common for both the Tx and Rx modes of the PAA. Therefore the desired goal, namely Tx and Rx with much common hardware is achieved. Note that extra RF switches are identical to those used for the DiBis and therefore they can be "implemented" on the DiBi itself. Similarly, the extra optical switches prior to the BIFODEL are identical to those within the BIFODEL and therefore they can be included within the

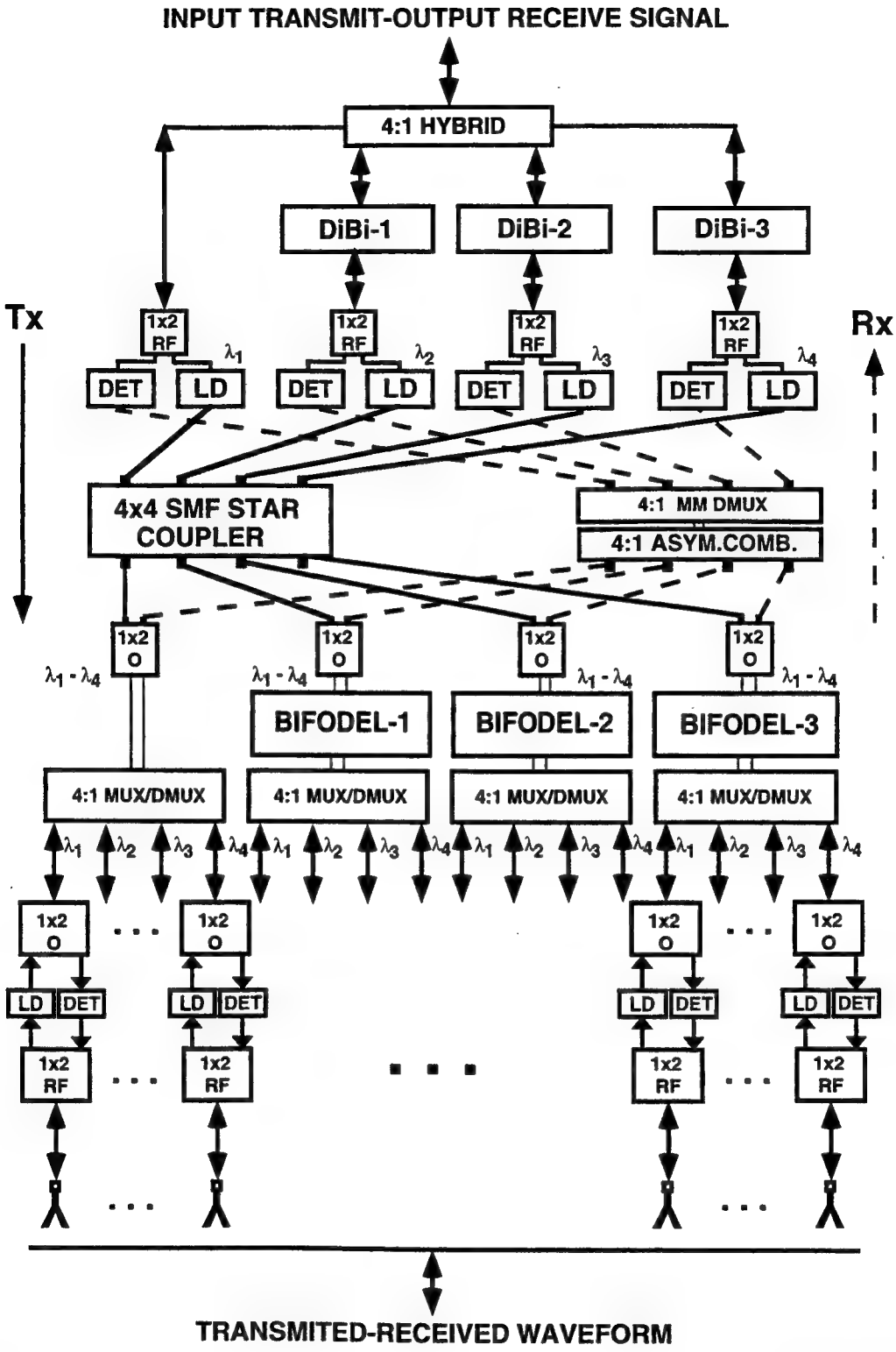

Figure 11.3 — Schematic of a combined low-loss Tx-Rx WDM TTD architecture for a 16 element PAA.

BIFODEL package. However, the optical switches within each PAA element are an issue, because they are expensive (>$1,000 a piece) and bulky (>1 in^3). Use of such switches increases the system cost dramatically. This problem can be eliminated if we use 1x2 fiberoptic combiners instead of a 1x2 switches. In this case the input of the combiner is connected to the MUX/DMUX output and the two outputs are connected to the output T/R module (one to the LD and one to the DET). Note that 1x2 fiberoptic combiners are passive, miniaturized low cost devices (under $20). However, they do have a fixed 3 dB loss (as compared with 1 dB for the best optical switches), which is the same for both division or combination modes because these devices are symmetric. This 3 dB loss is low enough to be accommodated in various system applications. Note that the 1x2 FO combiner solution can also be used in place of the 1x2 optical switches prior to the BIFODELs. However, because the total number of these switches is small ($\sqrt{K}$ for a K element PAA) and because they are located remotely from the antenna, their substitution may not be necessary.

11.3 Development of High Performance Rx Fiberoptic Links

For the 8-element Rx WDM TTD system the key component that must be developed is the receive FO link. This is because the required BIFODELs, associated MUXs, DiBis, and associated 4:1 RF combiner are identical to those required for the Tx system. For typical UHF-L band airborne surveillance radar TTD applications, the FO links must have the following characteristics: BW of 0.4-1.4 GHz, SFDR >70 dB-$MHz^{2/3}$, NF<3 dB, low phase error (<5° peak-to-peak across the band) and low amplitude ripple (<1 dB across the band). Developing low-cost FO links with the all the above characteristics is not an easy task. For example, the FO links we developed for the Tx WDM TTD prototype did satisfy the BW, SFDR, amplitude and phase errors, however, their NF was of the order of 20 dB. Such NF could be acceptable for Tx systems, however, it is absolutely unacceptable for the Rx mode.

In attempting to improve the link performance, we first designed and implemented several types of impedance matching networks between the input RF load and the LD. We found that such networks improve the NF somewhat but by no means they could result to NF of the order of 3 dB and maintain the wide BW. In view of this we switched to a much more complex LD driver approach involving a combination of passive-active driver. Using proprietary in-house developed CAD design, we designed and implemented several active and semi-active LD drivers. Unfortunately, due to time and budget constraints, we did not fully investigate several promising approaches. However, an all-active LD driver (consisting of a low cost, high SFDR gain block prior to the LD) did result in significant performance improvements; the overall link performance was well above the best performance published in the open literature for directly modulated CATV DFB LD-based fiberoptic links. Over a 0.2-2.5 GHz 3-dB BW the typical performance we achieved was: SFDR between 68-73 dB-$MHz^{2/3}$, NF~ 4.7 dB, phase error $<\pm 3^{\circ}$ and an overall link gain of about 15 dB. Over the 0.7-1.4 GHz BW of interest the amplitude ripple was below ±0.25 dB and the phase error was under ±1.7°. Figure 11.4 shows a network analyzer plot of the frequency response of the fiberoptic Rx active-driver link for a 2.3 GHz 3-dB bandwidth covering the 0.2-2.5 GHz band. Figure 11.5 shows a network analyzer plot of the frequency response of the fiberoptic Rx active-driver link for a 0.7 GHz 0.46-dB bandwidth covering the 0.7-1.4 GHz band. Finally, Figure 11.6 shows a plot of the phase error (i.e., deviation from linearity) of the FO link over the 0.7-1.4 GHz band. As Figure 11.6 indicates, the peak-to-peak phase error is 3.47°. Note that all 8 FO links had BW, amplitude and phase performance similar or better than that shown in Figures 11.4-11.6. However, their SFDR, NF, and gain performance did vary somewhat from link to link due (mostly) to LD performance variations. The specific values of SFDR, NF and gain for each of the 8 FO links we fabricated is shown in Table 11.2.

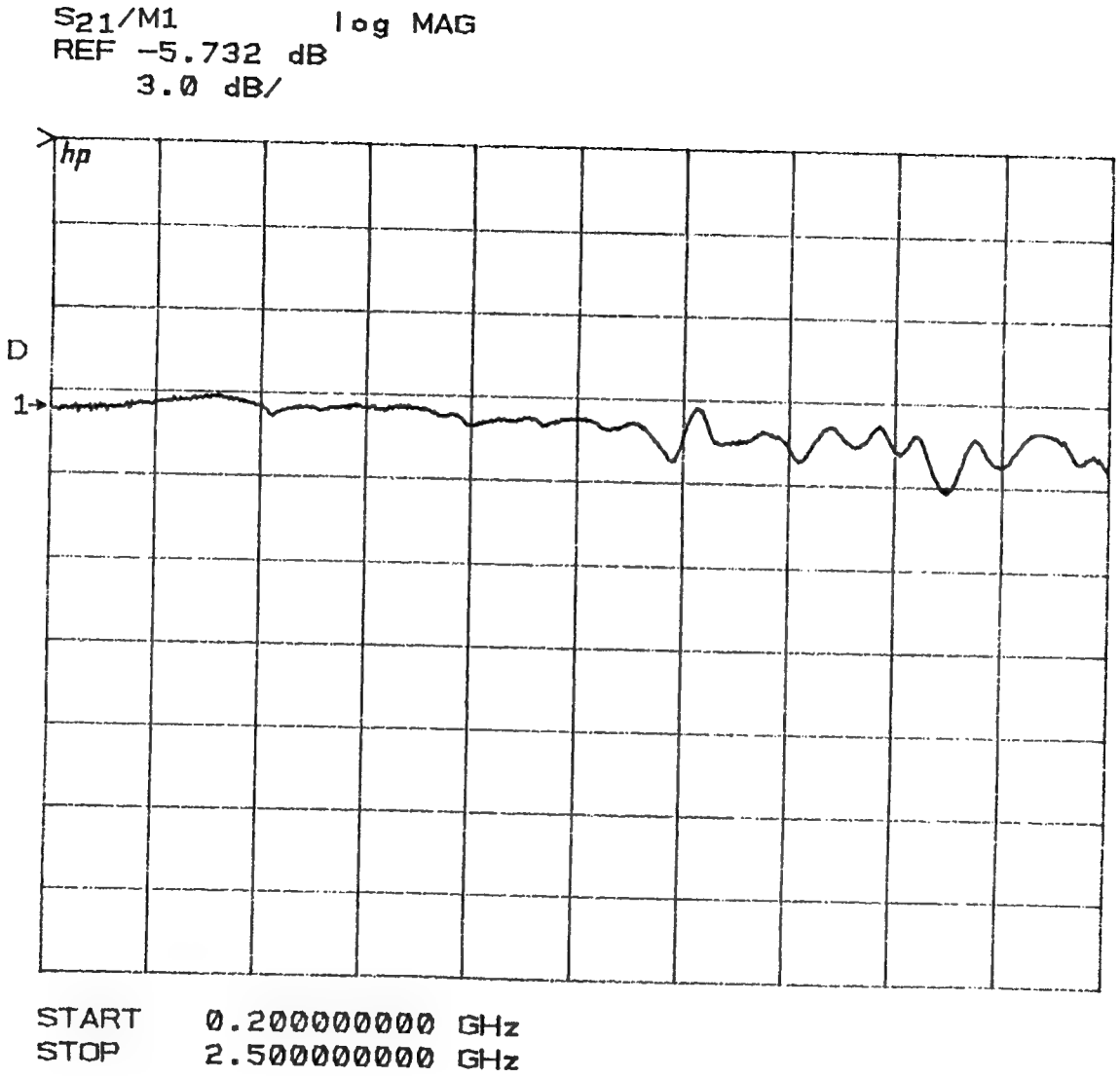

Figure 11.4 — Frequency response of the fiberoptic Rx active-driver link showing a 2.3 GHz 3-dB bandwidth covering the 0.2-2.5 GHz band.

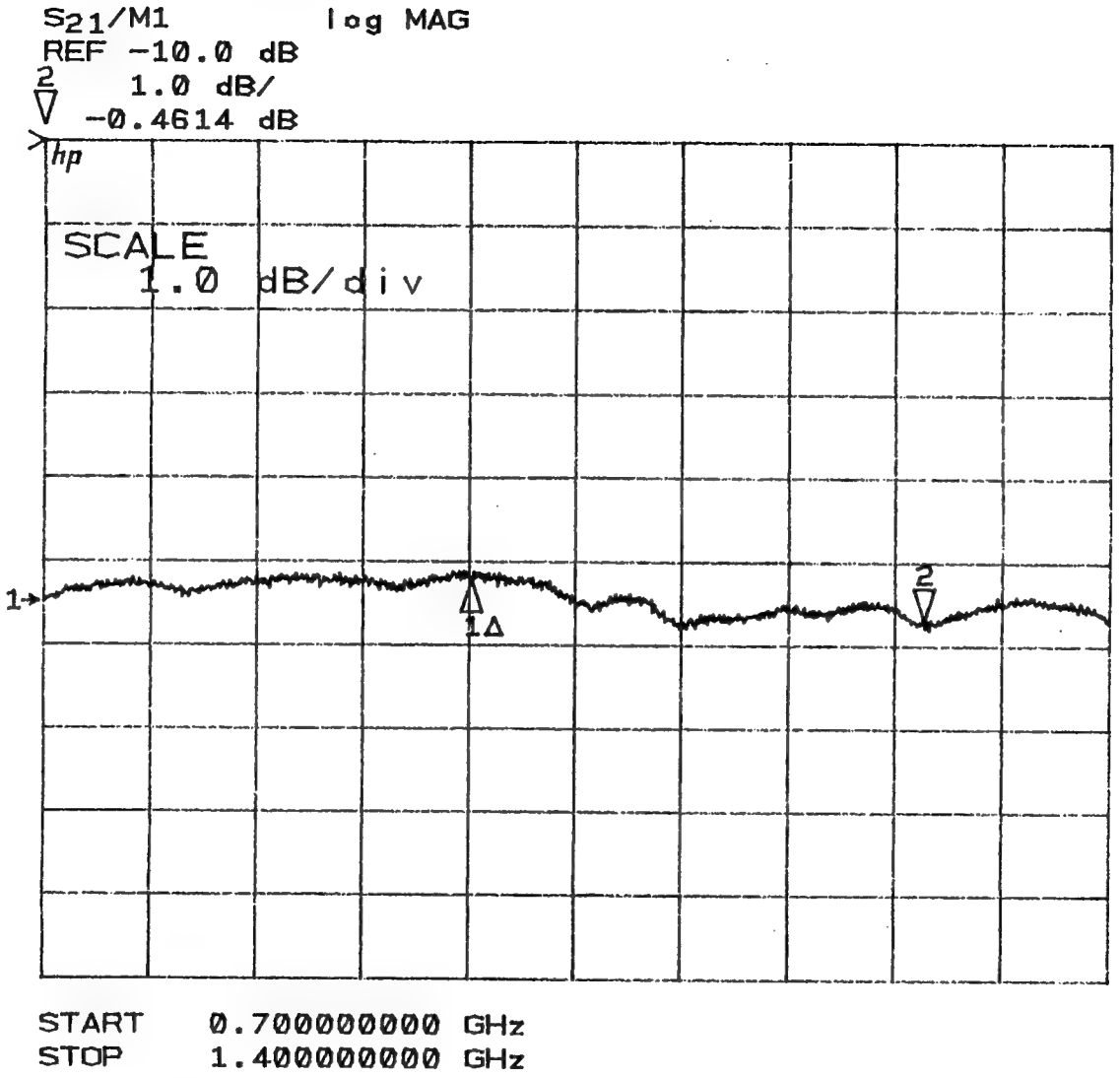

Figure 11.5 — Frequency response of the fiberoptic Rx active-driver link showing a 0.7 GHz 0.46-dB bandwidth covering the 0.7-1.4 GHz band.

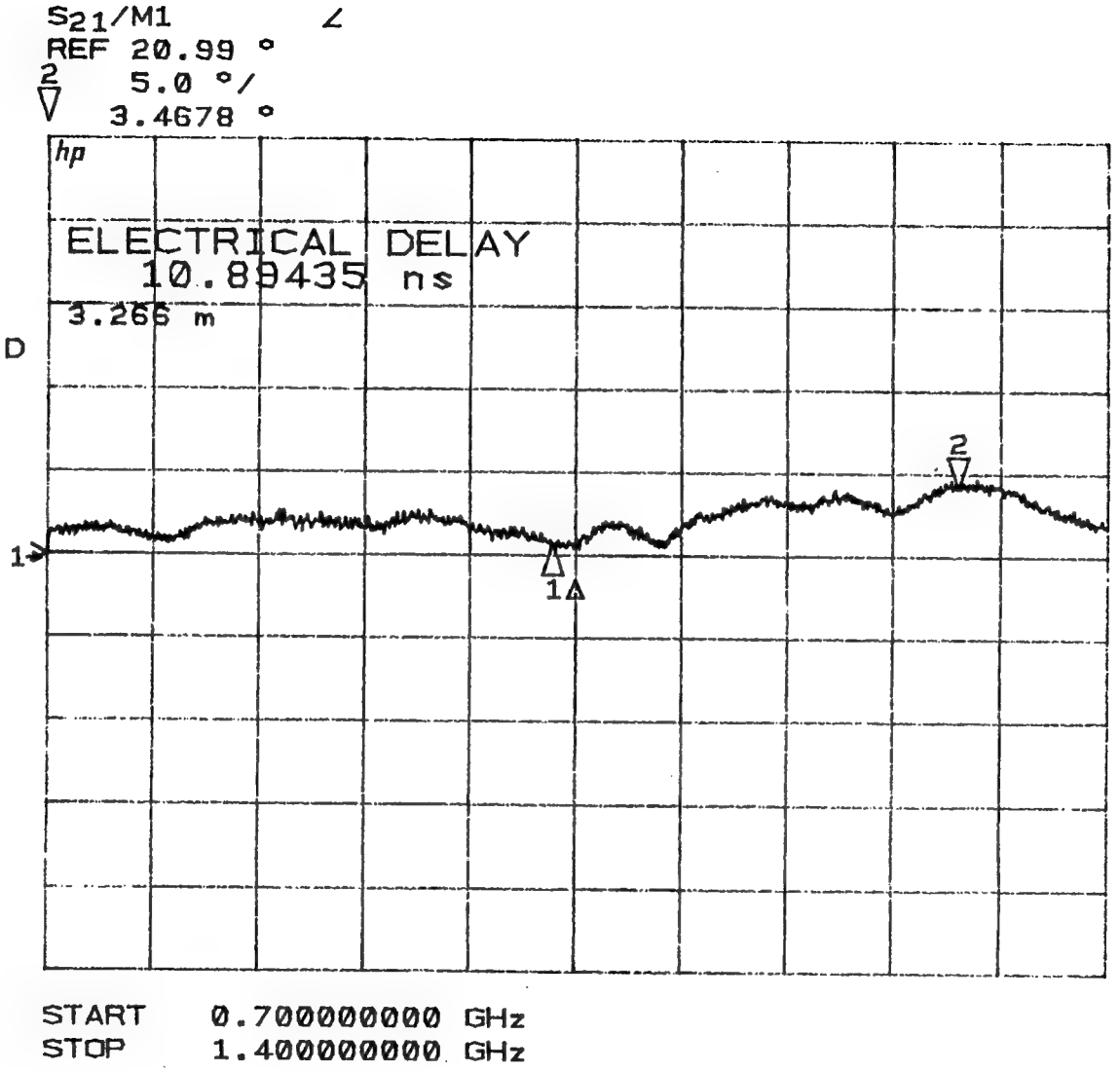

Figure 11.6 — Phase errors of the fiberoptic Rx active driver link over the 0.7-1.4 GHz band showing a peak-to-peak deviation of 3.47°.

TABLE 11.2 - SFDR, NF and gain for the 8 Rx fiberoptic links

Link #	SFDR (dB-MHz$^{2/3}$)	NF (dB)	Gain (dB)
1	68	5.2	15
2	73	4.7	17
3	67	4.7	15
4	68	4.7	15
5	69	5.8	14
6	70	4.7	17
7	73	4.2	17
8	67	5.2	15

Note that the above link performance was measured and verified several times during a 200 hour continuous laboratory testing. Each LD transmitter had (1) a network for temperature control of the LD module and (2) a feedback control network for regulating the LD current (these networks are similar to those used for the Tx WDM TTD prototype). The overall packaging of both the LD transmitter and DET receiver was also similar to that used for the Tx WDM TTD prototype.

In conclusion, the Rx FO links we developed have performance which is very near the performance required for future airborne surveillance systems. Specifically, the system requirements for BW, amplitude ripple, phase linearity and SFDR are satisfied whereas the NF is within 1.7 dB from the goal of 3 dB. Since we have explored only 50% of our active and semi-active drivers "ideas", we firmly believe that the NF can be improved to reach the goal of 3 dB. Furthermore we believe that this can be achieved with COTS electronic and optoelectronic components.

11.4 Binary Fiberoptic Delay Lines (BIFODEL) Selection

The 8-element Rx WDM TTD prototype requires the use of a single BIFODEL (see Figure 11.2). To match the required delays, we selected BIFODEL#1 from the Tx WDM TTD prototype. BIFODEL#1 was tested for over 100 hours and no performance degradation was found.

11.5 Binary Electronic Delay Lines (DiBi) Selection

The 8-element Rx WDM TTD prototype requires the use of all 3 DiBis (see Figure 11.2). These 3 DiBis were tested for over 100 hours and no performance degradation was found.

11.6 MUX/DMUX Selection and Temperature Control

As mentioned earlier in this report, the MUX/DMUX devices were sensitive to temperature variations. In view of this we decided to measure their response as a function of temperature with the objective of identifying the "appropriate" temperature range for good, stable performance. To accomplish this we assembled a small, temperature-controlled oven in which each of the 4 MUX/DMUX devices could be tested for temperatures above room temperature. Each of the DMUX outputs was monitored (for 100s of hours) in a spectrum analyzer and the overall output power was monitored as a function of temperature. The results of this test are shown in Table 11.3. As Table 11.3 shows, the performance of the 4 MUX/DMUX devices varies significantly with temperature. For the Rx WDM TTD prototype we require two such devices (see Figure 11.2) and thus we selected devices #1 and #3 because of their superior performance. (Device #3 was used prior to the BIFODEL and device #1 was used after the BIFODEL).

TABLE 11.3 - MUX/DMUX output variation (in dB RF) as a function of temperature

Temperature (°C)	Device #1 (dB RF)	Device #2 (dB RF)	Device #3 (dB RF)	Device #4 (dB RF)
<25	0	0	±0.2	±0.2
27	±0.2	±0.2	±0.3	±1.8
29	±0.5	±0.4	±0.3	±2.5
31	±0.6	±1.2	±0.4	dead
34	±1.2	±3.5	±0.4	dead

In addition, we designed and implemented a miniature heater on which we placed both MUX/DMUXs. The heater was used to stabilize the device temperature to +29° C. Thus, as long as the ambient temperature was at or below 29° C, the variation at the MUX/DMUXs outputs was virtually zero. The combination of device selection and heater, kept the overall output variation minimal (overall it was found to be significantly better than that of the Tx WDM TTD prototype). For temperatures below 29° C we measured an RF-equivalent loss of 5.6 dB per device, for a total of 11.2 dB for the MUX/DMUX combination.

11.7 Optical Isolator

Although all DFB LDs we used have an integral 30 dB optical isolator within their package, we still observed some reflections between the MUX device and the BIFODEL (Figure 11.2). To eliminate these reflections we used a single wide band isolator with at least 42 dB isolation over the 1301-1322 nm. The isolator was made by DiCon Fiberoptics, model IS-1310-A-F-N-P. This isolator was connected between the MUX and BIFODEL and completely eliminated the reflection problem. The penalty paid was a loss of ~0.6 dB optical (1.2 dB RF).

11.8 Electronic Attenuators For Amplitude Control

As Figure 11.2 shows, only 4 of the 8 channels go though a BIFODEL, and consequently, only 4 channels experience switching losses. These losses are dynamic, i.e., they vary as a function of the switch program. This is because in a 2x2 switch we can equalize only 3 of the 4 possible signal outputs and therefore at least one state will be different from the others. This problem is compounded by the fact that seven 2x2 switches are used for the 6-bit BIFODEL. For the Tx system, we equalized the BIFODELs relative to each other, i.e., we would accept variation as a function of the switch program, but, the variation would be the same from BIFODEL to BIFODEL. The 4 non-delayed channels were handled via the use of a single programmable optical attenuator which was adjusted as a function of the switch program dynamically (i.e., via the use of a PROM). For the Rx system that employs RF summation (see Figure 11.2) a single optical attenuator cannot work simply because there are 4 non-multiplexed channels. We solved this problem by using 4 in-house made electronic digital programmable attenuators. Each attenuator was connected at the DET output behind each non-multiplexed channel. These attenuators had a 4-bit resolution (0.5 dB, 1 dB, 2 dB, and 4 dB) for a total attenuation range of 7.5 dB. This range is wider than the BIFODEL variation range which is ~6 dB. The attenuators were made using COTS components. In particular, we used 1x2 FET switches identical to those used in the DiBis. The attenuator design incorporated delay and amplitude equalization for the various attenuation stages. Each attenuator was tested for BW, phase linearity, delay and amplitude equalization, and attenuation. The attenuators' performance was found to be excellent, and overall *transparent* to that of the remaining system.

11.9 Taper Implementation

For the Rx WDM TTD prototype, the taper we used was a 35-dB Chebyshev. For this tapper, the ideal relative powers of the 8 elements are as

follows: -16 dB, -7 dB, -2 dB, 0 dB, 0 dB, -2 dB, -7 dB, -16 dB. This tapper was implemented at the detector outputs as follows. First, we measured the relative RF power at each channel for a fixed RF input at the reference frequency of 1 GHz. Next we assigned the weakest channels towards the outer antenna elements were the required relative attenuation is large. The difference between actual and required attenuation was covered via the use of fixed RF attenuators located at the DET outputs. The overall precision in implementing the tapper was ± 1 dB which reduced the tapper effectiveness to about -30 dB.

11.10 Rx WDM TTD System Integration

The prototype system was assembled in a way similar to that described for the Tx system. Figure 11.7 shows a photograph of the prototype system undergoing laboratory testing. The 8 LD modules and the fiberoptic manifold are shown at the right of the photograph whereas the remaining system is shown at the left.

The system was packaged on the Tx WDM TTD prototype's chassis. The DiBis, their output 4:1 RF combiner, and the BIFODEL were placed at the same locations used for the Tx prototype. Above the plate housing the BIFODEL we mounted another plate on which we placed: (1) the MUX/DMUXs and their temperature controller, (2) the optical isolator, and (3) all the splices between: (i) the 4 fibers of the multiplexed part of the FO manifold, and (ii) the splices between MUX-isolator, isolator-BIFODEL, BIFODEL-DMUX and DMUX-detectors. On top of this plate we mounted another plate on which we placed: (i) the 8 detectors, (ii) the 4 programmable attenuators, and (iii) the 4 RF combiners (top level in Figure 11.7). Note that the detector board was made in a way similar to that described for the output modules of the Tx prototype. The detector and its board were housed in small aluminum boxes, the outputs of which were connected to the programmable attenuators via SMA connectors. The attenuators' outputs were directly connected to the RF combiners. The 4

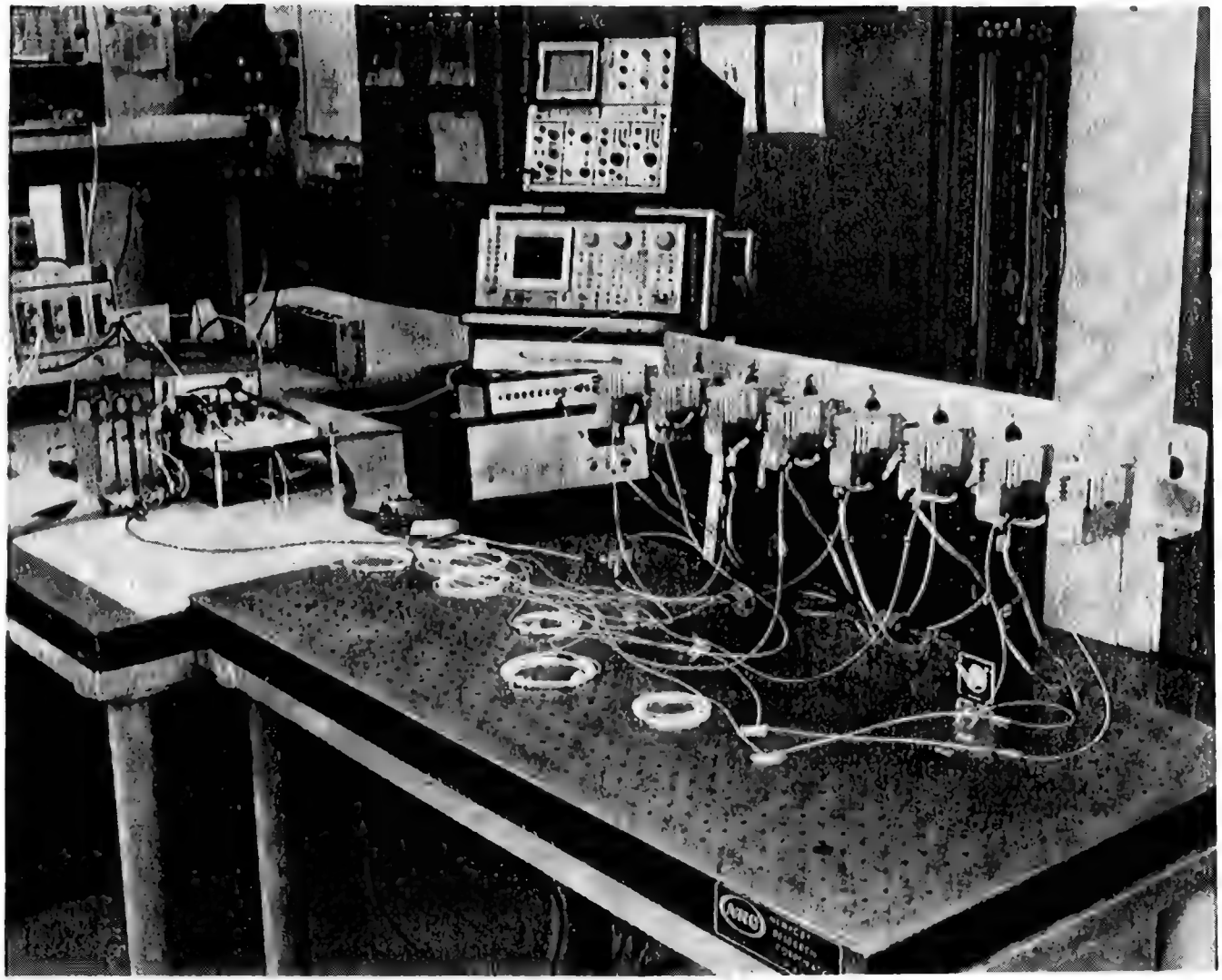

Figure 11.7 — Photograph showing the assembled Rx WDM TTD prototype undergoing testing in the Laboratory. The 8 LD modules for the receive modules and the FO manifold are shown to the right. The TTD system is shown in the left whereas the integrated power supply is shown in the middle.

outputs of the RF combiners were connected to the DiBis via precisely-cut coaxial cables. The DiBi outputs were connected to the output 4:1 RF combiner in a similar fashion.

11.11 Power Supply Integration

The power supplies for the full system were integrated in a single box shown in the center of Figure 11.7. This integrated power supply consists of two boxes mounted on top of each other. The bottom box contains the power supplies for: (1) the LD modules (LD current, LD driver, feedback control circuit, and LD cooler), (2) the detector modules, (3) the MUX/DMUX heater and control network, and (4) the programmable attenuators. The top box contains the power supplies for: (1) the DiBis, and (2) the BIFODELs. All power supplies were designed and fabricated in-house using low cost COTS components mainly form the PC Computer market. Prior to their use, the power supplies were tested for over 200 hours to ensure appropriate and sustainable performance.

11.12 Rx WDM TTD System Laboratory Testing

In addition to the various tests already described, the prototype Rx WDM TTD system was subjected to several other tests prior to the antenna range demonstration. A description of these tests follows.

(a) MUX/DMUX response as a function of temperature. For this test each of the 4 LD channels that correspond to the multiplexed part of the prototype system was driven by a different frequency but fixed power CW signal. The system response prior to the DiBis was observed on a spectrum analyzer while the ambient temperature was changed via the use of room heaters. As expected, for temperatures us to +28° C the RF power variation was insignificant. However, when the temperature was raised to about +30° C the differential RF power variation was increased to about 2.5 dB.

(b) Relative delay measurement. This test was performed for the purpose of testing the relative timing errors from the LD inputs to the DET outputs when the system was "looking" at 0° angle. We assigned channel #1 as the reference channel and we measured the relative delay for all remaining 7 channels. In all cases the relative timing errors were found to have a standard deviation similar to that of the BIFODELs, i.e., σ~1.45 ps. Next we measured the relative delays from the 2:1 RF combiners to the DiBi outputs. Again we found that the performance was acceptable with a σ~1.45 ps.

(c) Amplitude uniformity and tapper verification. In this test we measured the amplitude response of the full system (i.e., from each LD input to the 4:1 RF combiner's output) relative to element #4 (note that elements #4 and #5 are equal to each other and contribute most of the power to the system's output) via the use of a network analyzer. Figures 11.8 and 11.9 show the response of elements #5, #6, #7, and #8 relative to element #4 over the 0.6-1.6 GHz band. As these figures show, the relative "ripple" response is excellent: elements #4 and #5 are similar to within 0.5 dB, elements #4 and #6, #7 are similar to within 1 dB, and elements #4 and #8 are similar to within 1.5 dB over the entire 0.6-1.6 GHz band. Similar results were obtained for elements #1, #2, and #3. Note that Figures 11.8 and 11.9 also show the effects of tapering: elements #4 and #5 have the same power level, element #6 is 2 dB below #4 and #5, element #7 is 7 dB below #4 and #5 and element #8 is 16 dB below #4 and #5. Again, similar results were obtained for elements #1, #2, and #3.

(d) System insertion loss. The system IL was measured for the middle two elements (#4 and #5) for several look angles and was found to be IL=-27.4 dB $\pm$ 3 dB. The variation is due to the BIFODEL's switches which, as explained earlier, have an IL that varies up to 1 dB (per switch) for the 4

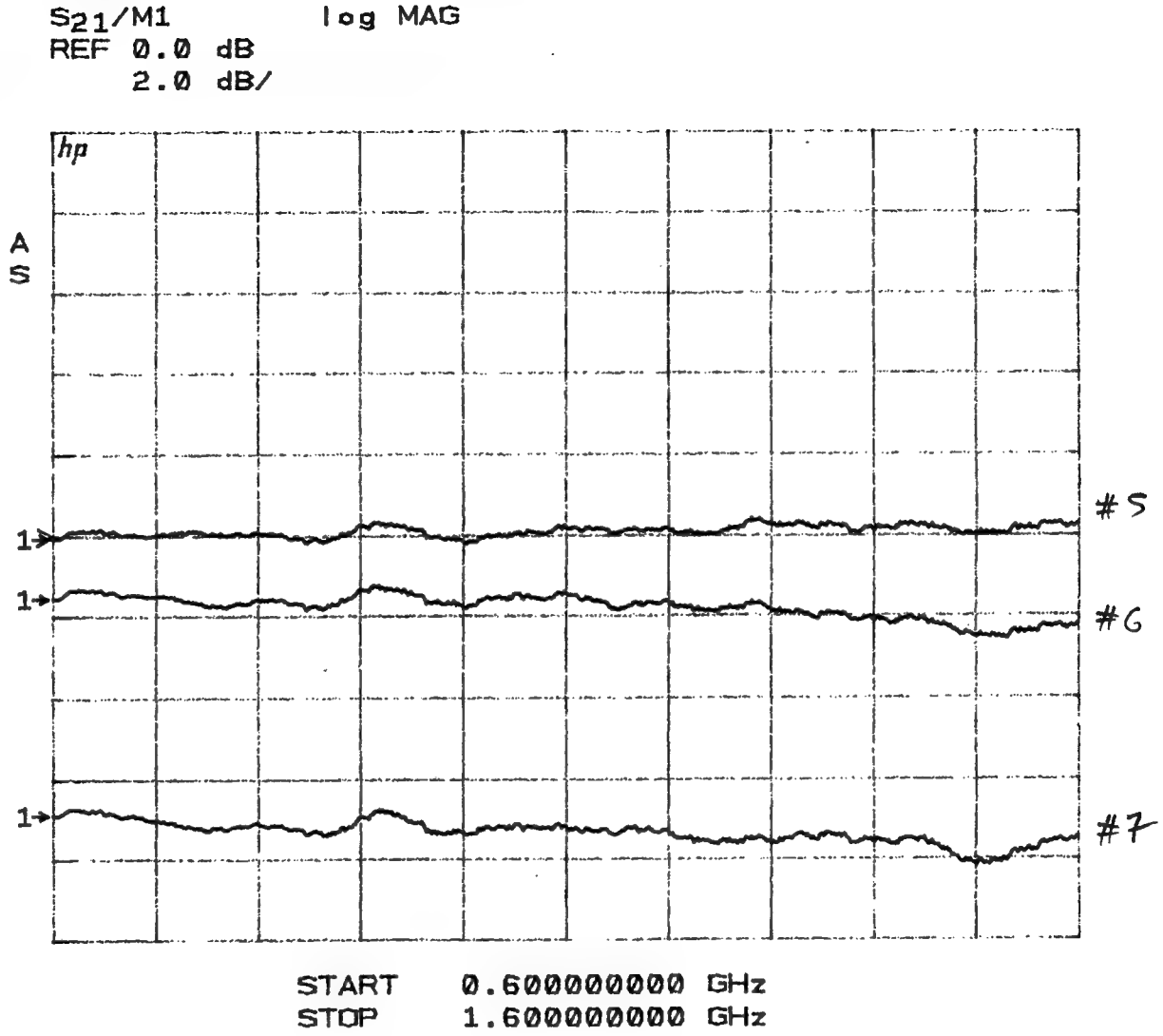

Figure 11.8 — Output response of elements #5, #6, and #7 relative to element #4 over the 0.6-1.6 GHz band (2dB scale).

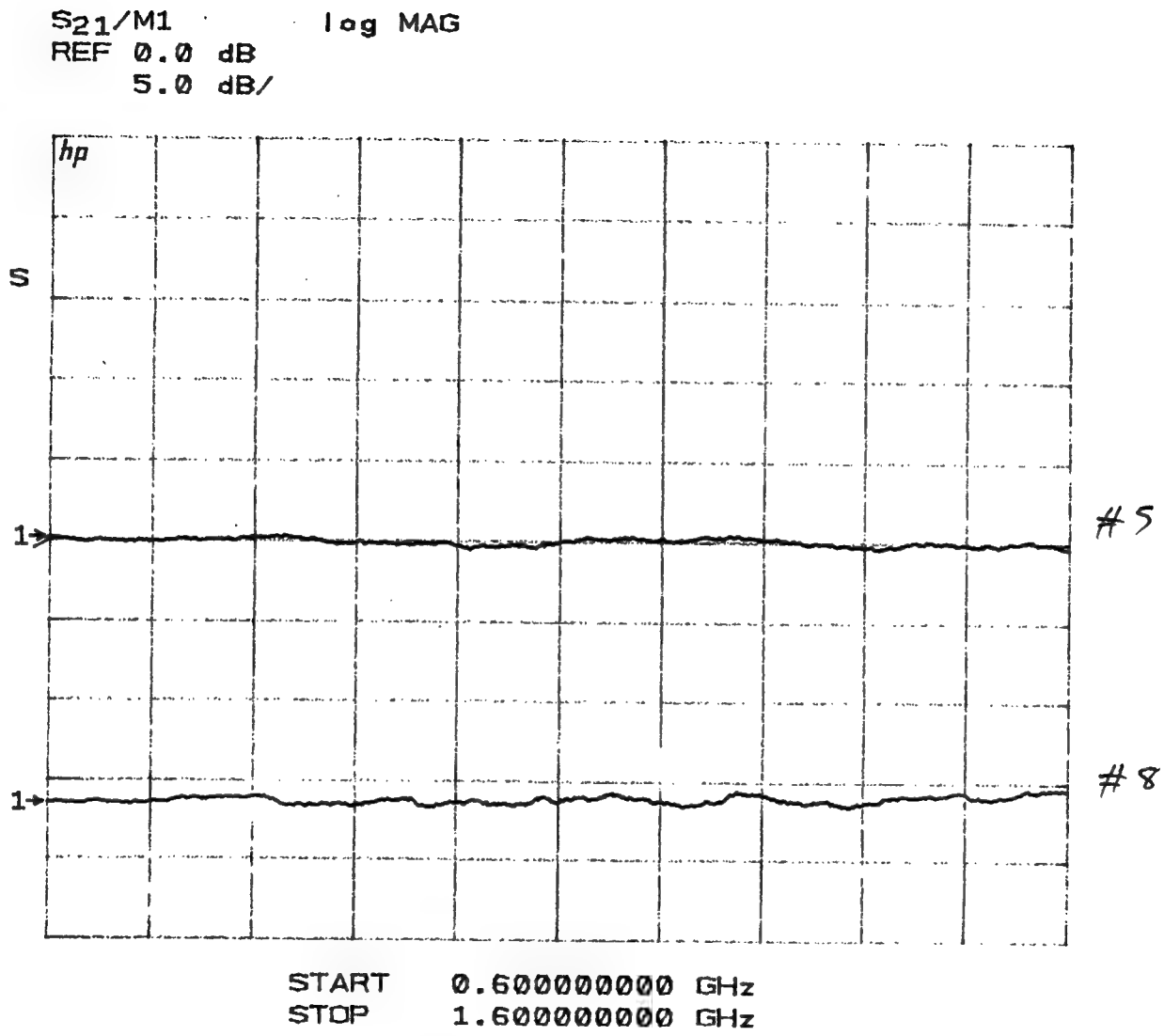

Figure 11.9 — Output response of elements #5, and #8 relative to element #4 over the 0.6-1.6 GHz band (5 dB scale).

switch output combinations. The -27.4 dB is due to the following components (all dBs are in RF): FO link =+ 15 dB, MUX/DMUX=-11.2 dB, Isolator=-1.2 dB, BIFODEL (average)=-21 dB, RF combiners' excess loss = -3.0 dB, and DiBi=-6 dB (i.e. the system optical loss was -33.4 dB and the RF loss was - 9 dB). The IL of the other elements can be found by simply adding the tapper loss to the -27.4 dB IL figure. Note that the 1 dB compression point for each FO link was also measured and it set the maximum RF input power to the system. For the 8 links the 1 dB point was in the range of -23 to -27 dBm, and thus for safe operation, we set the 1 dB compression point of the full system to -27 dBm. In practice however, we routinely operated with input RF levels no higher than -30 dBm.

(e) Coherent gain test. To perform this test we first set the system at 0° look angle and then excited *symmetric* system inputs by two CW signals which were equalized in both time and amplitude. By observing the system output on a spectrum analyzer for single channel excitation and for dual channel excitation, we were able to observe coherent gain. Table 11.4 shows the results obtained for an input power level (per channel) of -41.2 dBm.

TABLE 11.4 - Examples of system output for coherent gain test

Channel	Channel Output (dBm)	Sum Output (dBm)	Coherent Gain (dB)
4	-68.6	-62.8	5.8
5	-68.6	-62.8	5.8
3	-70.6	-65.1	5.5
6	-70.6	-65.1	5.5
2	-75.6	-70.0	5.4
7	-75.6	-70.0	5.4
1	-84.6	-79.9	5.3
8	-84.6	-79.9	5.3

As Table 11.4 shows there is clearly coherent gain for symmetrical pairs of system inputs. For the case of the two strongest inputs (#4 and #5) the gain is very close to the theoretical limit (5.8 vs 6.0 dB). Note that the deterioration of gain towards the outer elements is due to the low output level relative to the noise floor of the spectrum analyzer.

(f) Long term operation test. To ensure that most "near term" problems have been identified and eliminated, we operated the system in a CW mode for several 100s of hours. Every other day we measured the coherent gain of each symmetric pair of channels to verify proper operation. With the exception of one bad DiBi switch (which was replaced) no other problems were found.

11.13 System SFDR and NF analysis

As mentioned earlier, a practical, ready-for-system insertion Rx TTD system must satisfy several requirements including low NF (e.g., < 3 dB) and high SFDR (e.g., >70 dB-MHz$^{2/3}$). For our WDM TTD system, there are 3 key factors that influence the overall NF and SFDR: (1) DiBis, (2) FO links, and (3) system IL (not including FO links and DiBi loss). It is of interest to examine the effects of each of these factors onto the system NF and SFDR. A simple way to examine these effects is via a microwave analysis program such as the HP AppCAD. In this program, the user describes different system parts via their NF, gain, and 3rd order intercept point (IP3), and the program calculates the combined effect in terms of system NF, SFDR, SNR, gain, etc.

First, let us examine the performance of the FO link cascaded to a DiBi (i.e., no optical loss is assumed). For this analysis we will use the *average* performance obtained with the FO links and DiBis. Thus, for the FO link we will assume: NF=4.7 dB, gain=15 dB, IP3=9 dBm (corresponds to a SFDR of 69 dB-MHz$^{2/3}$). For the DiBi we will assume: NF=6 dB (this is equal to its IL),

gain=-6 dB and IP3=35 dBm (corresponds to a SFDR of 95 dB-$MHz^{2/3}$). The results of the AppCAD are shown in Figure 11.10 and demonstrate that, as expected, the DiBi effect on the system performance is minimal: the system NF is 4.84 dB and the system SFDR is 68.8 dB-$MHz^{2/3}$. Note that these small effects can be reduced via the use of a LNA prior to the DiBi.

Next we examine the performance of the FO link and the DiBi with a 28 dB (RF) loss "optical component" inserted in-between. Note that for simplicity, we will approximate the lossy optical component as an RF attenuator with the equivalent RF loss, located at the link's output. For our purposes this approximation is acceptable, however, for an accurate analysis, the optical loss must be taken into account *within* the FO link. The results of this analysis are shown in Figure 11.11. As expected, the overall system performance has greatly deteriorated: the NF is increased to 19.16 dB and the SFDR is decreased to 59.2 dB-$MHz^{2/3}$. This shows the *dramatic* effect that the optical loss could have on the system performance. The loss of system NF and SFDR as a function of optical loss (in dB RF) is shown in Figure 11.12. For that plot we have assumed FO links and DiBis with *average* performance. It can be seen that even modest optical loss (i.e., 5 dB optical) quickly deteriorates the system performance. For the actual prototype, the optical IL was 27.4 dB ± 3 dB, and thus the actual Rx WDM TTD system NF and SFDR are: >18 dB and <60 dB-$MHz^{2/3}$ respectively. Actual system NF and SFDR measurements in the laboratory have confirmed the above performance to within ± 2 dB.

The implication of the above results is very significant: *a high performance photonic TTD system must have minimal optical insertion loss and its overall performance cannot be better than that of the FO links involved.* For our WDM TTD system "minimal optical insertion loss" translates to optical loss reduction at all levels: BIFODELs, MUX/DMUX, and optical combiner. Possible solutions include: (i) use of an optical amplifier between the BIFODEL output and the DMUX input, (ii) use of very low loss asymmetric combiners and multi-mode

Hewlett-Packard	NoiseCalc	AppCAD

		1	2
Noise Figure	(dB)	4.70	6.00
Gain	(dB)	15.00	-6.00
IP3	(dBm)	9.00	35.00
δNF/δTemp	(dB/ºC)	0.000	0.000
δG/δTemp	(-dB/ºC)	0.000	0.000
System Temp.	(ºC)	25.0	
Input Power	(dBm)	-40.0	
Pout	(dBm)	-25.0	-31.0
δ NF/δ NF (Stage)		0.97	0.05
δ NF/δ G (Stage)		-0.03	0.00

Reference Temperature	(ºC)	25.0
Noise Bandwidth	(MHz)	1.00000

Cascade NF	(dB)	4.84
Noise Temperature	(ºK)	593.2
Signal-to-Noise Ratio	(dB)	69.2
Spur Free Dynamic Range	(dB)	68.8
Nominal Detectable Sig	(dBm)	-109.1

Cascade Gain	(dB)	9.00
Input Intercept Point	(dBm)	-6.0
Output Intercept Point	(dBm)	3.0
IM3 Output Level	(dBm)	-99.0

[F2]Compute [F4]Add Stage [F5]Print [F7]Erase [Esc]Exit

Enter 1st-stage Noise Figure in dB (at Reference Temperature)

Figure 11.10 — AppCAD output for the fiberoptic link and DiBi cascade.

Hewlett-Packard NoiseCalc AppCAD

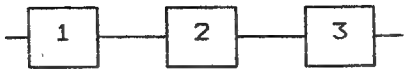

		1	2	3
Noise Figure	(dB)	4.70	28.00	6.00
Gain	(dB)	15.00	-28.00	-6.00
IP3	(dBm)	9.00	200.00	35.00
δNF/δTemp	(dB/ºC)	0.000	0.000	0.000
δG/δTemp	(-dB/ºC)	0.000	0.000	0.000

System Temp.	(ºC)	25.0	
Input Power	(dBm)	-40.0	
Reference Temperature	(ºC)		25.0
Noise Bandwidth	(MHz)		1.00000

		1	2	3
Pout	(dBm)	-25.0	-53.0	-59.0
δ NF/δ NF (Stage)		0.04	0.26	0.97
δ NF/δ G (Stage)		-0.96	-0.70	0.00

Cascade NF	(dB)	19.16	Cascade Gain	(dB) -19.00
Noise Temperature	(ºK)	23592.2	Input Intercept Point	(dBm) -6.0
Signal-to-Noise Ratio	(dB)	54.8	Output Intercept Point	(dBm) -25.0
Spur Free Dynamic Range	(dB)	59.2	IM3 Output Level	(dBm) -127.0
Nominal Detectable Sig	(dBm)	-94.8		

[F2]Compute [F4]Add Stage [F5]Print [F7]Erase [Esc]Exit
Enter 1st-stage Noise Figure in dB (at Reference Temperature)

Figure 11.11 — AppCAD output for the fiberoptic link, optical loss, and DiBi cascade.

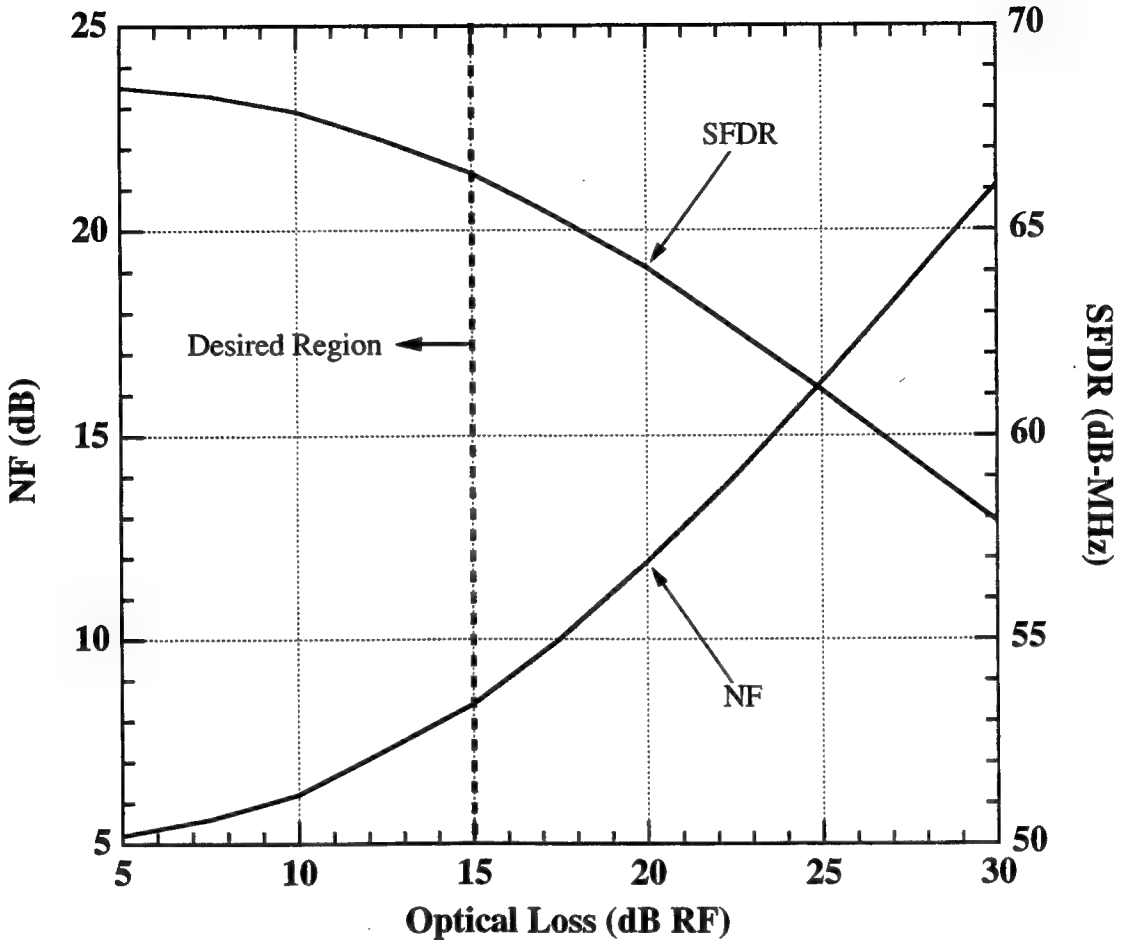

Figure 11.12 — Plot of the system SFDR and NF as a function of the system optical insertion loss (in dB RF).

DMUX, and (iii) use of transimpedance amplifiers at the detector output. In addition, low loss optical switches are necessary along with improved performance FO links.

12. Rx WDM TTD SYSTEM ANTENNA RANGE DEMONSTRATION

Upon completion of the prototype Rx WDM TTD system fabrication and laboratory testing, we proceeded with the demonstration at the antenna range. The antenna used was the same as that described in Section 10.1. The overall set-up as well as the type and method followed for each experiment was also similar with that described in Sections 10.1-10.2, with the difference being that the 2x4 element notch array which was used for transmission (rather than reception as for the Tx WDM TTD demonstration). In general, we operated the system outdoors, continuously for over 24 hours and with ambient temperatures exceeding (at times) 30° C. However, all our data were obtained during the morning and early evening when the ambient temperatures were below 29° C. This ensured that the MUX/DMUX temperature was kept at +29° C which in turn ensured that the overall system was working properly. In general, no serious problems were observed. Note that the RF power at the output of each receiving element (i.e., the RF power at the input of each LD module) was calculated to be -35.9 dBm (we arrive to this figure by using the following values: generator output power: 0 dBm, power amplifier gain: 35.5 dB, loss for a 231 ft coaxial cable: -27 dB, transmitter gain: +16.5 dB, space loss (192 ft propagation): -69.39 dB and Rx element gain: 8.4 dB).

Figures 12.1 and 12.2 show two views of the antenna range set-up including: (1) the 16-element PAA with the middle 8 elements driven by the Rx WDM TTD prototype, (2) the prototype Rx WDM TTD system (on top of the white cooler), (3) the fiberoptic manifold connecting the WDM TTD system and the PAA (white thin lines), (4) the integrated power supply (to the front of the white cooler), (5) the three-axis rotary positioner (under the PAA), and (6) the 4

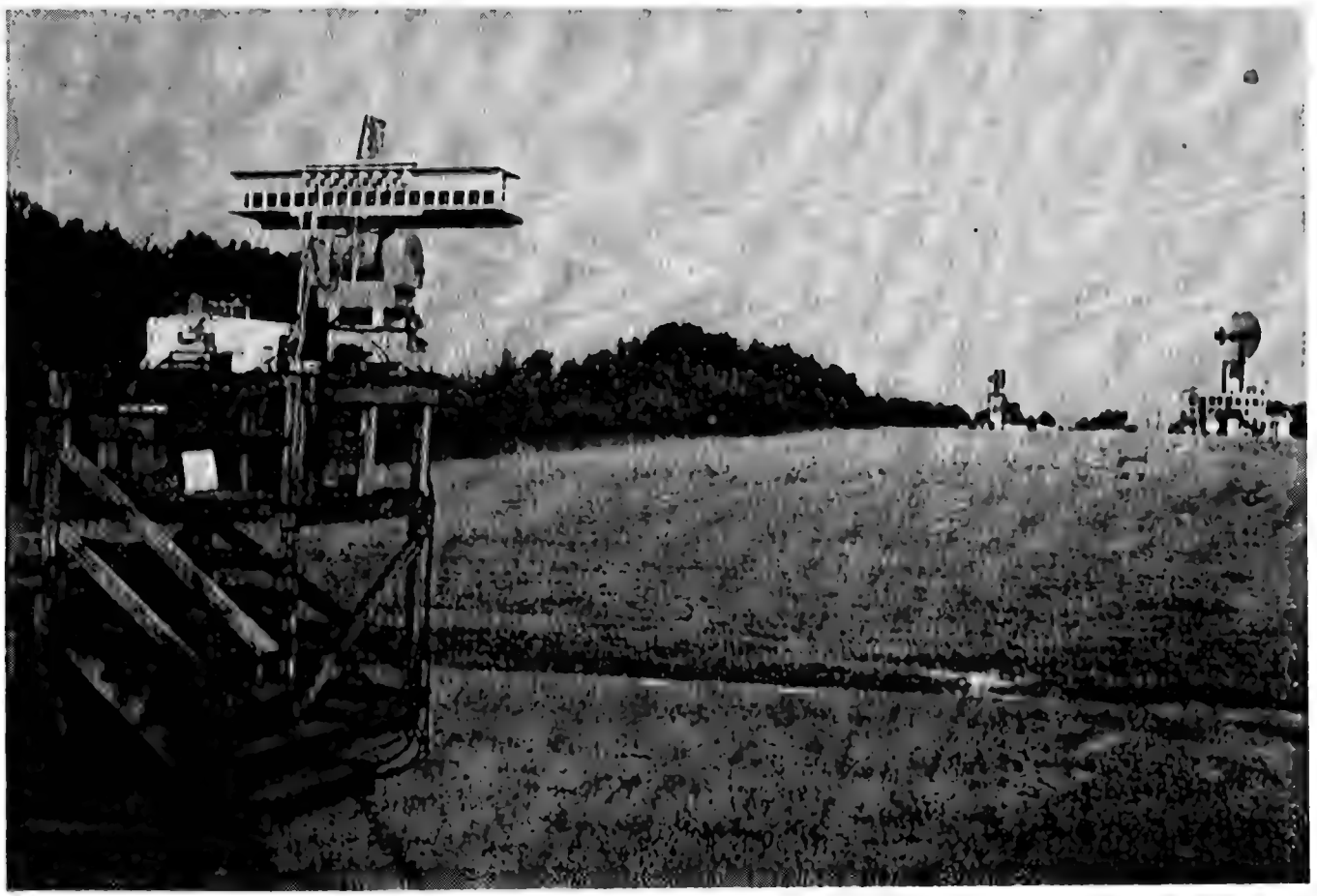

Figure 12.1 — Antenna-range setup showing the 8-element Rx WDM TTD-driven PAA mounted on a three-axis rotary positioner and the 4 element matching transmitter (middle right).

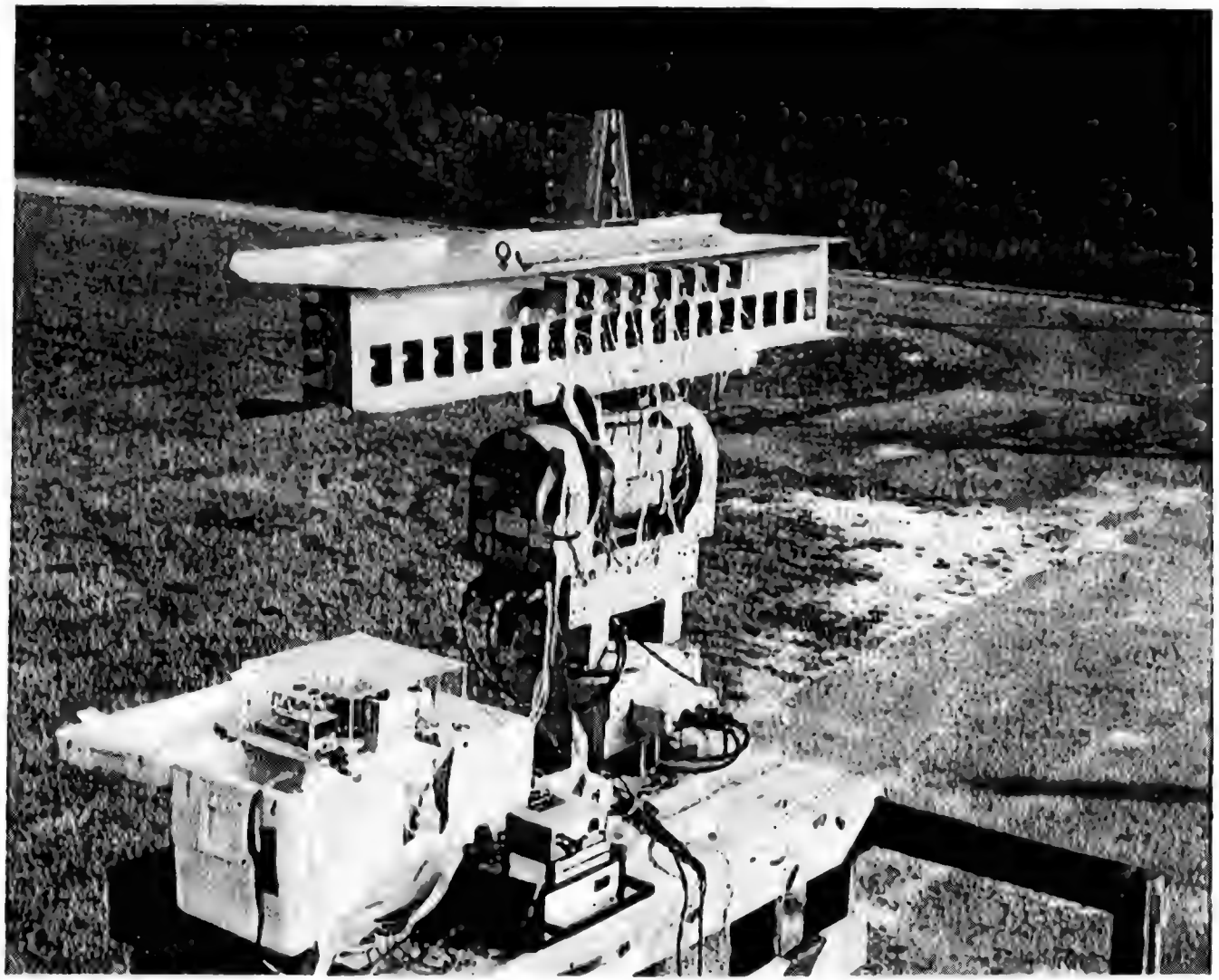

Figure 12.2 — Close-up view of the receiving PAA driven by the photonic Rx WDM TTD system.

element matching transmitter (far right in Figure 12.1 only). As Figure 12.2 shows, the LD modules were connected via L-type brackets directly on the antenna and above the radiating elements. Each interconnection between an LD module and a radiating element consisted of an in-house made coaxial cable (~1.5 ft length) and a small mechanical coaxial delay line (~50 psec total delay) which was used to equalize the delays between radiating elements and LD modules. This was accomplished via the use of the MTUNE program with the antenna receiving from the boresight.

The first experiment we performed was that of broadband reception as a function of angle (i.e., proof of the Rx TTD operation). Figure 12.3 shows squint-free antenna patterns for steering at the -42°, 0°, and +40° angles and for frequencies of 700, 900, 1000, 1100and 1400 MHz. As Figure 12.3 shows, in all cases stable, squint-free antenna patterns were recorded regardless of the operating frequency, which unambiguously demonstrates the TTD nature of the prototype Rx WDM TTD system; such patterns are not possible with phase steering. We have obtained similar results over the full range of steering angle covered by the TTD system and for any frequency covered by the BW of the antenna. We remind that the 700 - 1400 MHz BW results are limited by the antenna BW and not by the Rx WDM TTD system BW which is 0.2 - 2.5 GHz. It can be seen in Figure 12.3 that the -42° pattern at 1100 MHz is slightly different from the programmed angles by about -5°. We believe that this is due to a combination of errors due to: (1) antenna VSWR, (2) WDM TTD system phase error, and (3) coaxial cable/mechanical delay line VSWR. A similar but lesser problem can be seen for the +40° pattern and the frequencies of 700 and 900 MHz which are offset by -4°. We note that the ±1.0 dB antenna pattern gain variations are due to the characteristics of the element patterns rather than the TTD system.

The next experiment we performed was to accurately measure the sidelobes of the antenna patterns. Figure 12.4 shows the antenna pattern

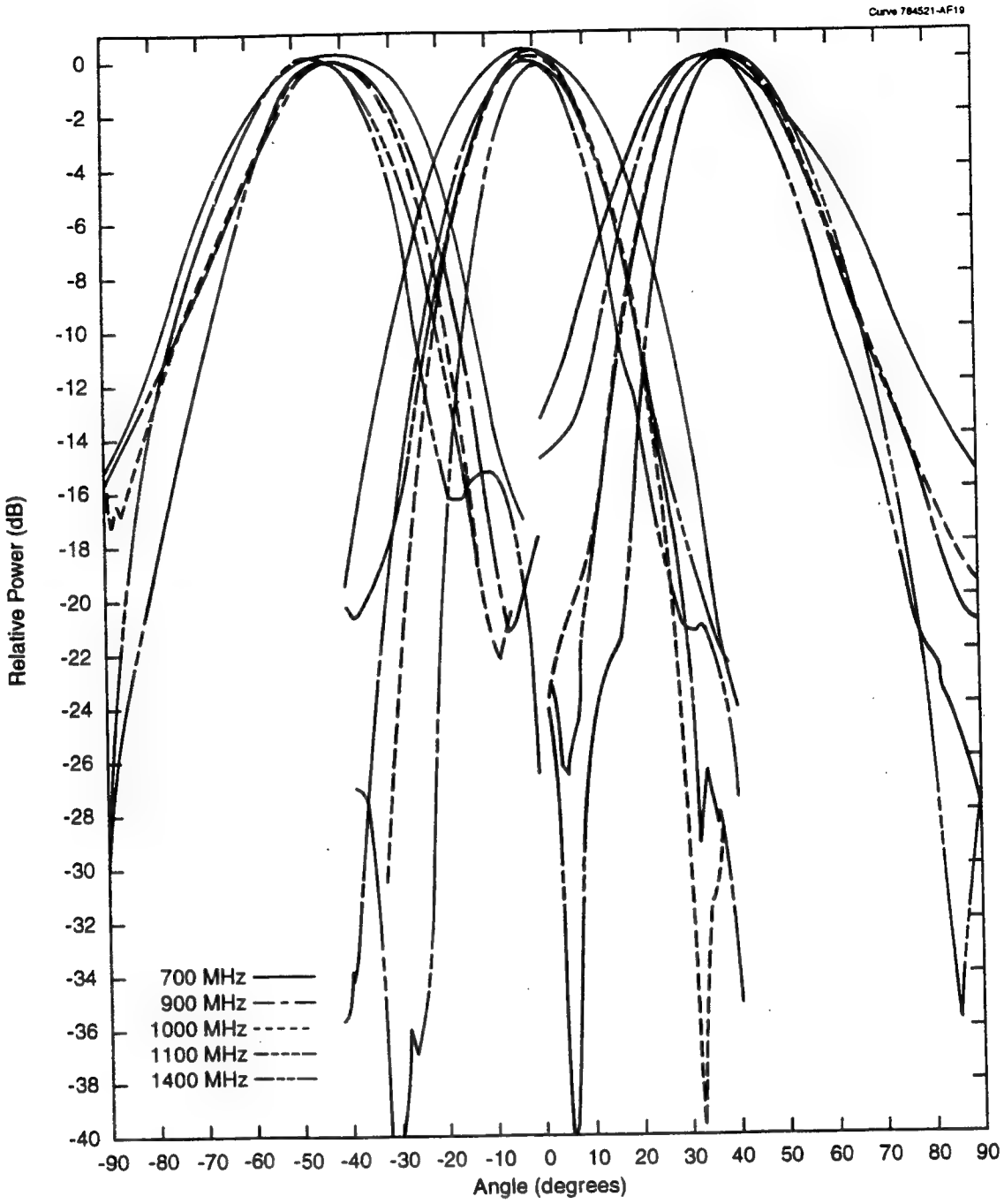

Figure 12.3 — Squint-free antenna patterns for steering at the -43°, 0°, and +39° angles and for frequencies of 700, 900, 1000, 1100, and 1400 MHz.

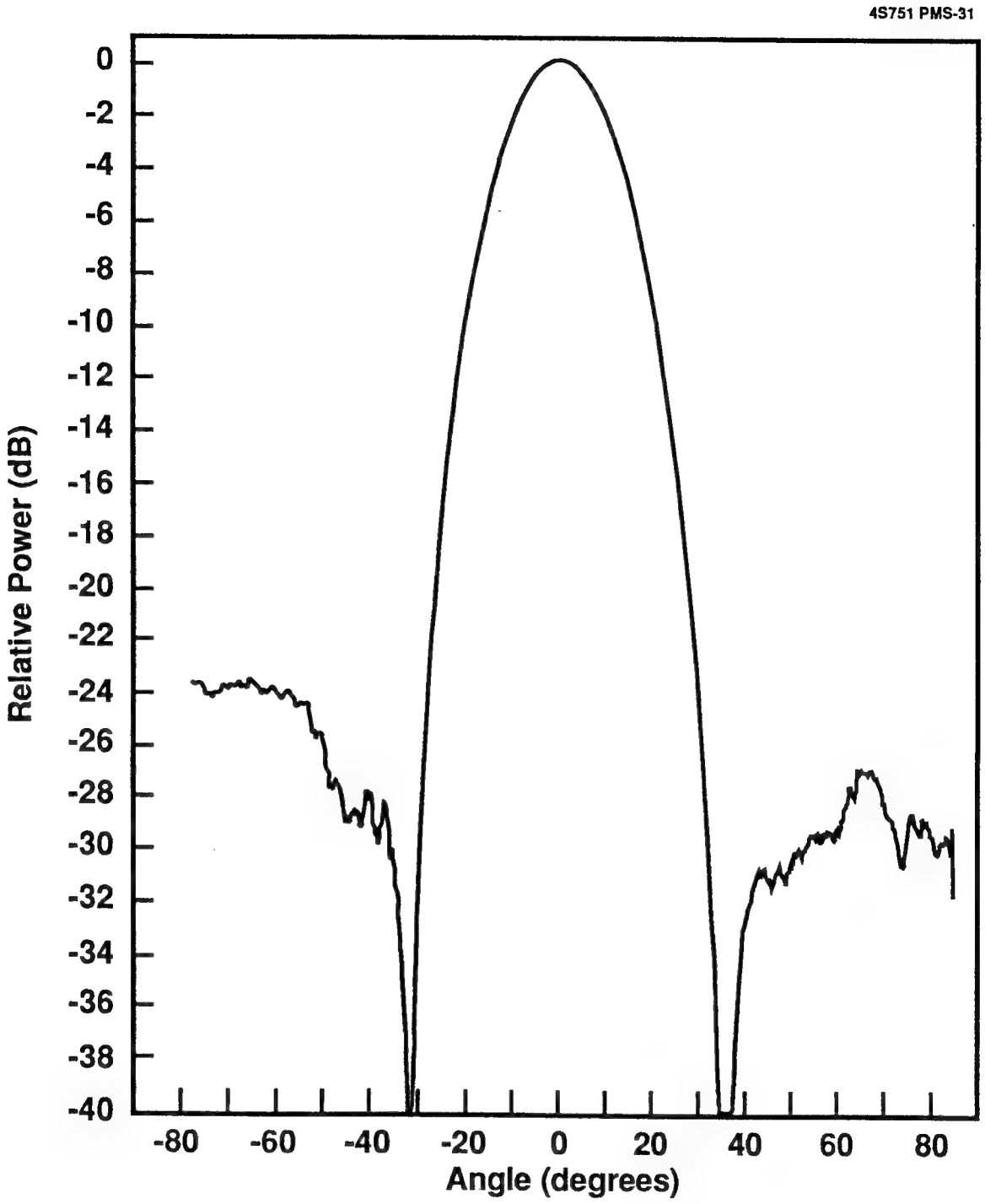

Figure 12.4 — Antenna pattern for a transmit frequency of 1000 MHz. showing sidelobe levels of -27 dB.

obtained for an antenna look angle of 0° and a frequency of 1000 MHz (similar patterns were recorder for other frequencies in the 700 - 1400 MHz range). From Figure 12.4 we see that the measured "right" sidelobe is about -27 dB whereas the "left" sidelobe is about -23 dB. We have determined that the "left" sidelobe was due to an actual reflection from an object that was not "movable" at the time of the experiment. The "right" sidelobe is within 3 dB of the theoretical sidelobes (i.e., the -30 dB level expected from the Chebychev taper) which proves that no serious errors were produced by the TTD system. We attribute the 3 dB difference to the combination cable-mechanical delay line VSWR mismatches for the 8 elements. Note that as Figure 12.4 shows (and similar to the Tx WDM TTD demonstration results), we routinely observed deep, e. g., < -40 dB, nulls in the antenna patterns. In view of the small number of antenna element used in these experiments, such deep nulls are associated with small time errors, which is consistent with the results obtained in the laboratory time error tests.

The last experiment we performed was to measure the system look-angle as a function of the DiBi and BIFODEL switch settings. Figure 12.5 shows an example of such patterns covering the -45° to +40° angular range for a frequency of 800 MHz. Similar to Figure 10.8, Figure 12.5 demonstrates the quantized (in binary form) resolution of the antenna driven by the TTD system. For example, the steering angle sequentially doubles as the TTD program is switched in turn from 000010 to 000100 to 001000 to 010000.

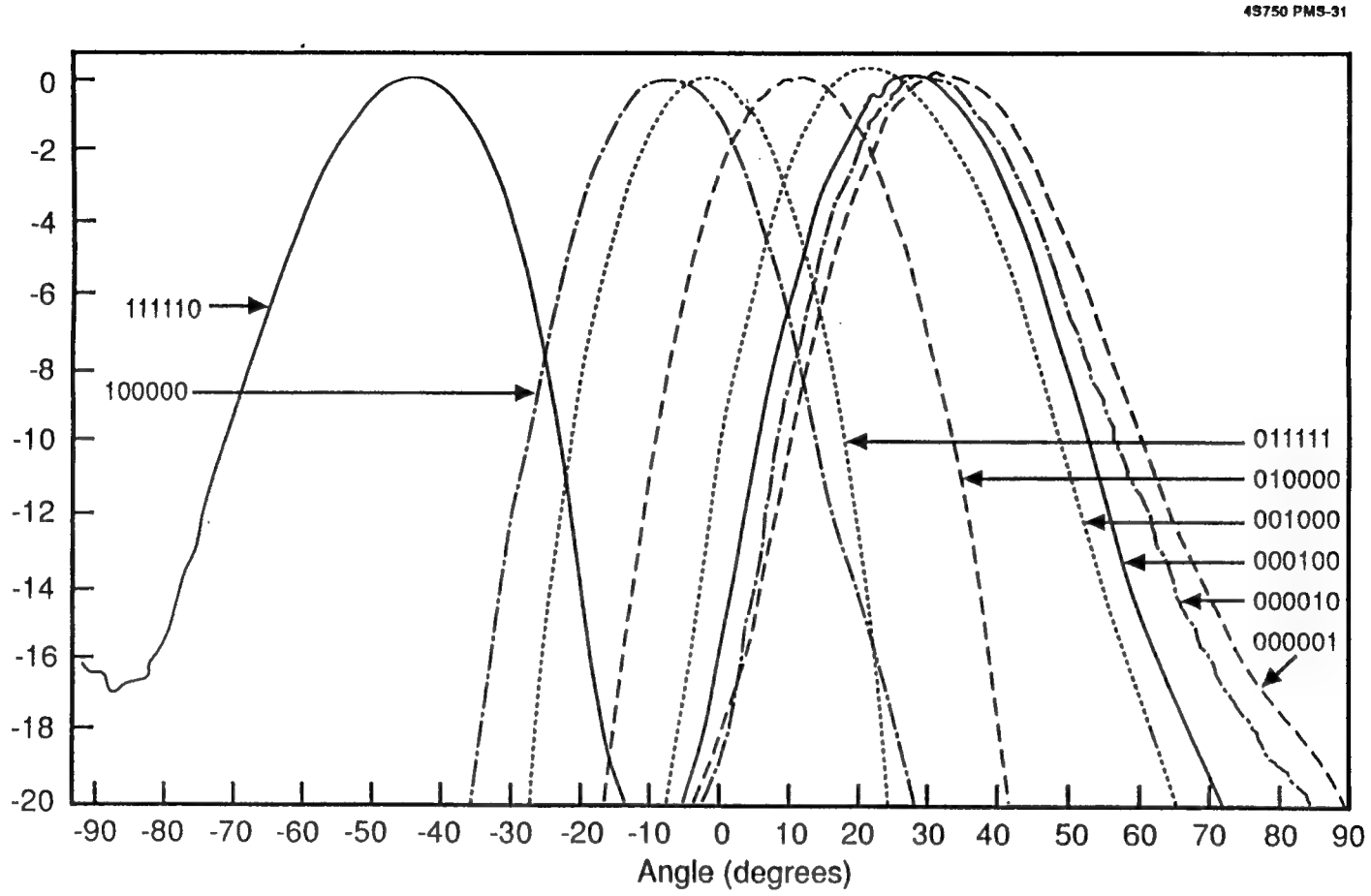

Figure 12.5 — Examples of antenna patterns as functions of DiBi and BIFODEL switch settings that cover the -45°-to-+40° angular range for a frequency of 800 MHz.

13. CONCLUSIONS

In this final report we have described the philosophy, design, fabrication, testing, and antenna range demonstration of a hybrid 16-element Tx, and an 8-element Rx 6-bit WDM TTD system that operates over the 0.2-2.5 GHz band. The hybrid WDM TTD architecture we used is based on a hardware-compressive scheme that uses optical WDM to greatly reduce the overall system volume; thus, as the system volume doubles, the number of antenna elements that can be steered quadruples. The prototype systems we have implemented are based on existing technology, and they are hybrid; they use binary fiberoptic delay lines (BIFODEL) only where low-cost binary electronic delay lines (DiBi) can not perform. In addition they use fiberoptic manifolds to carry the RF signals to and from the array antenna.

Both the 16-element Tx and the 8-element Rx WDM TTD systems have been successfully demonstrated at the Westinghouse antenna range using a 2x16 element broadband phased array antenna. Stable, squint-free antenna patterns have been obtained for both system modes, over the full 0.6 - 1.5 GHz antenna bandwidth and over the full TTD system scan range of about ±45°. The overall sidelobe level performance was found to be very close to the theoretical performance, which demonstrates that accurate time and amplitude performance has been achieved. In addition, we have verified both the system angular scan and angular resolution. Overall, the measured system performance is very close to that predicted by the design, and satisfies the key requirements of various scenarios of phased array antennas used in radar and communications applications.

To our opinion, the WDM TTD program was extremely successful and valuable. Much new knowledge and experience was gained for various aspects of the problem including "mapping" of system needs, compatible performance of optical and electronic devices, problem areas, etc. Several important

conclusions can be drawn from the work performed and the results achieved for this program, including:

- The WDM TTD architecture is indeed a true time delay steering system and compresses the overall hardware as expected.

- The WDM TTD architecture is bidirectional with over 80% of the hardware being common for the transmit and receive modes. However, the optical insertion loss varies for the two modes and thus different, switchable interfaces between the two levels of delay lines must be used for optimum operation.

- The fiberoptic manifolds used for transmit and receive work well and provide both high performance and flexibility.

- For the UHF-L band, the hybrid WDM TTD architecture is sufficient because DiBis with *excellent* performance can be made from low cost COTS.

- The performance of the DiBis is well superior to that of the BIFODELs and satisfy the needs of future high performance radar systems.

- The performance of BIFODELs needs significant improvements including: switching speed (down to 100s of ns), insertion loss (<2.5 dB optical or 5 dB RF), cost (down to 100s of $) and size (reduction by 5-10x).

- For *Transmit* the performance of directly modulated FO links is adequate for current and future system applications (BW, amplitude ripple, phase linearity, NF and SFDR are adequate).

• For *Receive* the performance of directly modulated FO links needs moderate improvements: NF must be reduced by 2-3 dB and SFDR must be increased by 1-2 dB (to >70 dB-$MHz^{2/3}$).

• The FO link cost is high and must be reduced by a factor of 2-5, i.e., to <$400.

• For *Transmit* the optical loss can be tolerated even though an optical amplifier could be used to alleviate the output module gain requirements.

• For *Receive* the optical loss is unacceptable since it deteriorates the system NF and SFDR to unacceptable levels. Much improvement is needed in the areas of: low loss optical switches, low loss asymmetric combiners, low loss MUXs, and low loss multi-mode DMUX.

• The overall system software is extremely simple and adequate.

• The overall time and amplitude errors are low (for both Tx and Rx operations) and satisfy foreseeable system needs without the need for dynamic correction. However, dynamic amplitude correction may be needed because of peripheral components' VSWR variations.

ACKNOWLEDGEMENTS

The authors would like to thank B. Hendrickson and J. Hunter of Rome Laboratory for their support throughout this work and J. Malingowski for his technical assistance.

REFERENCES

1. L. Cardone, "Ultra-wideband microwave beamforming technique," Microwave Journal, 121-131 (April, 1985).

2. D. Curtis, "Frequency domain analysis and performance of a true-time delay fiber optic beamforming network for array antennas," Proc. SPIE, Vol. 1217, 226-234 (1990).

3. W. Ng, A. Walston, G. Tangonan, J. Lee, I. Newberg, and N. Berstein, "The first demonstration of an optically steered microwave phased array antenna using true-time delay," J. Light. Technol., Vol. 9, No. 9, 1124-1131 (1991).

4. G. A. Koepf, "Optical processor for phased array antenna beam formation," Proc. SPIE, Vol. 477, 75-81, (1984).

5. P. R. Herczfeld and A. S. Daryoush, "Fiber-optic feed network for large aperture phased array antennas," Microwave Journal, 160-166 (August, 1987).

6. E. D. Toughlian and H. Zmuda, "A photonic variable RF delay line for phased array antennas," J. Light. Technol., Vol. 8, No. 12, 1824-1828 (1990).

7. R. D. Esman, M. J. Monsma, J. L. Dexter and D. G. Cooper, "Microwave true-time delay modulator using fiberoptic dispersion," Electron. Lett., Vol.28, No.20, 1905-1907 (1992).

8. R. Soref, "Optical dispersion technique for time-delay beam steering," Appl. Opt., Vol. 31, No. 35, 7395-7397 (1992).

9. M. Kondo, K. Komatsu, Y. Ohta, S. Suzuki, K. Nagashima, and H. Goto, "High-speed optical time switch with integrated optical 1x4 switches and single-polarization fiber delay lines," 4th Int. Conf. on Integrated Optics and Optical Fiber Communication, Tokyo, Japan (June 1983), E. I. Conf. No. 04967.

10. A. M. Levine, "Fiber-optic phased array antenna system for RF transmission," US. Patent No. 4028702, June 7, 1977; and in "Fiber optics for radar and data systems," Proc. SPIE, Vol. 150, 185-192 (1978).

11. W. Ng, A. Walston, G. Tangonan, I. Newberg, and J. J. Lee, "Wideband fiber-optic delay network for phased array antenna steering," Electron. Lett., Vol. 25, No. 21, 1456-1457 (1989).

12. W. Ng, G. Tangonan, A. Walston, I. Newberg, J. J. Lee, and N. Bernstein, "True-time delay steering of dual band phased array antenna using laser switched optical beam forming networks," Proc. SPIE, Vol. 1371, 205-211 (1990).

13. H. F. Taylor, "Optical fiber devices for signal processing," Proc. SPIE, Vol. 209, 159-165 (1979).

14. B. Lagerstroem, P. Svensson, A. Djupsjoebacka, and L. Thylen , "Integrated optical delay line signal processor," Proc. OFC/IOOC, Paper WK2, 1987, p. 176.

15. R. A. Thompson, "Optimizing photonic variable-integer delay circuits," OSA Topical Meeting on Photon Switching, Lake Tahoe, Paper FD4-1, March 1987.

16. A. P. Goutzoulis, D. K. Davies, and J. M. Zomp, "Prototype binary fiber optic delay line," Opt. Eng., Vol. 28, No. 11, 1193-1202 (1989).

17. A. P. Goutzoulis and D. K. Davies, "Hardware-compressive 2-D fiber optic delay line architecture for time steering of phased array antennas," Appl. Opt., Vol. 29, No. 36, 5353-5359 (1990).

18. D. L. Baldwin and A.G. Garas, "Architectures and performance of laser links in microwave phased array antenna systems," Proc. SPIE, Vol. 1217, 235-246 (1990).

19. A. P. Goutzoulis and D. K. Davies, "All-optical hardware-compressive wavelength- multiplexed fiber-optic architecture for true time delay steering of 2-D phased array antennas," Proc. SPIE, Vol. 1703, 604-614 (1992).

20. C. T. Sullivan et al., "Switched time delay elements based on AlGaAs/GaAs optical waveguide technology at 1.32 μm for optically controlled phased array antennas," Proc. SPIE, Vol. 1703, 264-271 (1992).

21. G. A. Magel and J. L. Leonard, "Phosphosilicate glass waveguides for phased-array radar time delay," Proc. SPIE, Vol. 1703, 373-378 (1992).

22. A. P. Goutzoulis, D. K. Davies, and J. M. Zomp, "Hybrid electronic fiber-optic wavelength-multiplexed system for true-time delay steering of phased array antennas," Opt. Eng., Vol. 31, No. 11, 2312-2322 (1992).

23. D. Dolfi, F. Michel-Gabriel, S. Bann, and J. P. Huignard, "Two-dimensional optical architecture for true-time delay beam forming in a phased array antenna," Opt. Lett., Vol. 16, No. 4, 255-257 (1991).

24. W. Ng, D. Yap, A. Narayanan, R. Hayes, and A. Walston, "GaAs optical time-shift network for steering a dual band microwave phased array antenna," Proc. SPIE, Vol. 1703, 379-383 (1992).

25. R. A. Soref, "Programmable time-delay devices," Appl. Opt., Vol. 23, No. 21, 3736-3737 (1984).

26. (i) A. P. Goutzoulis and D. K. Davies, "Wavelength-coded binary fiberoptic delay line for time steering of array antennas", US Patent 5125051, June 1992

(ii) A. P. Goutzoulis, "Partitioned optical delay line architecture for time steering of large 1-D array antennas", US Patent 5103495, April 1992

(iii) Ap. P. Goutzoulis, "Recirculating Binary Fiberoptic delay Line Apparatus for time steering", US Patent 5101455, March 1992.

27. S. Koul and B. Bhat, "Microwave and millimeter wave phase shifters," Vol.II, (Semiconductor and delay line phase shifters), Artech House, Norwood, MA, 1991.

28. J. R. Bois, S. Lazar, and P. L. Ouvrard, "Wide band MMIC delay line phase shifter (2-20 GHz)," Proc. IEEE GaAs Int. Symposium, 156-157 (1990).

29. N. K. Shankaranayanan, S. Elby, and K. Lau, "WDMA/Subacarrier FDMA lightwave networks: limitations due to optical beat interference", J. of Light. Tech. Vol . 9, No. 7, 931-943 (1991).

30. I. J. Bahl and D. K. Triverdi, " A designer's guide to microstrip line", Microwaves, 174-182 (May 1977)

*U.S. GOVERNMENT PRINTING OFFICE: 1996-710-126020096

MISSION

OF

ROME LABORATORY

Mission. The mission of Rome Laboratory is to advance the science and technologies of command, control, communications and intelligence and to transition them into systems to meet customer needs. To achieve this, Rome Lab:

a. Conducts vigorous research, development and test programs in all applicable technologies;

b. Transitions technology to current and future systems to improve operational capability, readiness, and supportability;

c. Provides a full range of technical support to Air Force Materiel Command product centers and other Air Force organizations;

d. Promotes transfer of technology to the private sector;

e. Maintains leading edge technological expertise in the areas of surveillance, communications, command and control, intelligence, reliability science, electro-magnetic technology, photonics, signal processing, and computational science.

The thrust areas of technical competence include: Surveillance, Communications, Command and Control, Intelligence, Signal Processing, Computer Science and Technology, Electromagnetic Technology, Photonics and Reliability Sciences.